

**Rational approaches in the development of novel  
5-Lipoxygenase inhibitors: Structure and Ligand  
Based Drug Design strategies**



**THESIS SUBMITTED FOR THE DEGREE  
OF**

*Doctor of Philosophy  
in  
Animal Sciences*

**Supervisor:**  
*Prof. P. Reddanna*

**By:**  
*Aparoy Polamarasetty*

**Department of Animal Sciences  
School of Life Sciences  
University of Hyderabad  
Hyderabad - 500 046  
India**

**February, 2010**

**Enrolment No. 05LAPH11**



**University of Hyderabad**  
**(Central University established in 1974 by act of parliament)**  
**HYDERABAD - 500 046, INDIA**

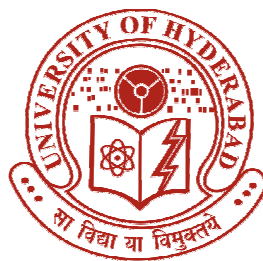
---

## **DECLARATION**

I hereby declare that the work embodied in this thesis entitled **"Rational approaches in the development of novel 5-Lipoxygenase inhibitors: Structure and Ligand Based Drug Design strategies "** has been carried out by me under the supervision of Prof. P. Reddanna and this has not been submitted for any degree or diploma of any other university earlier.

**Prof. P. Reddanna**  
**(PhD Supervisor)**

**Aparoy Polamarasetty**  
**(Research Scholar)**



University of Hyderabad  
(Central University established in 1974 by act of parliament)  
HYDERABAD - 500 046, INDIA

---

### CERTIFICATE

This is to certify that **Mr. Aparoy Polamarasetty** has carried out the research work embodied in the present thesis under my supervision and guidance for a full period prescribed under the Ph.D. ordinance of this University. We recommend his thesis entitled "**Rational approaches in the development of novel 5-Lipoxygenase inhibitors: Structure and Ligand Based Drug Design strategies**" for submission for the degree of Doctor of Philosophy in Animal Sciences of this University.

**Prof. P. Reddanna**  
(PhD Supervisor)

---

**Head**  
**Department of Animal Sciences**

---

**Dean**  
**School of Life Sciences**

---

## *Acknowledgements*

*I express my deepest sense of gratitude to my mentor, **Prof. P. Reddanna** for giving me an opportunity to work under his able guidance, providing the lab facilities and constant support throughout my work.*

*I would like to thank present Dean, School of Life Sciences, **Prof. M. Ramanatham** and former Dean **Prof. A. S. Raghavendra**, for allowing me to use the facilities of the school.*

*I would like to thank the present Head, Department of Animal Sciences, **Prof. S. Dayananda** and the former Head, **Prof. Aparna Dutta Gupta** for allowing me to use the department facilities.*

*I would like to thank **Prof. Arun Agarwal**, Director, Centre for Modelling, Simulation and Design, UoH, for allowing me to use the computational facilities.*

*I would like to thank members of doctoral committee, **Prof. K. Anand Kumar** and **Dr. Lalitha Guruprasad** for their valuable suggestions.*

*My special thanks to **Dr. M. Rami Reddy** for his constant encouragement and support. His dedication to work and perfectionism will have a far reaching impact on my life, academic and beyond.*

*I thank all the other faculty members of School of Life Sciences for their help during the course of my Ph.D. work, especially **Prof. Aparna Dutta Gupta** for her support in academic as well as other aspects of life.*

*My special thanks to **Mr. K. Kumar Reddy**.*

*My thanks to senior colleagues, **Dr. G.V. Reddy, Dr. Pulla Reddy, Dr. Kishore, Dr. K. Anil Kumar, Dr. Karnati R. Roy, Dr. Bharat, Dr. Sreedevi, Dr. Arunasree** and **Dr. Smita** for their help and support.*

*I wish to thank all my cooperative lab mates **Ramakrishna, Chandramohan, Nishanth, Roshan, Praveen, Jyotsna, Suresh, Chandrani, Naresh** and **Geetika** for their help and creating a cheerful work atmosphere.*

*I thank all my teachers since my childhood whose guidance and encouragement at each step was instrumental in shaping my career.*



*I am also thankful to **Mr. Shiva Kumar** for his assistance. The co-operation from the non-teaching staff of school of life sciences, **Mr. Jagan** and **Mr Ankineedu**, lab assistants **Mr. Nagesh** and **Mr. Balram** is greatly acknowledged.*

*I acknowledge **CSIR, New Delhi** for providing JRF and SRF in the form of financial assistance.*

*I thank all my friends at **UoH** for their timely help and support.*

*I fall short of words to thank my friends and family members, especially my mother and brothers **Anuroop** and **Abhiram** for their constant support and encouragement. They have been the pillars of growth and knowledge in my life.*

*Words fail me to express my appreciation to my wife **Srividya**, whose dedication, love and persistent confidence in me, has taken the load off my shoulder. She has provided my life a much needed momentum and direction.*

**Aparoy....✍**

## Contents

<b>I</b>	<b>General Introduction</b>	1-7
<b>1</b>	<b>Homology Modeling of 5-Lipoxygenase and docking studies</b>	8-62
1.1	Introduction	
	1.1.1. Introduction to Homology Modeling	
	1.1.2. Homology modeling of 5-LOX	
1.2	Materials and Methods	
	1.2.1. Construction of the 5-LOX model	
	1.2.1.1. Identification of template	
	1.2.1.2. Identification of metal binding site composition in LOXs using ANAMBS and MEDB	
	1.2.1.2.1. ANAMBS	
	1.2.1.2.2. MEDB	
	1.2.1.3. Incorporation of Ferrous atom in 5-LOX metal binding site	
	1.2.1.4. Refinement and validation of the 5-LOX model	
	1.2.2. Docking Studies	
	1.2.3. Energy Minimization Methods to validate binding site of 5-LOX model generated	
1.3	Results and discussion	
	1.3.1. Generation of 3D structure of 5-LOX	
	1.3.1.1. Template identification and alignment	
	1.3.1.2. Metal binding site composition in LOXs	
	1.3.1.3. Verification of iron binding site in 5-LOX model using ANAMBS	
	1.3.1.4. Verification of the stereo chemical quality of the refined model	
	1.3.1.5. Active site analysis	
	1.3.2. Docking studies	
	1.3.3. Energy minimization studies	
1.4	Conclusions	

<b>2</b>	<b>Development of 5-LOX inhibitors : Structure based lead optimization</b>	<b>63 - 83</b>
2.1	Introduction	
2.2	Methodology	
	2.2.1. Site point connection method	
	2.2.2. Binding site analysis	
	2.2.3. Lead optimization	
	2.2.3. <i>In vitro</i> 5-LOX inhibitory assay	
2.3	Results and discussion	
	2.3.1. Design of molecules	
	2.3.2. Docking and scoring	
	2.3.3. Biological evaluation	
	2.3.3.1. <i>In vitro</i> assay	
2.4	Conclusion	
<b>3</b>	<b>Pharmacophore modeling of 5-LOX inhibitors: A ligand based drug design approach</b>	<b>84 -117</b>
3.1	Introduction	
	3.1.1. Definition of pharmacophore	
	3.1.2. Pharmacophore Modeling	
	3.1.3. Catalyst	
	3.1.3.1. HypoGen theory	
	3.1.3.1. HipHop theory	
	3.1.2. Pharmacophore Modeling of 5-LOX	
3.2	Methodology	
	3.2.1. General methodology	
	3.2.2. Training set selection	
	3.2.3. Generation of Hypothesis	
	3.2.4. Pharmacophore evaluation	
3.3	Results and discussion	
	3.3.1. Generation of the model	
	3.3.2. Validation of the model	
3.4	Conclusion	

<b>4</b>	<b>Identification of 5-LOX inhibitors: Pharmacophore based approach</b>	<b>118-142</b>
4.1	Introduction	
	4.1.1. Selection on the basis of 2D property profiles	
	4.1.2. Selection by means of a target specific pharmacophore	
	4.1.3. Selection by means of receptor-ligand docking	
	4.1.4. Recent applications of pharmacophore based virtual Screening	
4.2	Methodology	
	4.2.1. Virtual screening	
	4.2.2. Biological evaluation	
	4.2.2.1. <i>In vitro</i> 5-LOX inhibition assay	
	4.2.2.2. <i>In vitro</i> anti-proliferative effects on COLO cell line	
4.3	Results and discussion	
	4.3.1. Screening and identification of potential 5-LOX inhibitors	
	4.3.2. Biological evaluation	
	4.3.2.1. <i>In vitro</i> assay	
	4.3.2.2. <i>In vitro</i> anti-proliferative effects	
4.4	Conclusion	
<b>5</b>	<b>Overall Conclusions</b>	<b>143-146</b>
6	References	147-160
7	List of Publications	161-162

## List of figures and tables

### Figures

- Fig. 1** Arachidonic acid metabolism
- Fig. 2** Pathological effects of 5-Lipoxygenase
- Fig. 3** Outline of the homology modeling process and its applications in drug discovery.
- Fig. 4** The two zones of sequence alignments, 'twilight' and 'safe' modeling zones.
- Fig. 5** Torsion angle of peptide
- Fig. 6** Ramachandran plot
- Fig. 7** Homology modeling and Structure Based Drug Design
- Fig. 8** Application of homology modeling techniques at different stages of drug discovery process within past two years
- Fig. 9** Hydropathy Index for the twenty natural amino acids (Kyte and Doolittle)
- Fig. 10** Features of the tool
- Fig. 11** Output obtained for Soybean Lipoxygenase (PDB id. 1YGE) using ANAMBS for a cutoff distance of 4 Å
- Fig. 12** The homepage of MEDB showing various search options
- Fig. 13** Working principle of tool ANAMBS and database MEDB developed
- Fig. 14** Alignment of Soybean LOX-3 (1NO3) and potato 5-LOX sequences. Essential sites for iron binding are denoted by asterisk (\*)
- Fig. 15** Iron binding site information obtained for LOXs in MEDB
- Fig. 16** Iron binding site in the C-terminal catalytic domain of 5-LOX
- Fig. 17** Profile-3D graph of the 5-LOX model
- Fig. 18** C $\alpha$  Trace of the template and the 5-LOX model
- Fig. 19** Secondary structures of (a) model and (b) template
- Fig. 20** Ramachandran plot of the 5-LOX model
- Fig. 21** Main chain parameters of the 5-LOX model
- Fig. 22** Side chain parameters of the 5-LOX model
- Fig. 23** ERRAT plot of the 5-LOX model

- Fig. 24** Hydrogen bonding interactions of NDGA with the protein
- Fig. 25** Hydrogen bonding interactions of BP1 with the protein
- Fig. 26** Hydrogen bonding interactions of BP2 with the protein
- Fig. 27** Hydrogen bonding interactions of BP3 with the protein
- Fig. 28** Structure-based lead generation and optimization
- Fig. 29** Scheme of site-point methods
- Fig. 30** The potential hydrogen bond interaction sites identified in the vicinity of the docked ligand.
- Fig. 31** O<sub>2</sub> conc. *vs* Time graph for various conc. of inhibitor
- Fig. 32** Various molecules designed using site points
- Fig. 33** The molecules designed and their molecular properties.
- Fig. 34** Inhibition concentration curve of S1 (IC<sub>50</sub> -157  $\mu$ M).
- Fig. 35** Inhibition concentration curve of S2 (IC<sub>50</sub> -137  $\mu$ M).
- Fig. 36** Inhibition concentration curve of S3 (IC<sub>50</sub> -8  $\mu$ M).
- Fig. 37** Inhibition concentration curve of S4 (IC<sub>50</sub> -6.4  $\mu$ M).
- Fig. 38** HypoGen theory
- Fig. 39** HipHop theory
- Fig. 40** Chemical structures of 5-LOX inhibitors in training set
- Fig. 41** Chemical structures of 5-LOX inhibitors in test set
- Fig. 42** Pharmacophore model of 5-LOX inhibitors generated by HypoGen
- Fig. 43** Interactions of most active molecule in training set.
- Fig. 44** The difference in total cost of hypotheses between the initial spreadsheet and 19 random spreadsheets after CatScramble run.
- Fig. 45** Correlation plot
- Fig. 46** Process for the ligand and receptor pharmacophore based virtual screening.
- Fig. 47** Process for the structure based virtual screening.
- Fig. 48** Summary of recently published virtual screening studies based on receptor-ligand docking
- Fig. 49** The virtual screening work flow followed.
- Fig. 50** One of the potential molecule identified, L11 mapped on to the

pharmacophore model.

- Fig. 51** Selected molecules (hits) and their molecular properties.
- Fig. 52** Effect of L11 on 5-LOX activities.
- Fig. 53** Effect of L13 on 5-LOX activities.
- Fig. 54** Interactions of L11 with 5-LOX
- Fig. 55** Effect of the two molecules on the proliferation of COLO-205 cell line.

### Tables

- Table-1** Comparison of results of the model and crystal structures of LOXs using ANAMBS
- Table-2** Experimentally measured  $IC_{50}$  values for the compounds and hydrogen bonding analysis of NDGA, BP1, BP2 and BP3.
- Table-3** Binding energies (kcal/mol) calculated using Eq.3
- Table-4** Calculated interaction energies (kcal/mol) for the designed compounds
- Table-5** Summary of successful applications of pharmacophore-based virtual screening.
- Table-6** Statistical parameters of the top 10 hypotheses of 5-LOX inhibitors generated by HypoGen program
- Table-7** Experimental and estimated (by Hypo1)  $IC_{50}$  values ( $\mu M$ ) of the training set compounds
- Table-8** Experimental and estimated (by Hypo1)  $IC_{50}$  values ( $\mu M$ ) of the test set compounds
- Table-9** Some of the potential hits identified

## Abbreviations

LOX	Lipoxygenase
LTs	Leukotrienes
HPETE	Hydroperoxyeicosatetraenoic acid
FLAP	5-Lipoxygenase activating protein
GERD	Gastroesophageal Reflux Disease
SRS-A	Slow-reacting substance of anaphylaxis
CML	Chronic myeloid leukemia
LSCs	Leukemia cancer stem cells
NMR	Nuclear magnetic resonance
PIR	Protein Information Resource
TrEMBL	Translated European Molecular Biology Laboratory
BLAST	Basic Local Alignment Search Tool
SCR	Structurally conserved region
SVR	Structurally variable region
PDB	Protein Data Bank
SGI	Silicon Graphics Interface
CHARMM	Chemistry at HARvard Macromolecular Mechanics
GOLD	Genetic Optimisation for Ligand Docking
AMBER	Assisted Model Building with Energy Refinement
MOE	Molecular Operating Environment
SAR	Structure Activity Relationship
Å	Angstrom units
GA	Genetic Algorithm
$\Delta E_{\text{bind}}$	Relative binding energy
$\Delta E_{\text{comp}}$	Interaction energies of a inhibitor in the complex



$\Delta E_{\text{sol}}$	Interaction energies of a inhibitor in solvated state
pH	Negative logarithm (base 10) of the molar concentration of dissolved hydrogen ions ( $\text{H}^+$ ).
DMSO	Dimethyl Sulfoxide
NDGA	Nordihydroguaiaretic Acid
BP	Benzyl Propargyl ether analog
L1-15	Ligand based designed compound 1-15
S1-4	Structure based designed compound 1-4
3-D	Three Dimensional
FBS	Fetal Bovine Serum
MTT	3-(4,5-Dimethylthiazol-2-Yl)-2,5-Diphenyltetrazolium Bromide

## List of figures and tables

### Figures

- Fig. 1** Arachidonic acid metabolism
- Fig. 2** Pathological effects of 5-Lipoxygenase
- Fig. 3** Outline of the homology modeling process and its applications in drug discovery.
- Fig. 4** The two zones of sequence alignments, 'twilight' and 'safe' modeling zones.
- Fig. 5** Torsion angle of peptide
- Fig. 6** Ramachandran plot
- Fig. 7** Homology modeling and Structure Based Drug Design
- Fig. 8** Application of homology modeling techniques at different stages of drug discovery process within past two years
- Fig. 9** Hydropathy Index for the twenty natural amino acids (Kyte and Doolittle)
- Fig. 10** Features of the tool
- Fig. 11** Output obtained for Soybean Lipoxygenase (PDB id. 1YGE) using ANAMBS for a cutoff distance of 4 Å
- Fig. 12** The homepage of MEDB showing various search options
- Fig. 13** Working principle of tool ANAMBS and database MEDB developed
- Fig. 14** Alignment of Soybean LOX-3 (1NO3) and potato 5-LOX sequences. Essential sites for iron binding are denoted by asterisk (\*)
- Fig. 15** Iron binding site information obtained for LOXs in MEDB
- Fig. 16** Iron binding site in the C-terminal catalytic domain of 5-LOX
- Fig. 17** Profile-3D graph of the 5-LOX model
- Fig. 18** C $\alpha$  Trace of the template and the 5-LOX model
- Fig. 19** Secondary structures of (a) model and (b) template
- Fig. 20** Ramachandran plot of the 5-LOX model
- Fig. 21** Main chain parameters of the 5-LOX model
- Fig. 22** Side chain parameters of the 5-LOX model
- Fig. 23** ERRAT plot of the 5-LOX model

- Fig. 24** Hydrogen bonding interactions of NDGA with the protein
- Fig. 25** Hydrogen bonding interactions of BP1 with the protein
- Fig. 26** Hydrogen bonding interactions of BP2 with the protein
- Fig. 27** Hydrogen bonding interactions of BP3 with the protein
- Fig. 28** Structure-based lead generation and optimization
- Fig. 29** Scheme of site-point methods
- Fig. 30** The potential hydrogen bond interaction sites identified in the vicinity of the docked ligand.
- Fig. 31** O<sub>2</sub> conc. *vs* Time graph for various conc. of inhibitor
- Fig. 32** Various molecules designed using site points
- Fig. 33** The molecules designed and their molecular properties.
- Fig. 34** Inhibition concentration curve of S1 (IC<sub>50</sub> -157  $\mu$ M).
- Fig. 35** Inhibition concentration curve of S2 (IC<sub>50</sub> -137  $\mu$ M).
- Fig. 36** Inhibition concentration curve of S3 (IC<sub>50</sub> -8  $\mu$ M).
- Fig. 37** Inhibition concentration curve of S4 (IC<sub>50</sub> -6.4  $\mu$ M).
- Fig. 38** HypoGen theory
- Fig. 39** HipHop theory
- Fig. 40** Chemical structures of 5-LOX inhibitors in training set
- Fig. 41** Chemical structures of 5-LOX inhibitors in test set
- Fig. 42** Pharmacophore model of 5-LOX inhibitors generated by HypoGen
- Fig. 43** Interactions of most active molecule in training set.
- Fig. 44** The difference in total cost of hypotheses between the initial spreadsheet and 19 random spreadsheets after CatScramble run.
- Fig. 45** Correlation plot
- Fig. 46** Process for the ligand and receptor pharmacophore based virtual screening.
- Fig. 47** Process for the structure based virtual screening.
- Fig. 48** Summary of recently published virtual screening studies based on receptor-ligand docking
- Fig. 49** The virtual screening work flow followed.
- Fig. 50** One of the potential molecule identified, L11 mapped on to the

pharmacophore model.

- Fig. 51** Selected molecules (hits) and their molecular properties.
- Fig. 52** Effect of L11 on 5-LOX activities.
- Fig. 53** Effect of L13 on 5-LOX activities.
- Fig. 54** Interactions of L11 with 5-LOX
- Fig. 55** Effect of the two molecules on the proliferation of COLO-205 cell line.

### Tables

- Table-1** Comparison of results of the model and crystal structures of LOXs using ANAMBS
- Table-2** Experimentally measured  $IC_{50}$  values for the compounds and hydrogen bonding analysis of NDGA, BP1, BP2 and BP3.
- Table-3** Binding energies (kcal/mol) calculated using Eq.3
- Table-4** Calculated interaction energies (kcal/mol) for the designed compounds
- Table-5** Summary of successful applications of pharmacophore-based virtual screening.
- Table-6** Statistical parameters of the top 10 hypotheses of 5-LOX inhibitors generated by HypoGen program
- Table-7** Experimental and estimated (by Hypo1)  $IC_{50}$  values ( $\mu M$ ) of the training set compounds
- Table-8** Experimental and estimated (by Hypo1)  $IC_{50}$  values ( $\mu M$ ) of the test set compounds
- Table-9** Some of the potential hits identified

## Abbreviations

LOX	Lipoxygenase
LTs	Leukotrienes
HPETE	Hydroperoxyeicosatetraenoic acid
FLAP	5-Lipoxygenase activating protein
GERD	Gastroesophageal Reflux Disease
SRS-A	Slow-reacting substance of anaphylaxis
CML	Chronic myeloid leukemia
LSCs	Leukemia cancer stem cells
NMR	Nuclear magnetic resonance
PIR	Protein Information Resource
TrEMBL	Translated European Molecular Biology Laboratory
BLAST	Basic Local Alignment Search Tool
SCR	Structurally conserved region
SVR	Structurally variable region
PDB	Protein Data Bank
SGI	Silicon Graphics Interface
CHARMM	Chemistry at HARvard Macromolecular Mechanics
GOLD	Genetic Optimisation for Ligand Docking
AMBER	Assisted Model Building with Energy Refinement
MOE	Molecular Operating Environment
SAR	Structure Activity Relationship
Å	Angstrom units
GA	Genetic Algorithm
$\Delta E_{\text{bind}}$	Relative binding energy
$\Delta E_{\text{comp}}$	Interaction energies of a inhibitor in the complex

$\Delta E_{\text{sol}}$	Interaction energies of a inhibitor in solvated state
pH	Negative logarithm (base 10) of the molar concentration of dissolved hydrogen ions ( $\text{H}^+$ ).
DMSO	Dimethyl Sulfoxide
NDGA	Nordihydroguaiaretic Acid
BP	Benzyl Propargyl ether analog
L1-15	Ligand based designed compound 1-15
S1-4	Structure based designed compound 1-4
3-D	Three Dimensional
FBS	Fetal Bovine Serum
MTT	3-(4,5-Dimethylthiazol-2-Yl)-2,5-Diphenyltetrazolium Bromide



## General Introduction

Lipoxygenases (LOXs) (linoleate: oxygen oxido reductase, EC 1.13.11.12) are a group of closely related non-heme iron containing dioxygenases. These enzymes catalyze the addition of molecular oxygen into Poly Unsaturated Fatty Acids (PUFAs) containing cis, cis 1-4 pentadiene structures to give their hydroperoxy derivatives. LOXs are essentially ubiquitous among eukaryotic organisms and have been demonstrated to exist in many tissues of numerous fungi, higher plants and animals [Gerwick, 1994; Funk, 1996]. Higher plants and animals contain multiple LOXs with at least eight identified in soybean, seven in mouse and five in humans [Boeglin *et al.*, 1998]. High levels of LOX expression is observed in few plant and animal tissues. They constitute a major portion of the proteins in soybeans, and 15-LOX represents one of the main proteins in rabbit reticulocytes during anemia. Soybean and potato are the well-characterized LOXs in plants. [Reddanna *et al.*, 1990; Chen *et al.*, 1998; Reddanna *et al.*, 1988; Nikolaev *et al.*, 1990]

PUFAs containing a series of cis double bonds act as suitable substrates for LOXs. LOXs are classified according to their positional specificity of arachidonate oxygenation into 5-, 8-, 9-, 11-, 12- and 15-LOXs [Rapoport *et al.*, 1979]. The prominent animal LOXs are 5-LOX, 8- LOX, 12-LOX and 15-LOX, while the plant LOXs are mostly 5-LOX and 15-LOX. The differing chain lengths of the most common substrates of plants (linoleic and  $\alpha$ -linoleic



acids, 18-carbon) and animals (arachidonic acid, 20-carbon) result in a plant 13-LOX or 9-LOX corresponding to a mammalian 15-LOX or 5-LOX.

LOX proteins have a single polypeptide chain with a molecular mass of 75–80 kDa in animals and 94–104 kDa in plants [Brash, 1999; Shibata *et al.*, 1995]. All LOXs have a two-domain structure, the small N-terminal  $\beta$ -barrel domain and a larger catalytic domain containing a single atom of non-heme iron. The catalytic iron is ligated in an octahedral arrangement by three conserved histidines, one His/Asn/Ser and the C-terminal isoleucine [Minor *et al.*, 1996]. The highest sequence identity between these LOXs is in the portion of the catalytic domain near the iron atom [Prigge *et al.*, 1997]. Though most of the LOXs insert molecular oxygen stereospecifically at 'S', recently 'R' LOXs also have been reported [Boeglin *et al.*, 1998; Sunitha *et al.*, 2005]. One of at least four LOX pathways of arachidonic acid metabolism, the 5-LOX pathway is the source of potent pro-inflammatory mediators [Brash, 1999]. LOX metabolites are potent physiological effectors in a variety of cellular responses, associated with normal host defense and inflammation. In particular, leukotrienes (LTs), the mediators of allergy and asthma are produced through the 5-LOX pathway.

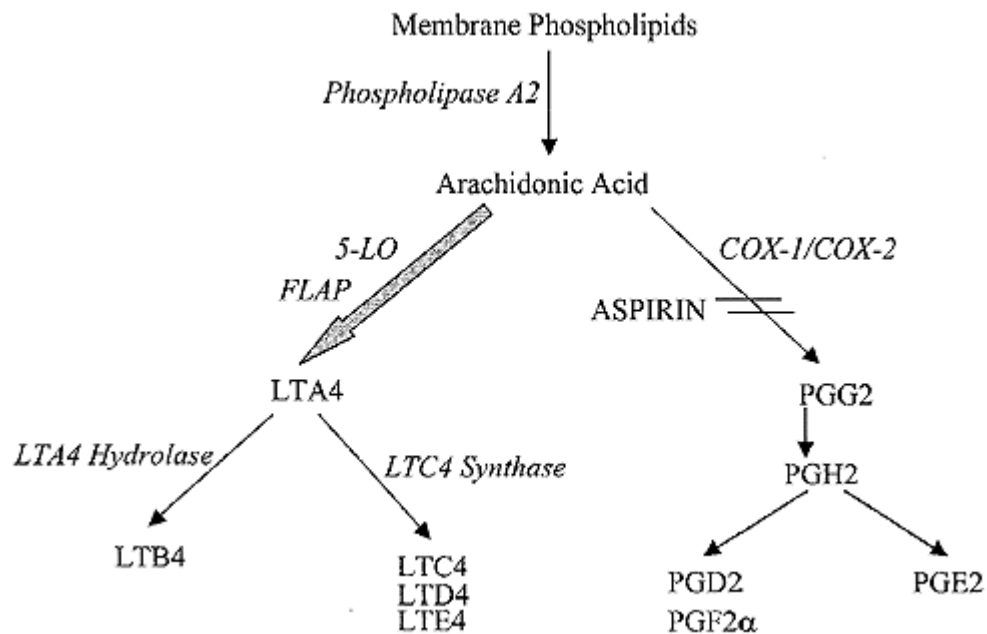


**Fig. 1:** Arachidonic acid metabolism

(<http://img.medscape.com/fullsize/migrated/405/963/ch1185.02.lieb.fig1.gif>)

The 5-LOX acts preferentially upon unesterified arachidonic acid, inserting molecular oxygen at the fifth carbon and forming the hydroperoxy intermediate, 5-hydroperoxyeicosatetraenoic acid (5-HPETE) (Fig. 1) [Funk, 2001]. The same enzyme then catalyzes a dehydration reaction, forming the unstable epoxide intermediate, leukotriene A<sub>4</sub> (LTA<sub>4</sub>). In intact inflammatory cells, the presence of 5-LOX activating protein (FLAP) is required to make this enzyme active [Dixon *et al.*, 1990]. LTA<sub>4</sub> can be further metabolized to LTB<sub>4</sub> by LTA<sub>4</sub> hydrolase or to LTC<sub>4</sub> by conjugation of glutathione at the sixth carbon by the action of LTC<sub>4</sub> synthase [Chang *et al.*, 1987]. Additional studies established

that LTC<sub>4</sub> and its extracellular metabolites LTD<sub>4</sub> and LTE<sub>4</sub> are the constituents of slow-reacting substances of anaphylaxis (SRS-A), but they are now more properly termed cysteinyl leukotrienes. The cysteinyl leukotrienes have been recognized to mimic many of the clinical manifestations of asthma, including sustained bronchoconstriction, hypersecretion of mucus, and airway edema. LTE<sub>4</sub> gets further metabolized to inactive LTF<sub>4</sub> by the action of  $\gamma$ -glutamyl transpeptidase. Also LTF<sub>4</sub> was shown to be formed directly from LTC<sub>4</sub> by the action of carboxypeptidase [Reddanna *et al.*, 2003].

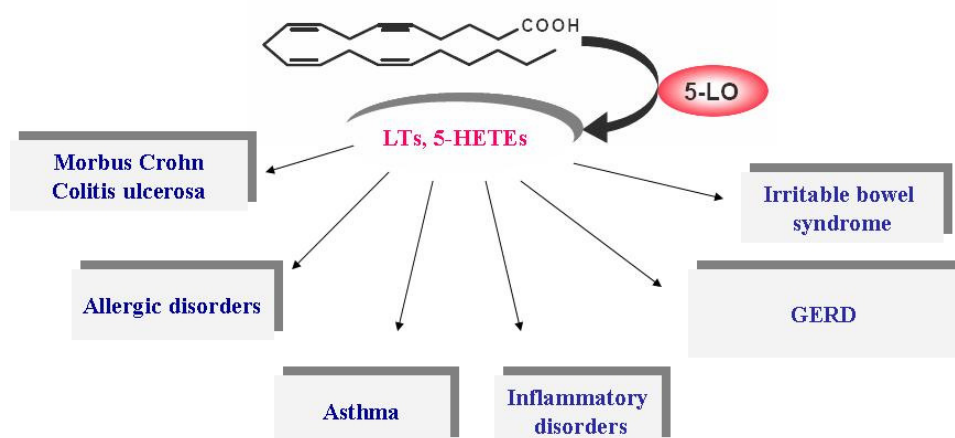


**Fig. 2:** Pathological effects of 5-LOX

Products of the 5-LOX pathway are thus important mediators of inflammation. Inhibitors of the 5-LOX pathway, therefore, have a therapeutic potential in a variety of inflammatory and allergic diseases. These efforts have resulted in the release of Zileuton (5-LOX inhibitor) and Montelukast

(leukotriene receptor antagonist) into the market for the treatment of asthma. It has been also reviewed that 5-LOX plays a key role in Gastroesophageal reflux disease (GERD). Elevated levels of leukotriene B-4 have been found in blood and joint fluid from patients with rheumatoid arthritis [Davidson *et al.*, 1983] and in colonic mucosa from patients with ulcerative colitis or Crohn's disease. LOX and their products are shown to play important role in tumor formation and cancer metastasis [Nie *et al.*, 2001]. High expression of 5-LOX was found in prostate, lung and other cancer cell lines [Anderson *et al.*, 1998; Avis *et al.*, 1996]. Recent studies have indicated that LOX inhibitors may be superior to leukotriene-receptor antagonists, as they block the action of the full spectrum of 5-LOX products whereas leukotriene receptor antagonists would produce narrower effects. Recently it has been shown that 5-LOX (ALOX5) is critical regulator for leukemia cancer stem cells (LSCS) in chronic myeloid leukemia (CML). Treatment of CML mice with a 5-LOX inhibitor also impaired the function of LSCS [Chen *et al.*, 2009]. Inhibition of 5-LOX by Vitamin E [Reddanna *et al.*, 1985] and benzyl propargyl ethers [Barhate *et al.*, 2002] has been reported. Currently an emerging strategy of therapeutic value consists of creating molecules with specific 5-LOX inhibition activity. In this study we have used structure based and ligand based drug design strategies to identify potential novel 5-LOX inhibitors.

Objectives framed for the study are:

1. Homology modeling of 5-LOX
2. Structure based lead optimization
3. Pharmacophore modeling of 5- LOX
4. Virtual screening
5. *In vitro* screening

# Chapter -I

## Homology Modeling of 5-Lipoxygenase and docking studies

## 1.1. Introduction

### 1.1.1. Introduction to Homology Modeling

Knowledge of the three-dimensional structure of a protein can often provide invaluable information. The structure can provide hints about functional and evolutionary features of the protein and in addition, structural information that is useful in drug design studies. The structure of a protein can, in theory, be obtained either by the use of experimental information, normally from X-ray crystallography or NMR spectroscopy or by computational techniques like comparative modeling or *ab initio* modeling or threading. The most widely used and accepted computational approach for structure prediction is homology modeling.

**Homology modeling**, also known as **comparative modeling** of protein refers to constructing an atomic resolution model of the "*target*" protein from its amino acid sequence and an experimental three-dimensional structure of a related homologous protein (the "*template*"). Homology modeling methods use the fact that evolutionary related proteins share a similar structure. Therefore, models of a protein with unknown structure (target) can be built based on an alignment of a closely related protein of known structure (template) (Fig 3). The steps involved in this process are: (i) identification of homolog that can be used as template(s) for modeling; (ii) alignment of the target sequence to the

template(s); (iii) backbone generation; (iv) loop modeling; (v) side-chain modeling; (vi) model optimization and (vii) validation of the model [Elmar Krieger *et al.*, 2003; Sánchez and Sali 1997].

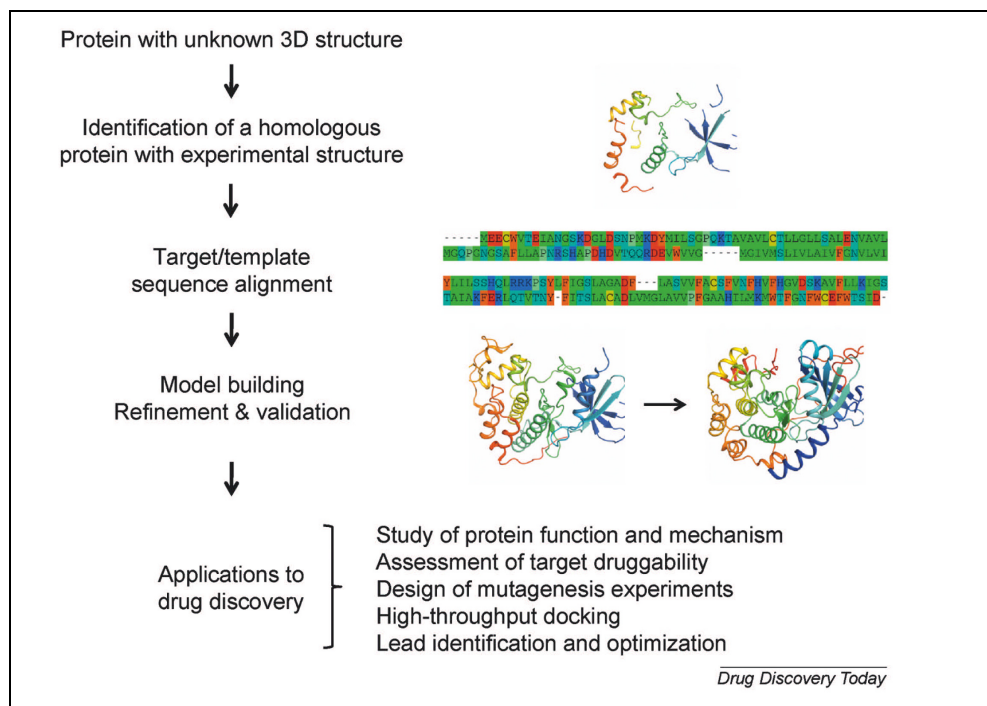


**Fig. 3:** Outline of the homology modeling process and its applications in drug discovery. Given the sequence of a protein with unknown structure, the first step is the identification of a related protein with known 3D structure that serves as template. An alignment of the target and template sequences is necessary to assign the correspondence between target and template residues. A model is then built for the target based on the alignment and structure of the template, and further refined and validated. This figure was prepared using Pymol (<http://www.pymol.org>).  
(Taken from: Cavasotto *et al.*, Drug Discov Today 14 (2009) 676-83).



*(i) Identification of homolog(s) that can be used as template(s) for modeling*

The first task in comparative modeling is to identify all protein structures related to the target sequence, some or one of which will be used as templates. This is greatly facilitated by the availability of protein sequence and structure, databases and softwares for the scanning of these databases. The target sequence can be searched against sequence databases, such as PIR, GenBank, or TrEMBL/SWISS-PROT, and/or structure databases, such as the Protein Data Bank. If the template is a close relative characterized by high percentage sequence identity (at least 40%) then one can obtain a model comparable in accuracy to a medium resolution X-ray structure, as shown in Fig. 4.

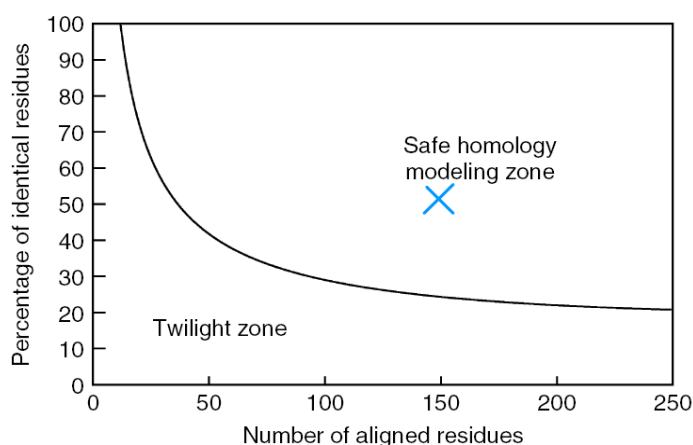


**Fig. 4:** *The two zones of sequence alignments.* Two sequences are practically guaranteed to fold into the same structure if their length and percentage sequence identity fall into the region marked as “safe.” An example of two sequences with 150 amino acids, 50% of which are identical, is shown (cross).

The tools which are available on World Wide Web to identify the template are:

1. [http://www.ncbi.nlm.nih.gov/cgi-bin/BLAST/nph-psi\\_blast/](http://www.ncbi.nlm.nih.gov/cgi-bin/BLAST/nph-psi_blast/)
2. <http://www.bmm.icnet.uk/~3dpssm/>
3. <http://www-cryst.bioc.cam.ac.uk/~fugue>
4. [http://bioinformatics.burnham-inst.org/pdb\\_blast](http://bioinformatics.burnham-inst.org/pdb_blast)

*(ii) Alignment of the target sequence to the template(s)*

Once the template structure/structures related to the target sequence are identified, the second task is to prepare a multiple alignment of the target sequence with the potential template structures. When pair wise sequence identity is over 25-30% (for more than 80 residues), alignment procedures are usually straightforward. Alignments may fail for less similarity protein sequences. There are many programs available for sequence alignment, but widely used program is CLUSTALW [Thompson *et al.*, 1994].

*(iii) Backbone generation*

When the alignment is ready, the actual model building can start. The most widely used approach in comparative modeling is to assemble a model from a small number of rigid bodies obtained from the aligned protein

structures [Greer, 1990; Blundell *et al.*, 1987]. The approach is based on the natural dissection of the protein structure into structurally conserved regions (SCRs), structurally variable regions (SVRs) or loops that connect them and side chains that decorate the backbone.

Creating the backbone is trivial for most of the model: One simply copies the coordinates of those template residues that show up in the alignment with the model sequence. If two aligned residues differ, only the backbone coordinates (N,  $C\alpha$ , C and O) can be copied. If they are the same, one can also include the side chain (at least the more rigid side chains, since rotamers tend to be conserved).

#### *(iv) Loop modeling*

In the majority of cases, the alignment between model and template sequence contains gaps i.e. loops or SVRs. The loops are generated by scanning a database of all known protein structures to identify the structurally variable regions that fit the anchor core regions and have a compatible sequence.

There are two main approaches to loop modeling:

**a. Knowledge based:** One searches the PDB for known loops with endpoints that match the residues between which the loop has to be inserted and simply copies the loop conformation. All major molecular modeling programs and servers support this approach (e.g., 3D-Jigsaw [Bates and Sternberg, 1999], Modeller [Sali and Blundell, 1993], Swiss-Model [Peitsch *et al.*, 2000], or WHAT IF [Vriend, 1990]).

**b. Energy based:** As in true *ab initio* fold prediction, an energy function is used to judge the quality of a loop. Then this function is minimized, using Monte Carlo or molecular dynamics techniques [Fiser *et al.*, 2000] to arrive at the best loop conformation. Often the energy function is modified (e.g., smoothed) to facilitate the search.

#### *(v) Side-Chain modeling*

The side chains are modeled based on their intrinsic conformational preferences and on the conformation of the equivalent side chains in the template structures.

*(vi) Model optimization*

Once an approximate model has been produced, the model needs to be refined further. The stereochemistry of the model is improved either by a restrained energy minimization or a molecular dynamics refinement. Idealization of bond energy and removal of unfavorable non-bonded contacts can be performed by energy minimization with force fields. The refinement of a primary model should be performed by 300-500 steps of steepest descent, followed by 500-1000 steps of conjugate gradient energy minimization. Models optimized by large steps of energy minimization (or molecular dynamics) usually move away from a control structure. It is thus necessary to keep the number of minimization steps to a minimum [Elmar Krieger *et al.*, 2003]. Constraining the position of selected atoms (such as C alpha or B-factor based function) in each residue generally helps avoiding excessive structural drift during force field computations. The modeling can be carried out using the softwares like MODELLER, INSIGHT-II, Discover Studio, etc.

*(vii) Validation of the model*

For a homology modeling from any source, it is important to demonstrate the structural features. Researchers have analyzed three-

dimensional structures of proteins from which basic principles of protein structure and folding have been developed. Several programs are available to assist in this analysis of correctness of a homology model. They are:

**a. PROCHECK:**

The aim of PROCHECK is to assess how normal or conversely how unusual, the geometry of the residues in a given protein structure is, as compared with stereo chemical parameters derived from well-refined, high resolution structures [Laskowski *et al.*, 1993]. PROCHECK is based on an analysis of ( $\phi$ ,  $\psi$ ) angles, peptide bond planarity, bond lengths, bond angles, hydrogen-bond geometry and side-chain conformations of known protein structures as a function of atomic resolution. Thus, the expected values of these parameters are known and can be compared to a modeled structure based on the atomic resolution of the structures from which the model was developed.

PROCHECK is available at

(<http://www.biochem.ucl.ac.uk/~roman/procheck/procheck.html>)

The criteria for analysis of correctness can include:

- ❖ Main chain conformations in the Ramachandran plot.
- ❖ Planar peptide bonds.
- ❖ Side chain conformations that correspond to those in the Rotamer library.
- ❖ Hydrogen bonding of polar atoms if they are buried.
- ❖ Proper environments for hydrophobic and hydrophilic residues.
- ❖ No bad atom-atom contacts.
- ❖ No holes inside the structure.

In order to check the stereo chemical quality of the structure, all bond lengths, dihedral angles including phi ( $\Phi$ ), psi ( $\Psi$ ) and omega and various chi angles of the side chains are calculated and examined. In polypeptide the main chain N-C $\alpha$  and C $\alpha$ -C bonds relatively are free to rotate. These rotations are represented by the torsion angles  $\Phi$  and  $\Psi$ , respectively. Fig. 5 shows the three main chain torsion angles of a polypeptide.

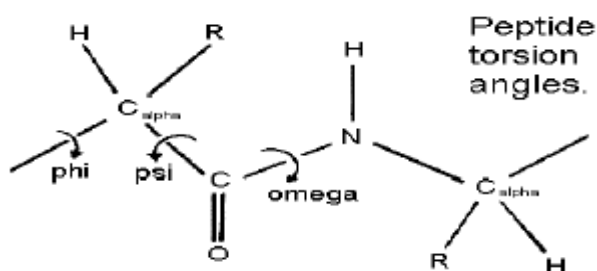
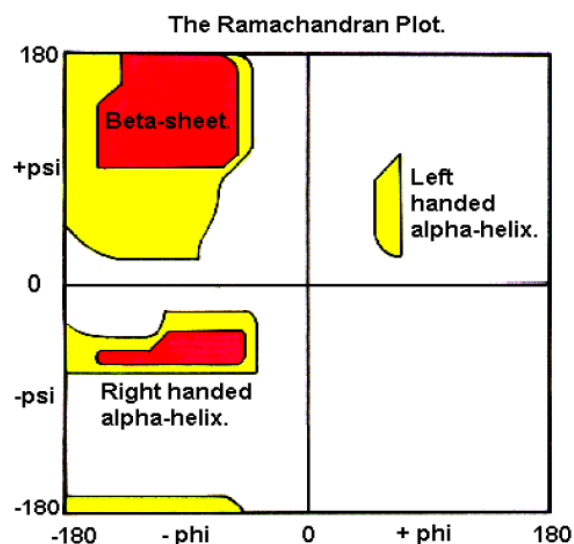


Fig. 5: Torsion angles of peptide

The  $\Phi$  and  $\Psi$  angles are plotted onto Ramachandran map from which the percentages of  $\Phi$ ,  $\Psi$  in the allowed and disallowed regions are calculated. In the Ramachandran plot, the structure is examined for close contacts between atoms. Angles which cause spheres to collide correspond to sterically disallowed conformations of the polypeptide backbone. In Fig. 6 the white areas correspond to conformations where atoms in the polypeptide come closer than the sum of their van der Waals radii. These regions are sterically disallowed for all amino acids except glycine which is unique in that it lacks a side chain. The red regions correspond to conformations where there are no steric clashes, i.e. these are the allowed regions namely the  $\alpha$ -helical and  $\beta$ -sheet conformations. The yellow areas show the allowed regions if slightly shorter van der Waals radii are used in the calculation, i.e. the atoms are allowed to come a little closer together, this brings out an additional region which corresponds to the left-handed  $\alpha$ -helix.





**Fig. 6:** Ramachandran plot showing disallowed region (white), allowed region (yellow) and most favourable region (red)

Disallowed regions generally involve steric hindrance between the side chain and main chain atoms. Glycine has no side chain and therefore can adopt  $\Phi$  and  $\Psi$  angles in all four quadrants of the Ramachandran plot. Hence it frequently occurs in turn regions of proteins where any other residue would be sterically hindered. Ideally, a good protein structure should have over **90%** of the residues in these "**core**" regions i.e. red color area in Fig. 6.

#### **b. ERRAT:**

ERRAT is a protein structure verification algorithm that is especially well-suited for evaluating the progress of crystallographic model building and refinement [Colovos *et al.*, 1993]. The program works by analyzing the

statistics of non-bonded interactions between different atom types. A single output plot is produced that gives the value of the error function *vs.* position of a 9-residue sliding window. By comparison with statistics from highly refined structures, the error values have been calibrated to give confidence limits. This is extremely useful in making decisions about reliability.

ERRAT protein submission server is available at <http://nihserver.mbi.ucla.edu/ERRATv2/>. The ERRAT program examines a PDB file, and generates a score based on the quality of the local structure surrounding each residue, as compared to the typical ranges of dihedral angles and side chain contacts observed in real proteins. The program generates a plot which gives a measure of the structure error at each residue in the protein. It also calculates an overall score for the structural quality.

### c. Profile 3D:

The model may contain some errors in the loop region and also in the wrong alignment of the sequence. These problems can be solved by checking the residue specific environments (e.g. All N-H and C=O functions are involved in hydrogen bonding and all polar residues buried) of all the residues. There are computational methods to evaluate numerical values representing the residue specific environment in a given structure. These

numerical values are called 3D profile scores. For a given model 3D profile scores are calculated from the template and used as control.

After the validation of the stereo chemical properties of the generated model it can be used for further studies. Homology modeling has become one of the most important steps in structure based drug design approaches for the proteins whose structure is not yet known (Fig. 7). Some of the studies in which homology modeling has been applied at different stages of drug discovery process are shown in Fig. 8.

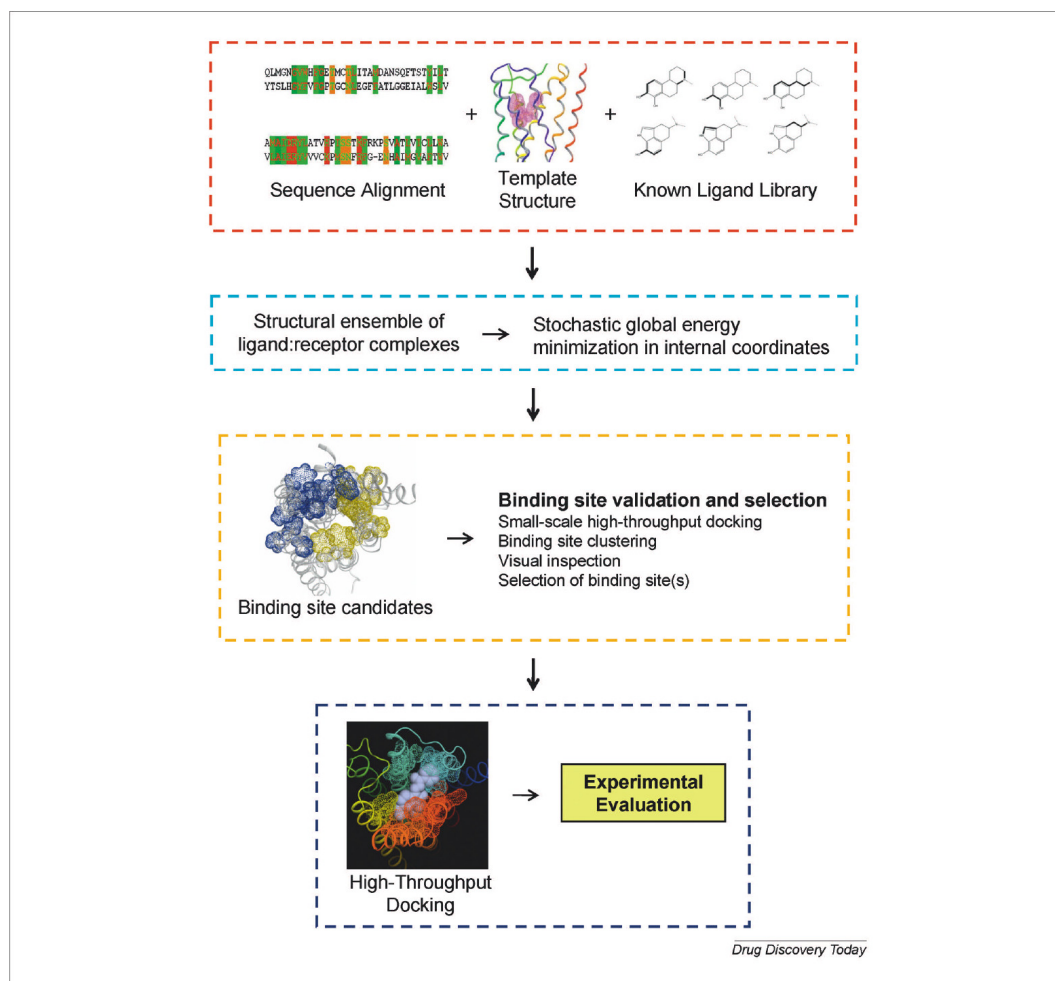


**Fig. 7:** *Homology modeling and Structure Based Drug Design* : Outline of the ligand-steered homology modeling method, in which information of known ligands is explicitly used to shape and optimize the binding site. Starting with the alignment between the template and target sequences, the structure of the target and a collection of known ligands of the target (red border), a structural ensemble of ligand:receptor complexes is generated and optimized through a stochastic global energy minimization in internal coordinates, eventually including experimental constraints (light blue border). Binding site candidates thus generated are validated through binding site clustering, small-scale highthroughput docking, analysis of known experimental interactions (if any), and visual inspection; one or more binding sites are selected (orange border), which could be later used in structure-based drug discovery projects (dark blue border).

(Taken from: Cavasotto *et al.*, Drug Discov Today 14 (2009) 676-83).

Receptor	Application
BC0371 (member of the enolase superfamily)	Study of protein function
M antigen	Study of protein function
RDH12	Assess the biological role of mutations in the binding site and their effect on the function of RDH12
Nod-like receptors	Understand the protein mechanism implicated in the immune response
Glut 1 transport receptor	Provide insights into the transport mechanism
NHE1	Understand the access mechanism of Na <sup>+</sup> /H <sup>+</sup> exchange
UreF	Study of protein mechanism
Prothrombinase (FXa-FVA)	Understand prothrombinase function and identify druggable pockets
ECE-2	Understand the loss of catalytic activity of ECE-2 via mutagenesis studies
Lunatic fringe (Lfng)	Explain the binding mode of O-linked fucose
MCH-R1	Structure-based lead discovery for antiobesity drugs
RSK-2	Docking-based screening for breast and prostate cancer lead discovery
Cannabinoid receptor 2, human adenosine A2A receptor, alpha-1-A-adrenoreceptor, adenosine 3 receptor	Binding mode prediction and elucidation of ligand:protein interactions
Peptide CGP38560 in complex with renin, Src kinase, PKC theta, GPR109A	Lead or compound optimization
Alpha-glucosidase	Structure-based virtual screening for antidiabetes lead discovery
Cdc25 phosphatases	Structure-based virtual screening for anticancer lead discovery
Protein tyrosine phosphatase SHP2	Structure-based virtual screening for anticancer lead discovery
CK1δ	Structure-based virtual screening to identify inhibitors for Alzheimer's disease
6-Phosphofructo-2-kinase (PFKFB3)	Structure-based virtual screening for inhibitors against glycolytic flux and tumor growth.

**Fig. 8:** Application of homology modeling techniques at different stages of drug discovery process within the past two years (Taken from : Cavasotto *et al.*, Drug Discovery Today 14 (2009) 676-83).

### 1.1.2. Homology modeling of 5-LOX

As the crystal structure of 5-LOX is yet to be elucidated, modeling studies will be helpful to obtain a consistent representation of the enzyme-inhibitor recognition events at the molecular level and furthermore, provide new insights that can be used to design novel therapeutic agents. The conserved structural pattern of all LOXs mainly at the catalytic site formed an advantage for building up an accurate homology model. The structure can provide hints about functional and evolutionary features of the protein and is also useful in drug design efforts.

To our best knowledge, the three dimensional (3D) experimental structure of 5-LOX is not known. To date, structural information for only four LOXs is available from the Protein Data Bank of Brookhaven (PDB, [www.rcsb.org/pdb](http://www.rcsb.org/pdb)): two isoforms from soybeans, 12S-LOX, LOX-1 and LOX-3 and one from rabbit reticulocytes, 15-LOX. In this study, the 3D model of 5-LOX is built by using homology modeling method based on the known structure of soybean LOX- 3 complexed with 4- nitrocatechol (PDB Id. 1NO3) [Jankun *et al.*, 2004]. The 3D model of 5-LOX is used to search the active site and carry out the binding studies by flexible docking and energy minimization

methods with known reported 5-LOX inhibitors, thereby further validating the generated model.

## 1.2. Materials and Methods

### 1.2.1. Construction of the 5-LOX model

#### 1.2.1.1. Identification of template

All simulations were performed on the SGI workstation by using InsightII software from Accelrys, USA [Accelrys Inc. InsightII; version 2000ed.: San Diego, CA]. The amino acid sequence of potato 5-LOX (Accession Id: AAD04258) is obtained from the databank in the National Center for Biotechnology Information, NCBI ([www.ncbi.nlm.nih.gov](http://www.ncbi.nlm.nih.gov)). The BLAST program against Protein Data Bank (PDB) [Berman *et al.*, 2000] available at NCBI was used to select a template structure for homology modeling of 5-LOX. The crystal structure of soybean LOX-3 (PDB code: 1NO3) was obtained from PDB database [Berman *et al.*, 2000] and it shares 63% sequence identity with 5-LOX. The first requirement in the construction of 5-LOX model is the sequence alignment among these templates. The sequence alignment is based on identifying structurally conserved regions (SCR) common to the template and target. The alignment from ClustalW program was used to build the initial model. To construct a protein model for the target sequence, we used the

InsightII/Homology program [Homology user guide, Accelrys, Inc., San Diego, USA; 1999] implemented on a Silicon Graphics workstation.

### **1.2.1.2. Identification of metal binding site composition in LOXs using ANAMBS and MEDB**

#### **1.2.1.2.1. ANALysis of Metal Binding Sites (ANAMBS):**

ANAMBS is a perl standalone tool developed in house for the identification of the microenvironment of a heteroatom environment in a protein. The tool can be used to analyze metal binding sites in protein structures determined by X-ray crystallography, NMR methods or other computational methods. Computer programs were written in order to extract relevant data from the PDB and extract the neighborhood of the metal atom.

The user is given an option to alter the cut off distance which ranges from 1 Å to 10 Å. In addition to the identification and visualization of the metal binding sites (MBS) the tool was further developed to calculate the hydrophobicity in the region. Hydrophobicity is calculated using the hydropathy index proposed by Kyte *et al.* (1982). Regions with a positive value are hydrophobic. In this scale each amino acid is given a hydrophobicity score between 4.6 and -4.6; 4.6 being the most hydrophobic, -4.6 the most hydrophilic (Fig. 9). As metals bind to centers of high hydrophilicity, the knowledge of



hydrophobicity within the metal binding site is of significance. Number of atoms within the cut-off region can be obtained. The order of amino acids in

R	K	N	D	Q	E	H	P	Y	W	S	T	G	A	M	C	F	L	V	I
-4.5	-3.9	-3.5	-3.5	-3.5	-3.5	-3.2	-1.6	-1.3	-0.9	-0.8	-0.7	-0.4	1.8	1.9	2.5	2.8	3.8	4.2	4.5

**Fig. 9:** *Hydropathy Index for the twenty natural amino acids (Kyte and Doolittle)*

the metal binding site, their distance and hydrophobicity within the metal binding site region is valuable information in addition to the generation of the 3D coordinates of the metal binding sites. The most probable coordinating atoms are also derived as output. The features of the tool are listed in Fig. 10. In most cases of pairs of homologous proteins, the coordinating amino acids and their orientation are conserved.

<b>1. FILE</b> a) Open PDB file b) Save Results c) Exit	<b>3. TOOLS</b> a) Get Residues b) 3D View MBS c) Generate Angle Matrix d) Generate Hydropathy Plot
<b>2. VIEW</b> a) View Heteroatom b) View FASTA c) View PDB Info	<b>4. HELP</b> a) About b) Manual

**Fig. 10:** *Features of the tool ANAMBS*

In ANAMBS there are three fields required to define a job. Firstly, a query PDB file is required in which the metal binding site environment is to be analyzed. Secondly, the metal group whose binding site is to be analyzed should be specified. Thirdly, the cut-off distance ranging from 1Å to 10Å should be defined. All the amino acids within a sphere of radius equal to the selected cut-off distance from the metal will be defined as metal binding site which is used for further analysis as shown in Fig. 11.

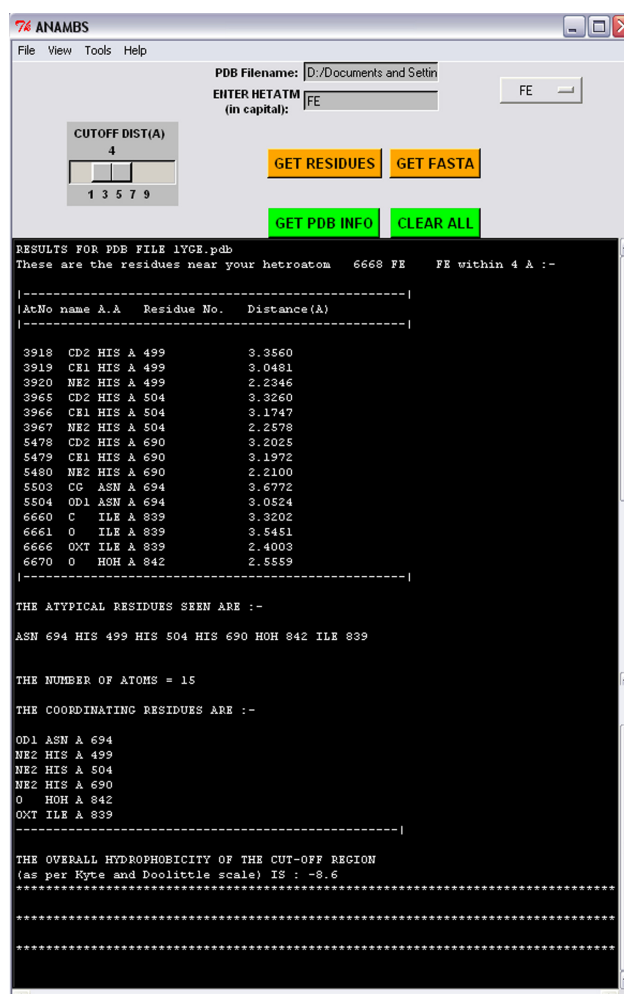
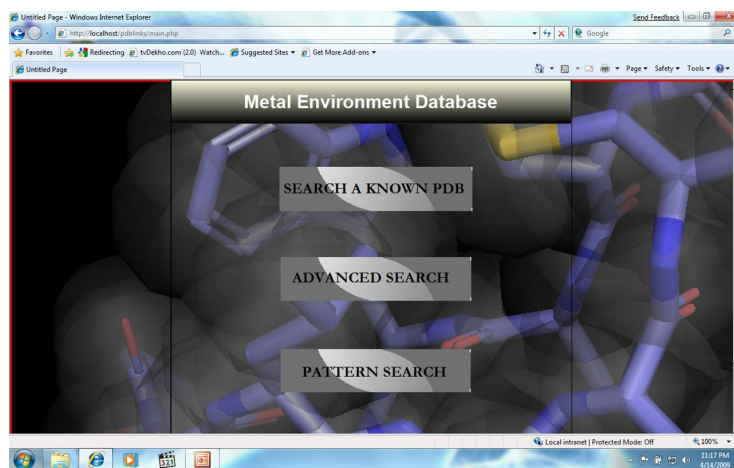


Fig. 11: Output obtained for Soybean LOX (PDB id. 1YGE) using ANAMBS for a cutoff distance of 4 Å

#### 1.2.1.2.2. Metal Environment DataBase (MEDB):

The database MEDB was built using the tool ANAMBS in a modified fashion. All the PDBs of the respective metalloproteins were obtained via RCSB advanced query interface and the tool was automated to access the input files and then stored in the web server. The homepage of the database directs to various search options as shown in Fig. 12. We have considered biologically significant metals like Ag, Au, Ca, Cd, Co, Cs, Cu, Fe, Hg, K, Mg, Mn, Na, Ni, Zn. The tool was used to scan all the obtained PDBs and then get the coordination environment and hydropathy data. ANAMBS uses a distance based algorithm to gather the metal coordination data and identifies the most probable atom candidates for coordination. The calculated data is then inserted into the database using automated in-house scripts. The working principle employed is shown in Fig. 13.



**Fig. 12:** The homepage of MEDB showing various search options

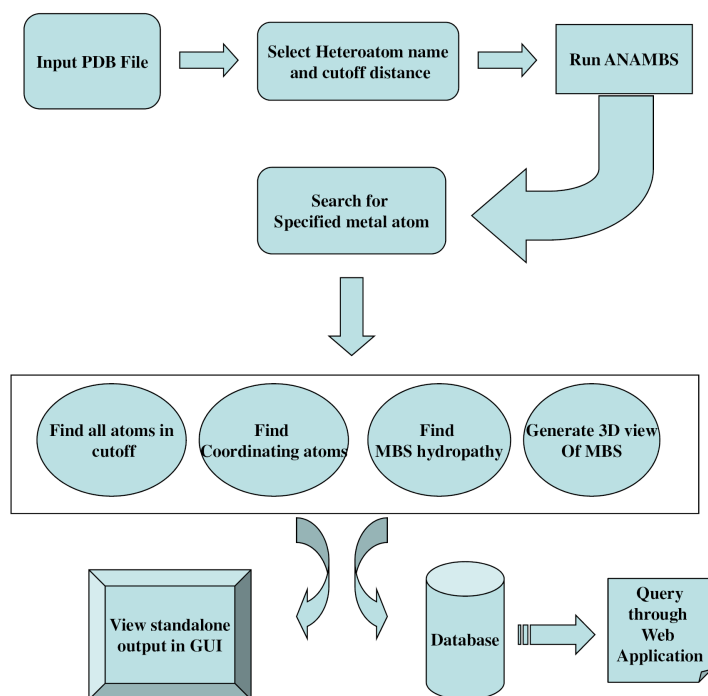


**Fig. 13:** Working principle of tool ANAMBS and database MEDB developed

The iron binding site composition in LOXs was analyzed and obtained using ANAMBS and MEDB.

### 1.2.1.3. Incorporation of Ferrous atom in 5-LOX metal binding site

Ferrous iron was added to the 5-LOX model using Builder module in InsightII so that the iron binding site is consistent with that of the site observed in crystal structures of other LOX isoforms. It was ligated to three histidines

(His525, His530 and His716), Asn720 and Ile864. The distances of iron from coordinating residues were measured and checked with ANAMBS tool.

#### 1.2.1.4. Refinement and validation of the 5-LOX model

Layers of water with thickness 5 Å were added to the whole protein using the SOAK program in the InsightII. A layer of water allows hydrophilic residues to interact with water instead of interacting with each other as they would do if modeled in vacuum. The protein model was energy minimized using CHARMM.cfc [CHARMM user guide, Accelrys, Inc., San Diego, USA; 1999] forcefield of CHARMM module in InsightII. Constraints were used so that the distance of Fe-N (His) is 2.1 to 2.3 Å and the distance between Fe-O (Ile) is 2.1 Å. The metal binding site was maintained fixed. The minimization was carried out using 300 steps of steepest descent followed by 500 steps of conjugate gradient to relieve all the bad contacts of the system. During the optimization procedure, the structure was verified by Profile-3D. The Profile-3D tests the validity of hypothetical protein structures by measuring the compatibility of the hypothetical structure with its own amino acid sequence [Profile-3D user guide, Accelrys, Inc., San Diego, USA; 1999]. To verify the protein model, the coordinates of the protein model were submitted to PROCHECK [Laskowski *et al.*, 1993] and ERRAT [Colovos *et al.*, 1993]. The

stereo chemical quality of the protein structures was examined by a Ramachandran plot using the PROCHECK program, the number of residues that are in the allowed or disallowed regions of Ramachandran plot determines the quality of the model. The ERRAT program was used to assess the false statistics of bad non-bonded interactions within the structure model.

### 1.2.2. Docking Studies

For our current docking studies four compounds were selected. One of them was a standard 5-LOX inhibitor namely, Nordihydroguaiaretic Acid (NDGA) having  $IC_{50}$  of 1.5  $\mu M$  [Reddanna *et al.*, 1985] and the other three (BP1, BP2 and BP3), analogs of benzyl propargyl ether, BP1: 1-(benzyloxy)hept-2-yn-4-ol having  $IC_{50}$  of 760  $\mu M$  [Barhate *et al.*, 2002], BP2: 1-[(4methylbenzyl)oxy]hept-2-yn-4-ol having an  $IC_{50}$  of 45  $\mu M$  and BP3: [(hept-2-yn-1-ylsulfanyl)methyl]benzene showing no inhibition of the 5-LOX activity [Barhate *et al.*, 2002].

The interactions of BP1-BP3 with 5-LOX active site residues were thoroughly studied to understand the 5-LOX structure better. Even though they were structurally not so diverse their activity varied greatly. Hence, more

emphasis was laid on interactions of NDGA and the three benzyl propargyl ethers in this study.

The ligands were built using the MOE from the Chemical Computing Group [MOE Program, Chemical Computing Group Inc., Montréal, Québec, Canada, 2003]. The structures of the ligands were energy minimized to a RMSD of 0.001kcal/mol using MMFF94X forcefield. Docking of the inhibitors into 5-LOX was carried out using GOLD [Jones *et al.*, 1997]. GOLD is based on the genetic algorithm. It performs docking of flexible ligands into proteins with partial flexibility in the neighborhood of the active site. The parameters used for GA were population size (100), selection pressure (1.1), number of operations (100,000), number of islands (5) and niche size (2). Operator parameters for crossover, mutation and migration were set to 95, 95 and 10 respectively. To quantitate the interactions in the protein-ligand complexes, the scoring function GOLD score was employed. Default cutoff values of 2.5 Å ( $d_{H-X}$ ) for hydrogen bonds and 4.0 Å for Van der Waals were employed. Based on the superimposition of the template, Soybean LOX-3 with 5-LOX 3D structure, active site was defined as a sphere of 10 Å centered on the inhibitor in the template. During docking, the default algorithm was selected. Input parameters of the GOLD were set to allow octahedral coordination geometry to iron. The number of poses for each inhibitor was set to 100, and early

termination was allowed if the top three bound conformations of a ligand were within 1.5 Å RMSD. After docking, the individual binding poses of each ligand were observed and their interactions with the protein were studied. The best and most energetically favorable conformation of each ligand was selected. Display and examination of the complexes was carried out using MOE program on windows and QUANTA [QUANTA, Accelrys Inc., San Diego, CA, USA] implemented on a SGI Octane2 workstation.

### 1.2.3. Energy Minimization Methods to validate binding site of 5-LOX model generated

The interactions of the four ligands with 5-LOX active site residues are thoroughly studied using the molecular mechanics calculations to understand the 5-LOX structure better and to get hints for better inhibitor design.

Molecular mechanics calculations are useful to calculate the binding energies, but these methods met with only limited success initially [Sansom *et al.*, 1992], due to the large approximations involved in the analysis (e.g., solvent model used, lack of entropic terms, *etc.*). A few successful studies evaluate interaction energies and ligand strain in analysis of various binding conformations of new analogs. The purine nucleoside phosphorylase (PNP) inhibitors [Montgomery *et al.*, 1993; Erion *et al.*, 1997] were designed



successfully using these methods. Minimization methods were also used successfully, for predicting relative binding affinities of protease inhibitors [Reddy *et al.*, 1998], COX-2 inhibitors [Reddy *et al.*, 2007] and fructose 1-6, bisphosphatase inhibitors [Reddy *et al.*, 2005] using energies obtained both in solvent as well as complex phases of each inhibitor.

In our study, the binding affinities of LOX inhibitors were estimated using energies obtained from minimization methods. The binding modes of the inhibitors were obtained by carefully aligning docked structures of the inhibitors in the homology model of the LOX enzyme in the active site. These inhibitors were evaluated by performing minimization calculations both in solvent and in complex using the AMBER [Singh *et al.*, 1986] force field. The following are the technical details used for estimating relative binding affinities using energy components obtained from minimizations of each inhibitor both in solvent as well as in complex phases.

Molecular mechanics calculations (energy minimizations) on all the structures were performed using the BORN module of the AMBER program. A four-stage protocol was set up for energy minimizations of the protein-inhibitor complex. Minimization at each stage was performed using 100 steps of steepest descent and 1500 steps of conjugate gradient algorithms for

minimization. In the first stage, only the water molecules were minimized, keeping the inhibitor and the protein (in the complex calculation) fixed. The purpose of this step is to relieve any bad contacts involving water molecules in the initially solvated system. In the second stage, only hydrogens in the system were allowed to relax. This step relaxes the hydrogen atoms prior to relaxing heavy atoms. It was performed because the hydrogen locations are not specified by the X-ray structure and because adjustments in hydrogen atom locations are necessary to improve hydrogen bond geometries. In this third stage, all atoms of the protein were fixed, while allowing all the atoms of the inhibitor and the solvent to move during optimization. This stage allows for the relaxation of the inhibitor with respect to the protein and establishes the preferred interactions (e.g., hydrogen bonds). In the fourth and final stage, all the atoms of residues within 25 Å from the center of the inhibitor (water molecules, protein atoms and the ligand) were allowed to relax.

A four-stage protocol was also established for energy minimization of the solvated inhibitor. These minimizations were carried out using periodic boundary conditions in all directions and each stage involved 100 steps of steepest descent and 1500 steps of conjugate gradient optimization. In the first stage of minimization, only the water molecules were minimized keeping the inhibitor (*i.e.*, the solute) fixed. In the second stage, only hydrogens in the

system were allowed to relax. In the third stage, all the atoms of the inhibitor were allowed to move while fixing the solvent during the optimization. In the fourth stage of the solvent calculation, all water molecules and all the atoms of the inhibitor were allowed to relax.

The minimized structures for all the inhibitors in the complexed and solvated states were used for calculating the following energy variables:

$$\Delta E_{\text{bind}}(\text{Intra}) = E_{\text{com}}(\text{Intra}) - E_{\text{sol}}(\text{Intra}) \quad (1)$$

$$\Delta E_{\text{bind}}(\text{Inter}) = E_{\text{com}}(\text{Inter}) - E_{\text{sol}}(\text{Inter}) \quad (2)$$

where,  $\Delta E_{\text{bind}}(\text{Intra})$  and  $\Delta E_{\text{bind}}(\text{Inter})$  are relative intra and intermolecular binding interaction energies of an inhibitor, respectively, and  $E_{\text{com}}(\text{Intra})$ ,  $E_{\text{com}}(\text{Inter})$ ,  $E_{\text{sol}}(\text{Intra})$  and  $E_{\text{sol}}(\text{Inter})$  are intra and intermolecular interaction energies of an inhibitor in the complexed and solvated states, respectively. The total binding energy,  $\Delta E_{\text{bind}}(\text{Total})$ , of inhibitor is given by,

$$\Delta E_{\text{bind}}(\text{Total}) = \Delta E_{\text{bind}}(\text{Intra}) + \Delta E_{\text{bind}}(\text{Inter}) \quad (3)$$

### 1.3. Results and Discussion

There are many examples where homology modeling techniques have supported the drug discovery process especially in the target identification and/or validation, lead identification as well as lead optimization with respect to potency and selectivity.

Although various 5-LOX inhibitors have been synthesized or discovered to date, the direct mechanism by which they interact with 5-LOX is poorly understood due to the deficiency of structural information about 5-LOX. The 3D structural model of 5-LOX was reported earlier by Du *et al.*, (2006) and Charlier *et al.*, (2006). Du *et al.*, (2006) developed 3D model of 5-LOX using rabbit 15-LOX as the template and performed molecular docking simulation analyses to predict binding free energies for the inhibitors. The correctness of the constructed 3D structural model of 5-LOX was supported by the correlation with the  $K_D$  values measured by SPR assay. There are limitations in obtaining sufficient quantity of the purified 5-LOX in stable form from mammalian sources, so potato tubers are frequently employed as the source for large amounts of 5-LOX [Whelan *et al.*, 1988] in screening specific inhibitors. Hence, in our study, we modeled 5-LOX, performed docking studies with already reported inhibitors (NDGA, BP1, BP2 and BP3) and further calculated relative

binding energies of docked inhibitors using energy minimization calculations. Thus the model generated has been evaluated for its accuracy.

The protein model presented here can be used for designing inhibitors for human 5-LOX because of the high similarity among LOXs in the catalytic domain containing conserved metal binding residues [Brash, 1999]. The conserved structural pattern of all LOXs mainly at the active site residues formed an advantage for building up a reasonable homology model. The structure can provide hints about functional and evolutionary features of the protein and is also useful in drug design efforts.

The extent of information derived from the homology model depends on the quality of the model. Since the accuracy of the homology model is related to the degree of sequence identity and similarity between the template and target, template search and sequence alignment is a crucial step in any homology modeling.

### 1.3.1. Generation of 3D structure of 5-LOX

#### 1.3.1.1. Template identification and alignment

The BLASTP searches of PDB identified the crystal structure of Soybean LOX (PDB id: 1NO3) as the template structure. A pair wise alignment of the sequences of the template and the target is presented in Fig. 14. The structurally conserved regions were determined by multiple sequence alignment, which is based on the Needleman and Wunsch Algorithm [Needleman *et al.*, 1970].

1NO3	-----MLGG-LLHRGH-----KIKGTVVLMRKNVLDVNSVTSVGGIIGQGLDLVGSTLDTL	50
5-LOX	MNIGQIMGGRELFGGHDDSKVKGTVMKKNALDFT-----DLAGSLTDIA	47
1NO3	TAFLGRSVSLQLISATKADANG--KGKLGKATFLEGIIITSLPTLGAG-QSAFKINFEWDD	107
5-LOX	FDVLGQKVSFQLISSVQGDPTNGLQGKHSNPAYLENSLFTLTPLTAGSETAFGVTFDWNE	107
1NO3	GSGIFGAFYIKNFMQTEFFLVSLTLEDIPNHGSIHFVCNSWIYNAKLFKSDRIFFANQTY	167
5-LOX	EEGVFGAFIIKNTHINEFFLKSLLTLEDVPHGKVHFDNCNSWVYPSFRYKSDRIFFANQPY	167
1NO3	LPSETPAPLVKYREEELHNLRCDGTGERKEWERIYDYDVYNDLGDPPKGENHARPVLGDN	227
5-LOX	LPSTPELLRKYRENEELLTRGDGTGKREAWDRIYDIYNDLGNPDQGENVRTTLGGS	227
1NO3	DTFPYPRRGRTGRKPTRKDPNSESER----SNDVYLPDEAFGHKSSDFLTGKSVSQ	282
5-LOX	AEYYPYPRRGRTGRPPTRTDPKSESRIPLLLSLDIYVPRDERFGLHKMSDFLTGKSVSQ	287
1NO3	NVLPLLQSAFDLNTPREFDSFDEVHGLYSGGIKLEPT---DIISKISPLPVLKEIFRTD	338
5-LOX	FILPELHALFDG--TPNEFDSFEDVLRLYEGGIKLEQGLPKALTAIPELMIKELLRTD	345
1NO3	GEQALKFPPPKVIQVSKSAWMTDEEFAREMLAGVNPILRCLKDFPPRKLDSQVYGDHT	398
5-LOX	GEGLIRFPPTPLVIKDSKTAWRTDEEFAREMLAGVNPILRCLKDFPPRKLDSQVYGDHT	405
1NO3	SQITKEHLEPNLEGLTVDEAIQNKRLFLLDHHDPIMPYLRINATSTKAYATRTILFLKN	458
5-LOX	STITAHEHIEDKDLGLTVDEAMNNKLFILNHHDLILIPYLRINTTTITKSYASRTLLFLQD	465
1NO3	DGTLRPLATELSLPHFQGDQSGAFSQVFLPADEGVESIIWLLAKAYVVVNDSCYHQLS-H	517
5-LOX	NGSLKPLATELSLPHPDGDFGVTSKYVTPSDQGVESIIWLLAKAYVAVNDAGVHQLSH	525
1NO3	WLNTHAVVEPFIIATNRHLSVVHPIYKLLHPHYRDTMNINGLRLSLVNDGGVIEQTFW	577
5-LOX	WLNTHAVIEPFVIATNRQLSVLHPIHKLLYPHFRDTMNNINASARQILINAGGVLESTVFQ	585
1NO3	GRYSVEMSAVVYKDWVFTDQALPADLIKRGMAIEDPSCPHGIRLVIEDYFYTVDGLEIWD	637
5-LOX	SKFALEMSAVVYKDWVFPDQALPADLVKRGVAVEDSSPHGVRLLIEDYFYAVDGLIWS	645
1NO3	AIKT-VHEYVFLYYKSDDTLREDPELQACWKELVEVGHGDKKNPWWPKMQTREELVEAC	696
5-LOX	AIKSWVTDYCSFYYSDEILKDNELQAWWKELREVGHGDKKNPWWPEMETPELIDSC	705
1NO3	AIITWTASALHAAVNFGQYPYGGILNRPTLSRRFMPEKGSAYEELRNPNQKAYLKTIT	756
5-LOX	TTIITWIASALHAAVNFGQYPYAGYLENRPVSRFMPEPGTFEYELKKNPDKAFKLTIT	765
1NO3	PKFQTLIDLSVIEILSRHASDEVYLGERNPNWTSOTRALEAFKRFGNKLAQIENKLSER	816
5-LOX	AQLQTLGVSLSVIEILSRHTTDEIYLGQRESPEWTKDKEPLAADFPGKKLTIDIEKQIIQR	825
1NO3	NNDEKLNRNRCGPVQMPYTLTLLPSSKEGLTFRGIPNSISI	855
5-LOX	NGDNILNRSRGPVNAPTYTLTLLPSSKEGLTFRGIPNSVSI	864

**Fig. 14:** Alignment of Soybean LOX-3 (1NO3) and 5-LOX sequences. Essential sites for iron binding are denoted by asterisk (\*)

### 1.3.1.2. Metal binding site composition in LOXs

Metal binding site composition in LOXs was obtained from MEDB as shown in Fig. 15. The structural pattern was found to be conserved at the iron binding site. Iron coordinates with 5 amino acids, 3 Histidines His<sub>n</sub>, His<sub>n+5</sub>, His<sub>>n+5</sub>; Asn/His and the terminal Ile. The 6<sup>th</sup> position is occupied by water molecules in crystal structure and is replaced by Substrate/Inhibitor. The hydropathy value is -8.3 or -8.6 in all LOXs; -8.6 when Asn occupies the 4<sup>th</sup> coordinate site of the iron and -8.3 when His is present. This is due to the difference in the Kyte and Doolittle hydropathy index values of Asn (-3.5) and His (-3.2).

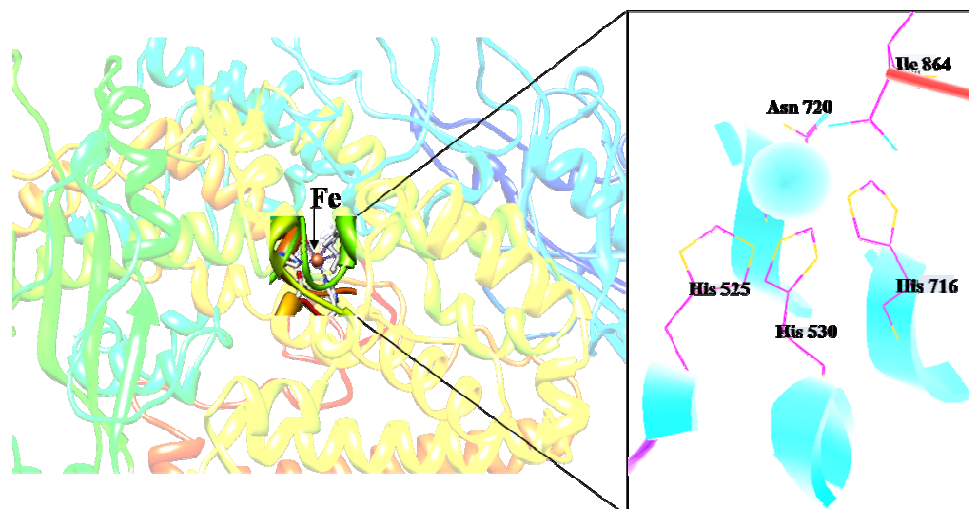
METAL ENVIRONMENT DATABASE				
<b>QUICK LINKS</b> <a href="#">Home page</a> <a href="#">Main page</a> <a href="#">Advanced search</a> <a href="#">Pattern search</a> <a href="#">Known PDB with 3D view</a>	<b>DATABASE OF PROBABLE METAL COORDINATING ATOMS</b> TABLE: <a href="#">links</a> <a href="#">Printer Friendly</a> <a href="#">Export to Excel</a> <a href="#">Export to Word</a> lipoxxygenase <input type="text"/> Search (*) <a href="#">Reset search criteria</a> <a href="#">Advanced Search</a> <a href="#">Hide highlight</a> <input checked="" type="radio"/> Exact phrase <input type="radio"/> All words <input type="radio"/> Any word			
	PDB (*)	CLASS (*)	NAME (*)	COORDINATING ATOMS (*)
	pd2b2nq.ent	OXIDOREDUCTASE	INSIGHTS FROM THE X-RAY CRYSTAL STRUCTURE OF CORAL 8R- <b>LIPPOXYGENASE</b> : CALCIUM ACTIVATION VIA A C2-LIKE DOMAIN AND A STRUCTURAL BASIS OF PRODUCT CHIRALITY	CA A2200-->   OD1 ASN A 416   OD1 ASP A 391   O ASP A 417   OE2 GLU A 419   O PHE A 418   O THR A 390
	1F8N.pdb	OXIDOREDUCTASE	<b>LIPPOXYGENASE</b> -1 (SOYBEAN) AT 100K, NEW REFINEMENT	FE2 840-->   OD1 ASN A 694   NE2AHIS A 499   NE2 HIS A 504   NE2 HIS A 690   O HOH 841   OXT ILE A 839
	1JNQ.pdb	OXIDOREDUCTASE	<b>LIPPOXYGENASE</b> -3 (SOYBEAN) COMPLEX WITH EPIGALLOCATHECHIN (EGC)	FE2 A 858-->   OD1 ASN A 713   O19 EGT 871   NE2 HIS A 518   NE2 HIS A 523   NE2 HIS A 709   OXT ILE A 857
HYDROPATHY (*) CA A2200-->-11.9 FE2 840-->-8.6 FE2 A 858-->-8.6 FE2 858-->-8.6 FE2 A 858-->-8.6 FE2 A 858-->-8.6 FE2 A 858-->-8.6 FE2 A 858-->-8.6 FE2 A 858-->-8.6 FE2 840-->-5.1 FE2 A2100-->-8.6 FE A1854-->-8.6 FE A 901-->-8.6 FE2 A 840-->-8.3 FE2 A1099-->-8.6 FE A 840-->-8.3 FE A 840-->-8.6 FE A 840-->-8.6 FE A 840-->-8.6 FE A 840-->-8.6 FE A 858-->-8.6 FE A 858-->-8.6				
<b>2F8Q.pdb</b> <b>21UJ.pdb</b> <b>21UK.pdb</b> <b>2POM.pdb</b> <b>3DVS.pdb</b> <b>1FGM.pdb</b> <b>1FGO.pdb</b> <b>1FGQ.pdb</b> <b>1FGR.pdb</b> <b>1FGT.pdb</b> <b>1HU9.pdb</b> <b>1IK3.pdb</b>	OXIDOREDUCTASE	INSIGHTS FROM THE X-RAY CRYSTAL STRUCTURE OF CORAL 8R- <b>LIPPOXYGENASE</b> : CALCIUM ACTIVATION VIA A C2-LIKE DOMAIN AND A STRUCTURAL BASIS OF PRODUCT CHIRALITY	FE2 A2100-->   ND2 ASN A 947   NE2 HIS A 757   NE2 HIS A 762   CE1 HIS A 943   O ILE A1066	FE2 A2100-->-8.6
	OXIDOREDUCTASE	CRYSTAL STRUCTURE OF SOYBEAN <b>LIPPOXYGENASE</b> -B	FE A1854-->   OD1 ASN A 708   NE2 HIS A 513   NE2 HIS A 518   NE2 HIS A 704   O ILE A 853	FE A1854-->-8.6
	OXIDOREDUCTASE	CRYSTAL STRUCTURE OF SOYBEAN <b>LIPPOXYGENASE</b> -D	FE A 901-->   OD1 ASN A 720   NE2 HIS A 525   NE2 HIS A 530   NE2 HIS A 716   OXT ILE A 864	FE A 901-->-8.6
	OXIDOREDUCTASE	REVISED STRUCTURE OF RABBIT RETICULOCYTE 15S- <b>LIPPOXYGENASE</b>	FE2 A 840-->   NE2 HIS A 361   NE2 HIS A 366   NE2 HIS A 541   ND1 HIS A 545   OXT ILE A 663	FE2 A 840-->-8.3
	LYASE, OXIDOREDUCTASE	ALLENE OXIDE SYNTHASE 8R- <b>LIPPOXYGENASE</b> FROM PLEXAURA HOMOMALLA	FE2 A1099-->   ND2 ASN A 947   NE2 HIS A 757   NE2 HIS A 762   NE2 HIS A 943   OXT ILE A1066	FE2 A1099-->-8.6
	OXIDOREDUCTASE	<b>LIPPOXYGENASE</b> -1 (SOYBEAN) AT 100K, N694H MUTANT	FE A 840-->   NE2 HIS A 499   NE2 HIS A 504   NE2 HIS A 690   ND1 HIS A 694   O HOH 1522   OXT ILE A 839	FE A 840-->-8.3
	OXIDOREDUCTASE	<b>LIPPOXYGENASE</b> -1 (SOYBEAN) AT 100K, Q495A MUTANT	FE A 840-->   OD1 ASN A 694   NE2 HIS A 499   NE2 HIS A 504   NE2 HIS A 690   O HOH 1665   OXT ILE A 839	FE A 840-->-8.6
	OXIDOREDUCTASE	<b>LIPPOXYGENASE</b> -1 (SOYBEAN) AT 100K, Q495E MUTANT	FE A 840-->   OD1 ASN A 694   NE2 HIS A 499   NE2 HIS A 504   NE2 HIS A 690   O HOH 1472   OXT ILE A 839	FE A 840-->-8.6
	OXIDOREDUCTASE	<b>LIPPOXYGENASE</b> -1 (SOYBEAN) AT 100K, Q697E MUTANT	FE A 840-->   OD1 ASN A 694   NE2AHIS A 499   NE2 HIS A 504   NE2 HIS A 690   O HOH 1429   OXT ILE A 839	FE A 840-->-8.6
	OXIDOREDUCTASE	<b>LIPPOXYGENASE</b> -1 (SOYBEAN) AT 100K, Q697N MUTANT	FE A 840-->   OD1 ASN A 694   NE2 HIS A 499   NE2 HIS A 504   NE2 HIS A 690   O HOH 1594   OXT ILE A 839	FE A 840-->-8.6
	OXIDOREDUCTASE	<b>LIPPOXYGENASE</b> -3 (SOYBEAN) COMPLEX WITH 4-HYDROPEROXY-2- METHOXY-PHENOL	FE A 858-->   O8 4HM A 861   OD1 ASN A 713   NE2 HIS A 518   NE2 HIS A 523   NE2 HIS A 709   OXT ILE A 857	FE A 858-->-8.6
	OXIDOREDUCTASE	<b>LIPPOXYGENASE</b> -3 (SOYBEAN) COMPLEX WITH 13(S)-HYDROPEROXY- 9(Z),11(E)-OCTADECADIENOIC ACID	FE A 858-->   O22B13R A1860   O22A13S A1859   O22C9OH A1861   OD1 ASN A 713   NE2 HIS A 518   NE2 HIS A 523   NE2 HIS A 709   OXT ILE A 857	FE A 858-->-8.6
Page 1 of 2 Records 1 to 20 of 32				
©2009 Prof. Reddanna Research Group Database maintained and updated by Prof. Reddanna Research Group				

Fig. 15: Iron binding site information obtained for LOXs in MEDB. It can be seen that the iron binding site is conserved across all LOXs available in the PDB.



### 1.3.1.3. Verification of iron binding site in 5-LOX model using ANAMBS

Comparison of numerous LOX crystal structures led to the identification of highly conserved residues [Prigge *et al.*, 1997] and important residues involved in iron chelation [Zhang *et al.*, 1993; Funk *et al.*, 2001]. The iron binding site of the model was verified using ANAMBS. The iron atom in 5-LOX model follows the structural pattern at the active site residues that is conserved in all LOXs. It is in distorted octahedral geometry. There are five amino acid ligands, the imidazole N atoms of three histidine residues His525, His530 and His716; carboxylate oxygen of the C-terminal isoleucine Ile864 and the carboxyl oxygen of the amide of an asparagine Asn720 (Fig. 16). The results of the model were compared with all the existing crystal structures of LOXs and summarized in Table-1.



**Fig. 16:** Iron binding site in the C-terminal catalytic domain of 5-LOX

**Table-1:** Comparison of results of the model and crystal structures of LOXs using ANAMBS. The amino acids within the cutoff distance of 3Å from iron are listed.

PDB ID	Amino acids with in the cut-off distance	Hydrophobicity with in the cut-off distance	Number of atoms within the region
1F8N	ASN 694 HIS 499 HIS 504 HIS 690 ILE 839	-8.6	17
1FGM	HIS 499 HIS 504 HIS 690 HIS 694 ILE 839	-8.3	16
1FGO	ASN 694 HIS 499 HIS 504 HIS 690 ILE 839	-8.6	14
1FGQ	ASN 694 HIS 499 HIS 504 HIS 690 ILE 839	-8.6	14
1FGR	ASN 694 HIS 499 HIS 504 HIS 690 ILE 839	-8.6	17
1FGT	ASN 694 HIS 499 HIS 504 HIS 690 ILE 839	-8.6	14
1YGE	ASN 694 HIS 499 HIS 504 HIS 690 ILE 839	-8.6	14
1Y4K	HIS 499 HIS 504 HIS 690 ILE 839	-5.1	12
3BNB	ASN 694 HIS 499 HIS 504 HIS 690 ILE 839	-8.6	17
3BNC	ASN 694 HIS 499 HIS 504 HIS 690 ILE 839	-8.6	14
3BND	ASN 694 HIS 499 HIS 504 HIS 690 ILE 839	-8.6	14
3BNE	ASN 694 HIS 499 HIS 504 HIS 690 ILE 839	-8.6	15
1HU9	ASN 713 HIS 518 HIS 523 HIS 709 ILE 857	-8.6	14
1IK3	ASN 713 HIS 518 HIS 523 HIS 709 ILE 857	-8.6	14
1JNQ	ASN 713 HIS 518 HIS 523 HIS 709 ILE 857	-8.6	13
1LNH	ASN 713 HIS 518 HIS 523 HIS 709 ILE 857	-8.6	14
1N8Q	ASN 713 HIS 518 HIS 523 HIS 709 ILE 857	-8.6	13
1NO3	ASN 713 HIS 518 HIS 523 HIS 709 ILE 857	-8.6	16
1RRH	ASN 713 HIS 518 HIS 523 HIS 709 ILE 857	-8.6	13
1RRL	ASN 713 HIS 518 HIS 523 HIS 709 ILE 857	-8.6	13
2FNQ	ASN 947 HIS 757 HIS 762 HIS 943 ILE1066	-8.6	16
3DY5	ASN 947 HIS 757 HIS 762 HIS 943 ILE1066	-8.6	17
1IUJ	ASN 708 HIS 513 HIS 518 HIS 704 ILE 853	-8.6	14
1IUK	ASN 720 HIS 525 HIS 530 HIS 716 ILE 864	-8.6	14
2P0M	HIS 361 HIS 366 HIS 541 HIS 545 ILE 663	-8.3	16
1LOX	HIS 361 HIS 366 HIS 541 HIS 545 ILE 663	-8.3	15
3D3L	ASN 544 HIS 360 HIS 365 HIS 540	-13.1	13
5-LOX model	HIS 525 HIS 530 HIS 716 ASN720 ILE864	-8.6	15

#### 1.3.1.4. Verification of the stereo chemical quality of the refined model

The model initially generated was energy minimized in CHARMM after addition of the Ferric ion. The final model obtained was verified with Profile-3D and Structure Alignment in InsightII. The overall self-compatibility score for this protein without the heteroatom is 342.899719 which is higher than the lower score 178.423093 and close to the top score 396.495761. The Profile-3D graph of the model is shown in Fig. 17.

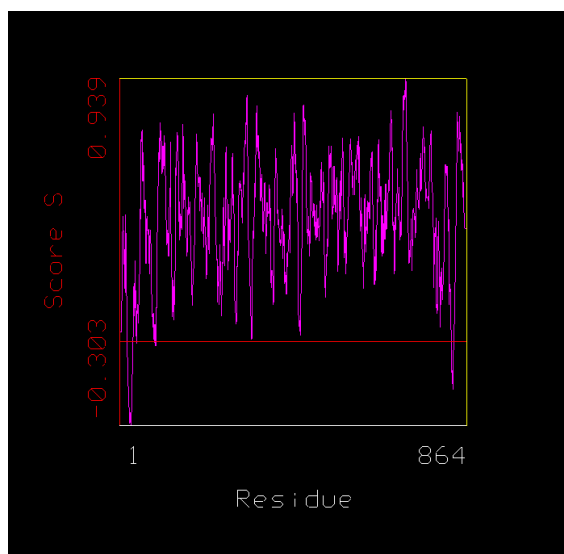


**Fig. 17:** *Profile-3D graph of the model.* It is observed that most of the aminoacids have very good score.

The RMSD of the equivalent C $\alpha$  atoms between the crystal structure 1NO3 and the model structure of 5-LOX is 0.621534, indicating that the overall structures are highly identical and that the homology model is reliable.

The C $\alpha$  trace of both the template and the model is shown in Fig. 18. The overall secondary and tertiary structures of both the proteins are quite similar (Fig. 19). The stereochemical quality of the 5-LOX model was checked using PROCHECK and ERRAT. (<http://nihserver.mbi.ucla.edu/ERRATv2/>).

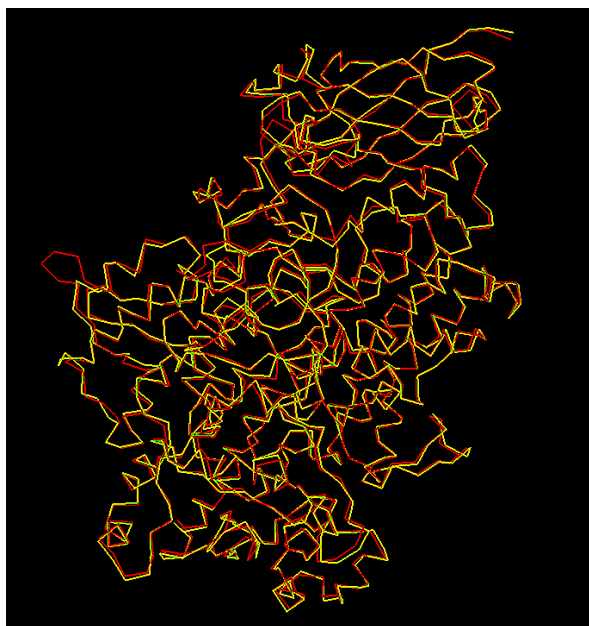


**Fig. 18:** *C $\alpha$  Trace of the template and the model.* Yellow colour shows the template and red shows the model

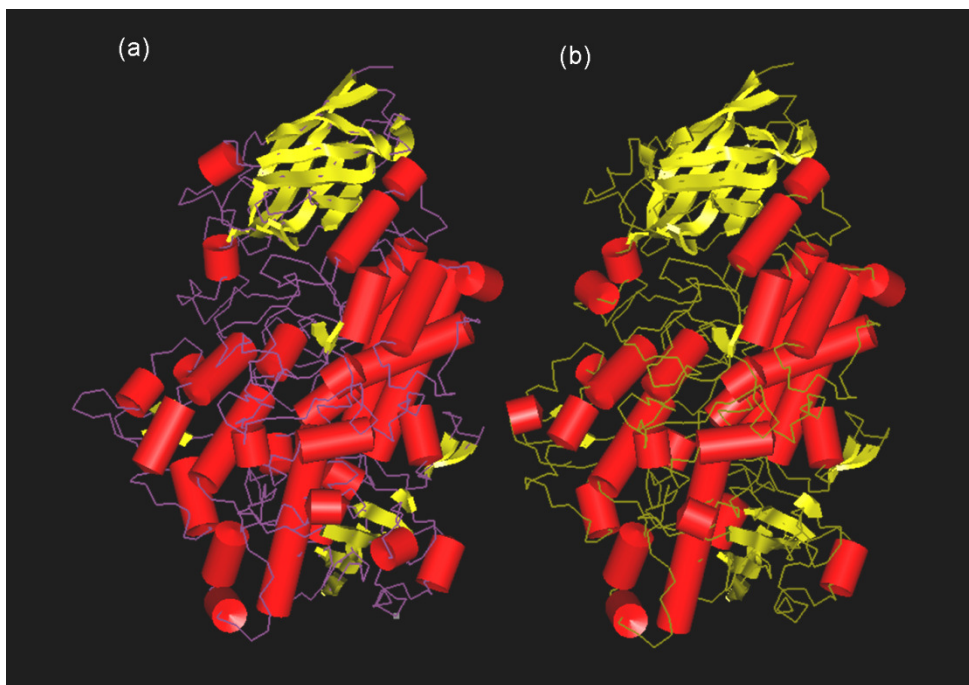
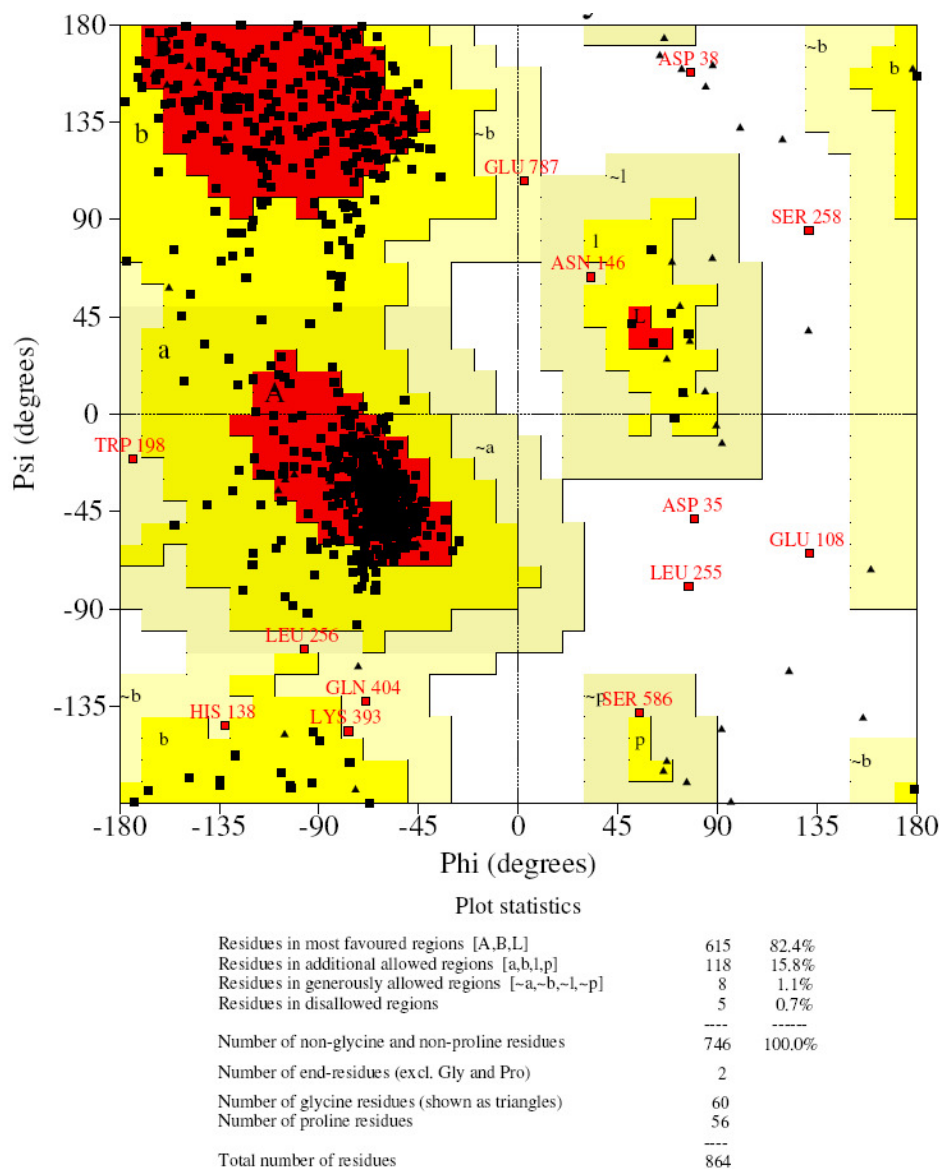


**Fig. 19:** Secondary structures of (a) model and (b) template

Ramachandran plot of this minimized model showed that 99.3% of the residues were located in the allowed regions (82.4% most favored) and only 0.7% (5 residues) outside the allowed regions (Fig. 21). As these disallowed residues are far from the 5-LOX active site they may not significantly contribute to its function. Other parameters (Main chain, Side chain) show that the quality of the model is good (Fig. 20-22). The ERRAT results showed that the overall quality factor of the protein was good with a score of 88.318 (Fig. 23).



Based on an analysis of 118 structures of resolution of at least 2.0 Angstroms and R-factor no greater than 20%, a good quality model would be expected to have over 90% in the most favoured regions.

**Fig. 20:** Ramachandran plot of the 5-LOX model. The amino acids in the red shaded region are in favourable region, amino acids in yellow shaded region are in additionally allowed region, amino acids in cream shaded region are in generously allowed region and those in white shaded region are in the disallowed region. The results show that only 5 residues of the 5-LOX model are in the disallowed region and 82.4% in the most favored region.

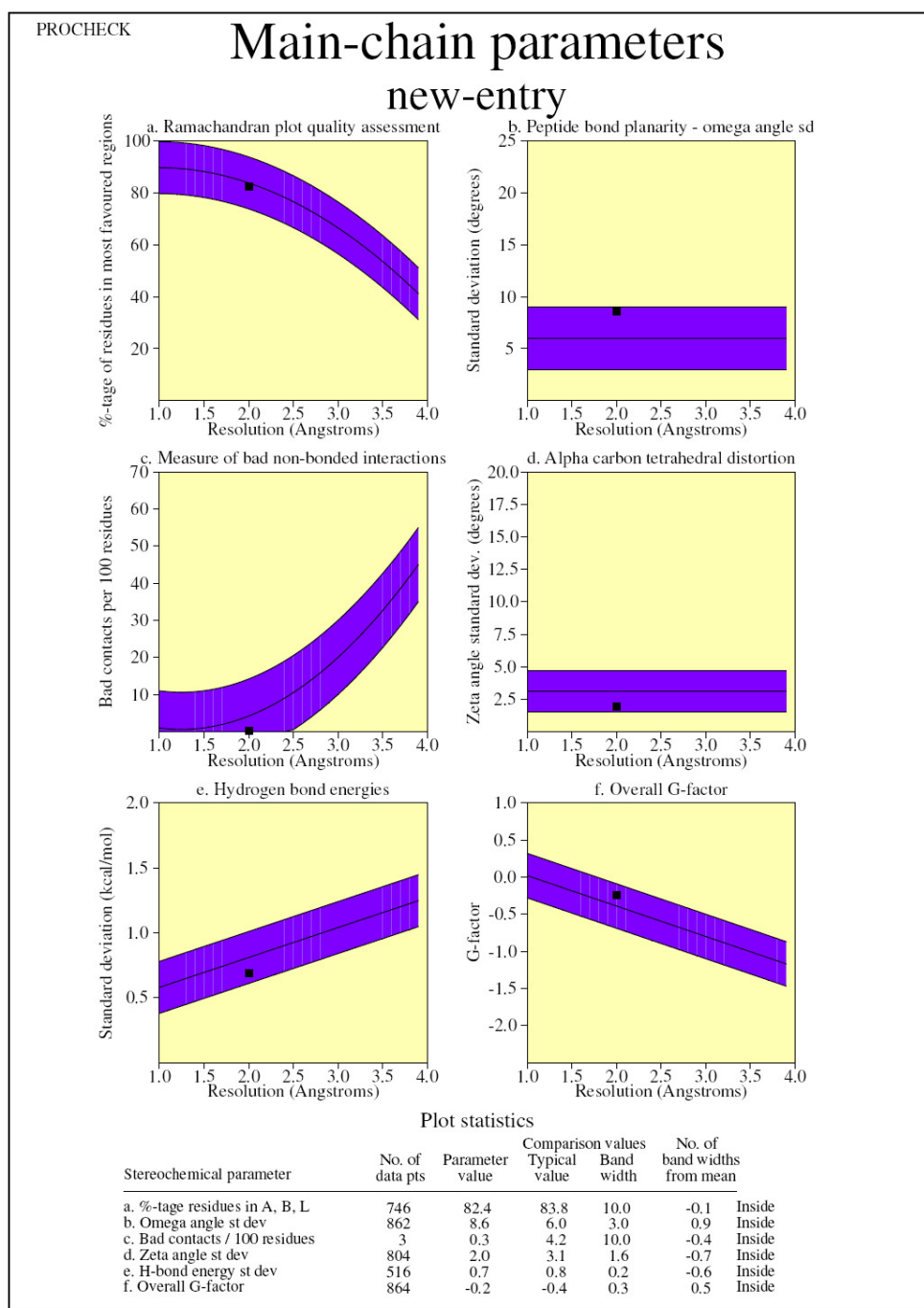


**Fig. 21:** Main chain parameters of 5-LOX model. The six graphs on the main chain parameters show how the structure (Solid Square) compares with well refined structures at a similar resolution. The dark band represents the results from well refined structures and the central line is the least squares fit. The width of the band on either side corresponds to the deviation about the mean. The results show that the 5-LOX model is within the results from well defined structures.

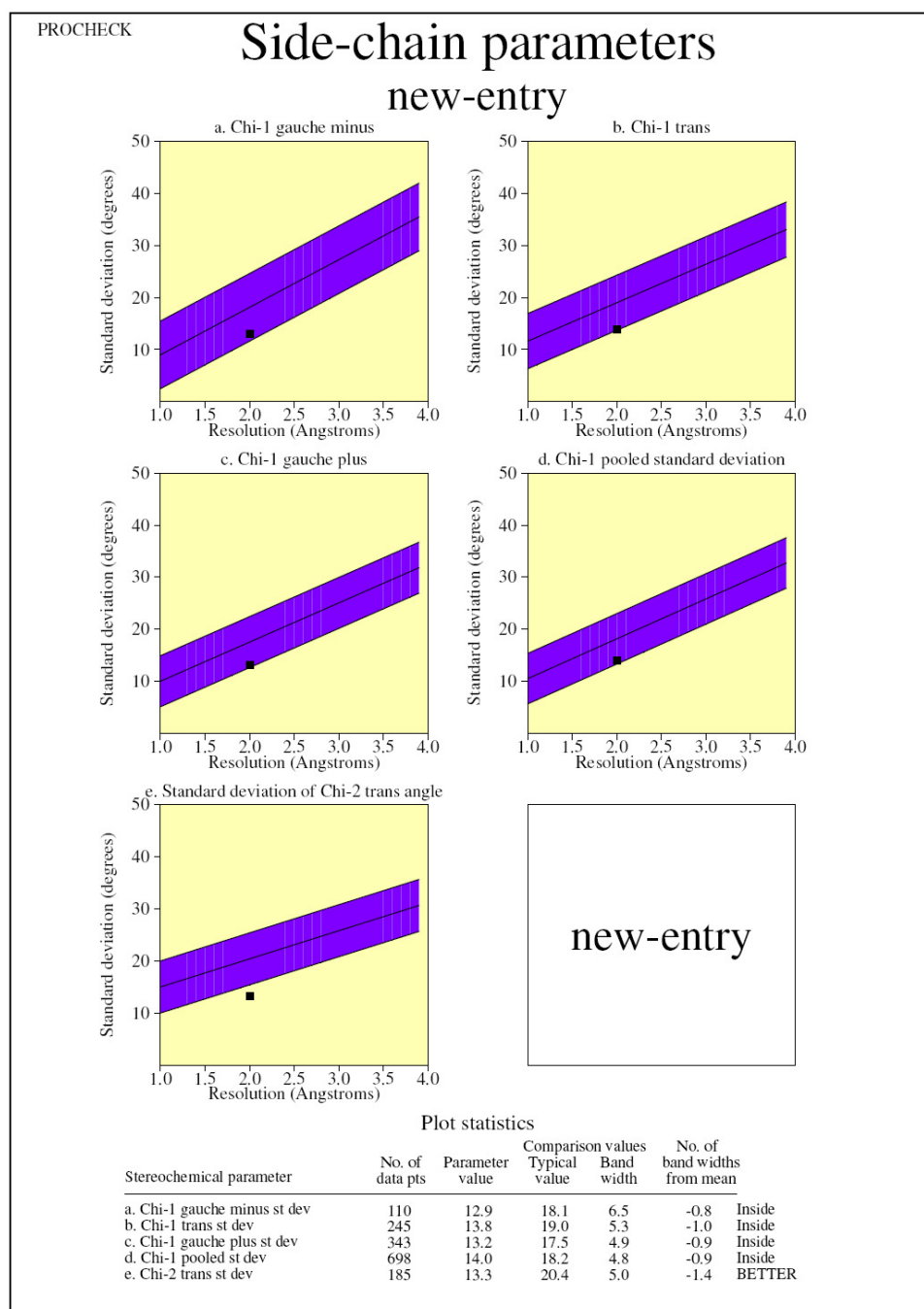
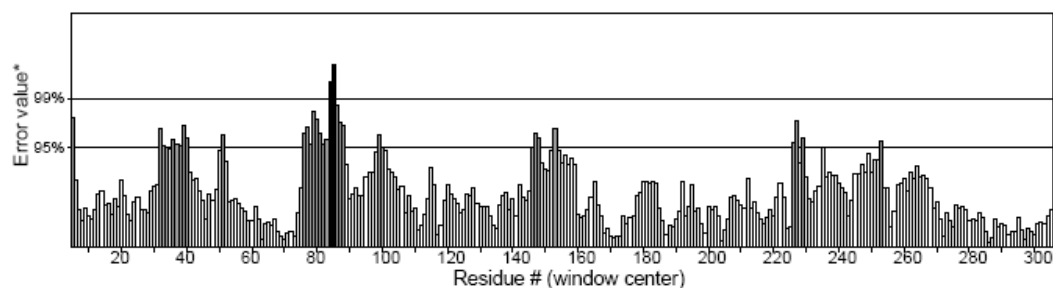


**Fig. 22:** Side chain parameters of 5-LOX model. The five graphs on the side chain parameters show how the structure (Solid Square) compares with well refined structures at a similar resolution. The dark band represents the results from well refined structures and the central line is the least squares fit. The width of the band on either side corresponds to the deviation about the mean. The results show that the 5-LOX model is within the results from well defined structures.

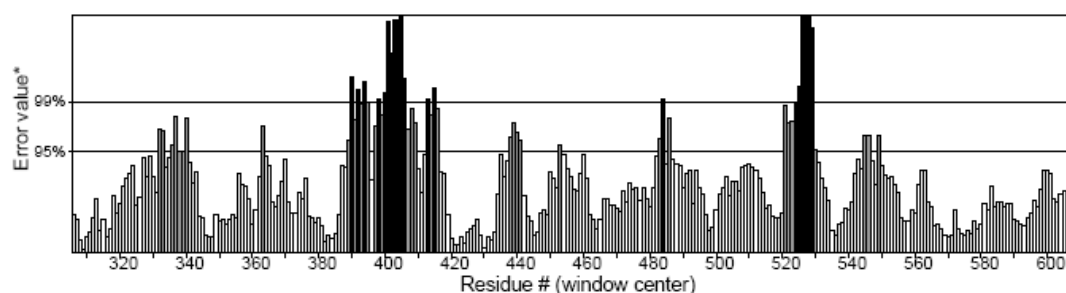


Overall quality factor\*\*: 88.318



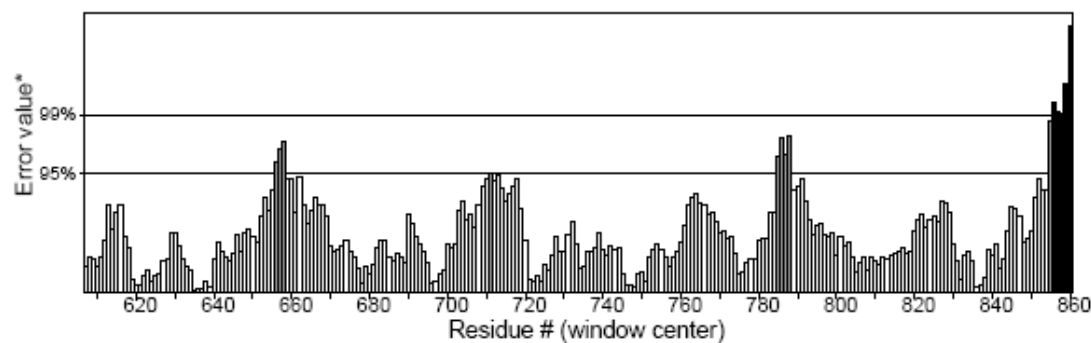
\*On the error axis, two lines are drawn to indicate the confidence with which it is possible to reject regions that exceed that error value.

\*\*Expressed as the percentage of the protein for which the calculated error value falls below the 95% rejection limit. Good high resolution structures generally produce values around 95% or higher. For lower resolutions (2.5 to 3Å) the average overall quality factor is around 91%.



\*On the error axis, two lines are drawn to indicate the confidence with which it is possible to reject regions that exceed that error value.

\*\*Expressed as the percentage of the protein for which the calculated error value falls below the 95% rejection limit. Good high resolution structures generally produce values around 95% or higher. For lower resolutions (2.5 to 3Å) the average overall quality factor is around 91%.



\*On the error axis, two lines are drawn to indicate the confidence with which it is possible to reject regions that exceed that error value.

\*\*Expressed as the percentage of the protein for which the calculated error value falls below the 95% rejection limit. Good high resolution structures generally produce values around 95% or higher. For lower resolutions (2.5 to 3Å) the average overall quality factor is around 91%.

**Fig. 23:** ERRAT plot of the 5-LOX model. The overall measure of quality is given at the top of the plot and each bar in the histogram is shaded according to the significance of the local structural error.

#### 1.3.1.5. Active site analysis

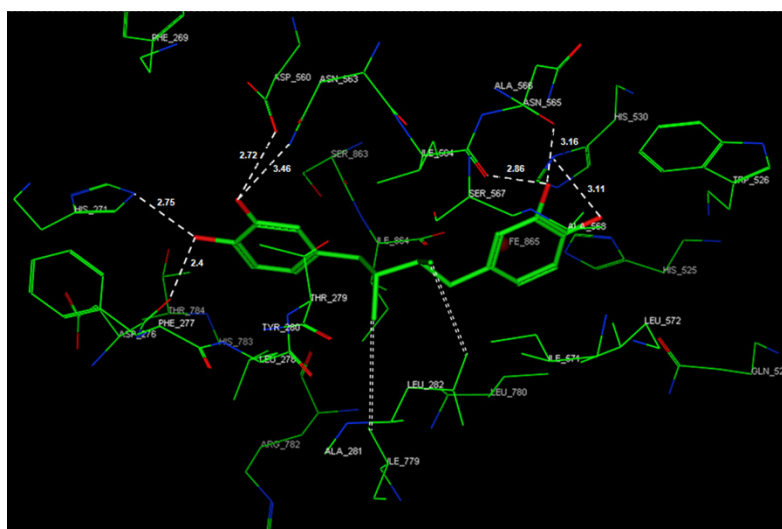
The sixth coordination position of iron faces an open cavity that usually accommodates the substrate/inhibitor. Fe-O distance with Ile864 is 2.10 Å. Fe-N distance with the Histidines 525, 530 and 716 is between 2.1-3 Å.

The overall folding pattern of LOXs is conserved across the available 3D structures and is also recognized in the 5-LOX model. It is composed of two folding units; a small N-terminal  $\beta$ -barrel domain, suggested to interact with lipids and a larger C-terminal catalytic domain, mainly composed of  $\alpha$ -helices, and containing the active site, i.e. iron-binding site and the substrate binding cleft. Based on the superimposition of soybean LOX-3 and 5-LOX 3D structures, active site was defined as a sphere of 10 Å centered on the inhibitor co-crystallized with soybean LOX-3. It was observed that the active site of 5-LOX was quite similar to that of the soybean LOX. Polar residues like Gln521, Glu787, His530, His525, His271, His783, Thr784, Arg782, Asp276, Arg559, Asp560, Asn563, Asn565, Asn720, Ser567, Ser863 and Thr279 were distributed along the 5-LOX active site channel. Acidic amino acids Asp276, Asp560 and basic amino acids His525, His530 were present in the active site channel and play vital role in ligand binding. The knowledge of the orientation of these

active site residues is extremely useful in designing a potential inhibitor of 5-LOX.

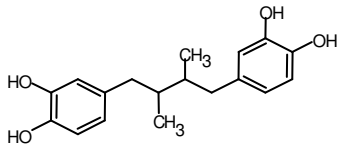
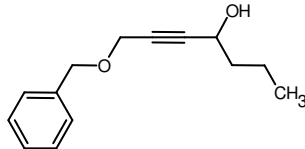
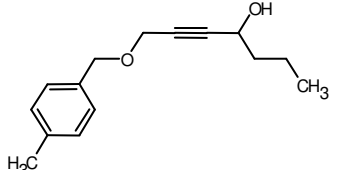
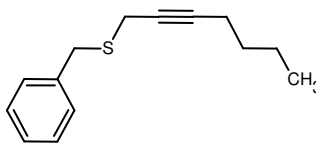
### 1.3.2. Docking studies

We used the GOLD methodology for the docking studies of NDGA, BP1, BP2 and BP3 into the 5-LOX structure. The interactions of NDGA with 5-LOX were studied using MOE and QUANTA. It was observed that NDGA was located in the center of the active site and was stabilized by hydrogen bonding interactions. In the molecule there were four hydroxyl moieties, each forming hydrogen-bonding interactions with the active site amino acids as shown in Fig. 24, Table-1.



**Fig. 24:** *Hydrogen bonding interactions of NDGA (Compound 1) with the protein*

**Table-2:** Experimentally measured  $IC_{50}$  values for the compounds and hydrogen bonding analysis of NDGA, BP1, BP2 and BP3. NI = No inhibition.

S.No	Compound	Experimental $IC_{50}$ ( $\mu$ M)	Aminoacids in 5-LOX with which hydrogen bonds are formed
NDGA		1.5	His271, Asp276, Asp560, Asn563, Ile564 and Asn565
BP1		760	His530 and Asn565
BP2		45	His530 and Asn565
BP3		NI	No hydrogen bonds

In the first hydroxyl group oxygen makes hydrogen bonding interactions with the side chain of His271 ( $O \cdots N_{\epsilon} = 2.75 \text{ \AA}$ ) and the hydrogen atom makes hydrogen-bonding interactions with the main chain of Asp276 ( $OH \cdots O = 2.4 \text{ \AA}$ ). In the second hydroxyl group, the hydrogen atom forms hydrogen bonding interactions with OD2 of Asp560 ( $OH \cdots OD2 = 2.72 \text{ \AA}$ ) and the oxygen atom forms two hydrogen bonds with amide group of Asn563 ( $O \cdots ND2 = 3.46 \text{ \AA}$ ). In the third hydroxyl group, hydrogen atom forms hydrogen bond with the

main chain atom of Ile564 ( $\text{OH} \cdots \text{O} = 2.86 \text{ \AA}$ ) and oxygen atom forms two hydrogen bonds with Asn565 ( $\text{O} \cdots \text{ND2} = 3.16 \text{ \AA}$ ). In the fourth hydroxyl group, hydrogen atom forms one hydrogen bond with His 530 ( $\text{OH} \cdots \text{ND1} = 3.11 \text{ \AA}$ ). And also, NDGA picks-up hydrophobic interactions with Leu282, and Ile779 protein residues.

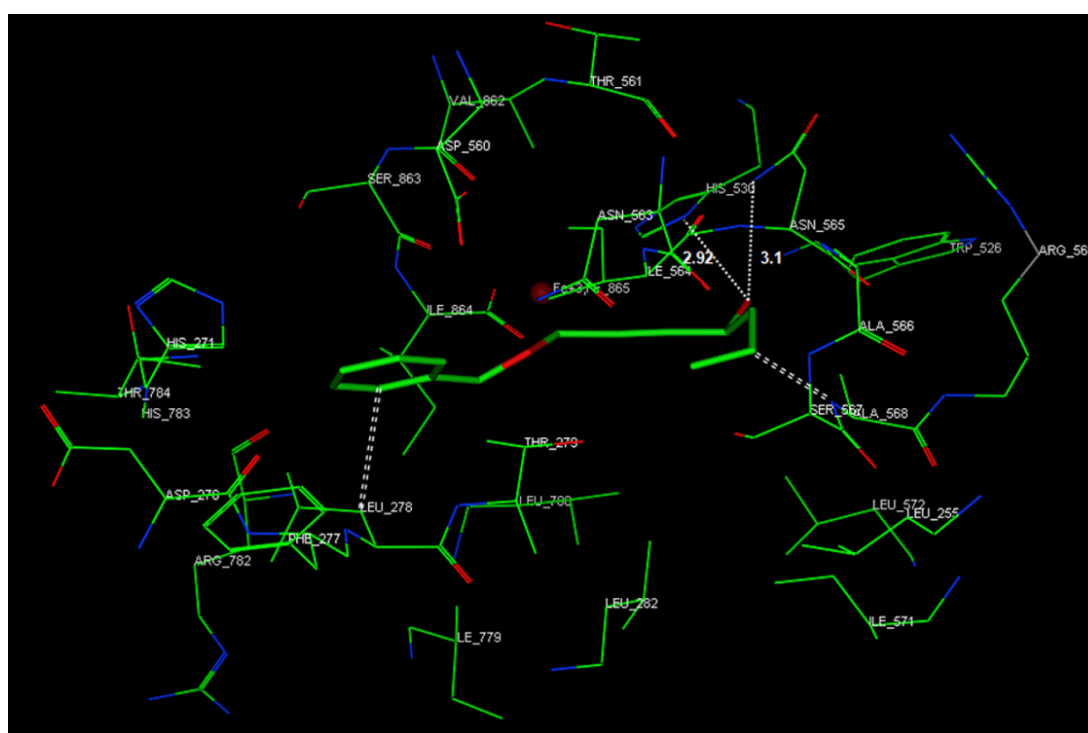


**Fig. 25:** *Hydrogen bonding interactions of BP1 with the protein.* Hydrogen bond interactions are shown in single dotted line. Hydrophobic interactions are shown in double dashed line.

In addition, NDGA was firmly bound in the open cavity that is in the sixth coordination of the iron atom and thus prevents the access of the substrate to the catalytic site of the enzyme efficiently. Hence, it has a very low  $IC_{50}$  and possesses high affinity. BP1 formed three hydrogen bonds with 5-LOX (Fig. 25). The hydroxyl group oxygen forms two hydrogen-bonding interactions with ND2 (*via*. HD1 and HD2) of Asn565 ( $O \cdots ND2 = 3.10 \text{ \AA}$ ). The hydrogen atom forms hydrogen bond with ND1 of His530 ( $O-H \cdots ND1 = 2.92 \text{ \AA}$ ). BP2 forms the same number of hydrogen bonding interactions as BP1. In addition, the methyl group of this compound gains strong hydrophobic interactions with Thr784 (Fig. 26). As a result the BP2 is more potent inhibitor than the BP1 to 5-LOX. BP3 did not form any hydrogen bond interactions with the protein except a few hydrophobic interactions (Fig. 27) with the protein residues. There were no strong interactions to stabilize BP3 in the 5-LOX active site; hence it showed no inhibition of 5-LOX. The residue Asn720 present in the 5-LOX active site may act as a ligand for iron and is a very important amino acid for the enzyme's activity. Based on the comparison of the number of hydrogen bonds formed between the NDGA and BP1 with the 5-LOX indicates that the NDGA is more potent inhibitor of 5-LOX than BP1.

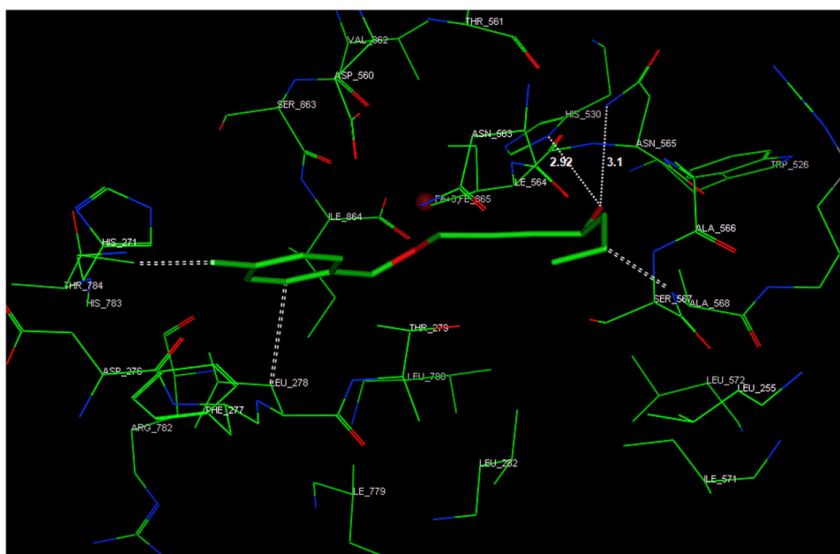


**Fig. 26:** *Hydrogen bonding interactions of BP2 with the protein.* Hydrogen bond interactions are shown in single dotted line. Hydrophobic interactions are shown in double dashed line.

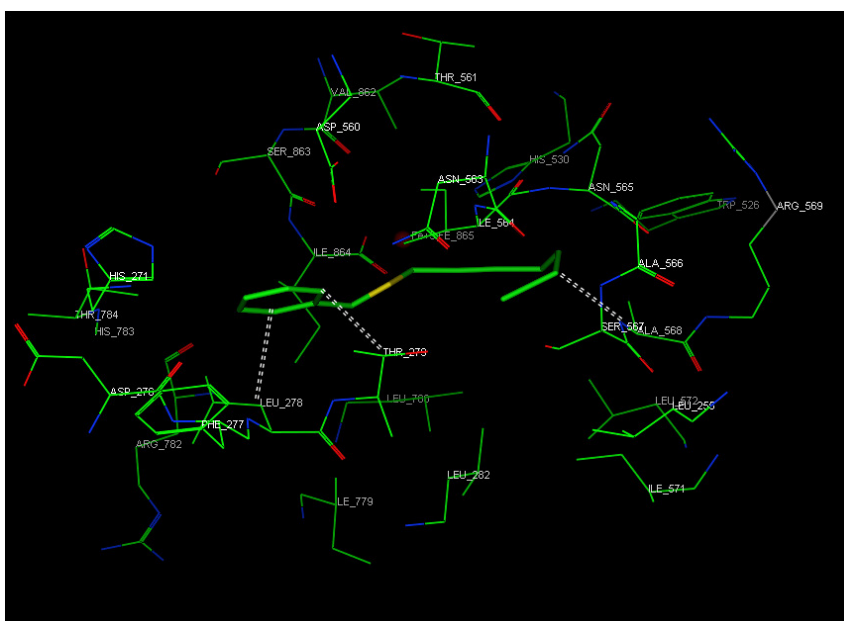


**Fig. 27:** *Hydrogen bonding interactions of BP3 with the protein.* Hydrogen bond interactions are shown in single dotted line. Hydrophobic interactions are shown in double dashed line.

These results correlate well with the experimental results. The protein model presented here can also be used as a guide for human 5-LOX inhibitors due to the high similarity in LOXs in the catalytic domain containing conserved metal binding residues [Montgomery *et al.*, 1993].

The accuracy of a homology model built depends strongly on the degree of homology with the template sequence. The homology modeling methodology we used here for constructing the 5-LOX model may be adequate because the model is based on a sequence homology of ~63% with the template. After energy minimization, the refined model structure is obtained. The final refined model is assessed by Profile-3D and Procheck, and the results showed that this model is reliable. However, to consider structural information about the target as well, a theoretical 3D model of 5-LOX was elaborated by homology with Soybean LOXs, based on consensus alignment of the sequences. The 5-LOX active site was then characterized from a structural point of view and used to study the docking of selected inhibitors. This shed new light on the binding features of the enzyme. The active site pocket in the protein model constructed is conserved among all the LOXs. Asn720 forms the fifth coordination with iron, hence is very important residue. The accuracy of the protein model is reflected in a docking and interactions study with benzyl propargyl ether inhibitors.



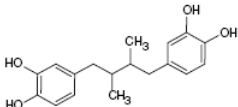
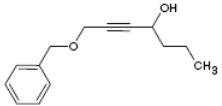
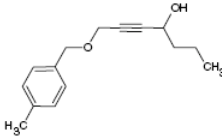
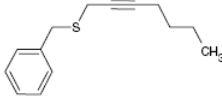
The docking results correlate well with the activity measured for the ligands, confirming the feasibility of the current modeling methodology used. The docking study shows that the amino acids in the ligand binding area are Gln521, Asn563, Asn565, Ser567, Thr279, His525, Trp526, His530, Asp276, Asp560, Ile564, Leu572, Leu780 and Ile864, which are consistent with the template. Finally, hydrogen bonds analysis identified the important hydrogen bonds between enzyme and inhibitor. The present study is a step towards the characterization of 5-LOX and its interaction with ligands. Fundamental understanding of the molecular details of inhibitors/5-LOX interactions remains very rudimentary in contrast with the extensive studies carried out on the localization and activation of the enzyme. This model can be considered as a working tool for generating hypotheses and designing further experimental studies and more precise predictions of function and drug binding.

### **1.3.3. Energy minimization studies**

The docking and minimization results correlated well with the activity measured for all the inhibitors which further validated the homology model (Table-3). This model was considered as a working tool for generating hypotheses and designing further experimental studies, and more precise predictions of function and binding affinities of inhibitors. The homology

model of 5-LOX generated was further used for the identification of novel potential 5-LOX inhibitors.

**Table-3:** Binding energies calculated using the Eq. 3 and the experimentally measured IC<sub>50</sub> values for the compounds considered in the validation study

S. No.	Ligand name	Ligand structure	$E_{bind}$ (Total) (kcal/mole)	Experimental IC <sub>50</sub> (μM)
1	Nordihydroguaiaretic acid (NDGA)		-25.5	1.5
2	1-(benzyloxy)-2-heptyn-4-ol		-11.6	760
3	1-[(4methylbenzyl)-oxy]-2-heptyn-4-ol		-21.4	45
4	[(Hept-2-yn-1-ylsulfanyl) methyl]benzene (or) 1-(benzylsulfanyl)-2-heptyne		10.5	NI

The minimization results correlated well with the activity measured for all the inhibitors which further validates the homology model. Docking studies have resulted in identification of crucial amino acids in the active site which can be targeted in Structure based drug design studies.

5-LOX, an important enzyme involved in the LTs synthesis pathway, has aroused considerable interest and been developed as a major target for the discovery of anti-inflammatory agents. Although various 5-LOX inhibitors

have been synthesized or discovered to date, the direct mechanism by which they interact with 5-LOX is poorly understood due to the deficiency of structural information about 5-LOX. The 3D structural model of 5-LOX was reported earlier by Du *et al.*, (2006) and Charlier *et al.*, (2006). Du *et al.*, (2006) developed 3D model of 5-LOX using rabbit 15-LOX as the template and performed molecular docking simulation analyses to predict binding free energies for the inhibitors. The correctness of the constructed 3D structural model of 5-LOX was supported by the correlation with the  $K_D$  values measured by SPR assay. There are limitations in obtaining sufficient quantity of the purified 5-LOX in stable form from mammalian sources, so potato tubers are frequently employed as the source for large amounts of 5-LOX [Whelan *et al.*, 1988] in screening specific inhibitors. Hence, in our study, we modeled 5-LOX, performed docking studies with already reported inhibitors (NDGA, BP1, BP2 and BP3) and further calculated relative binding energies of docked inhibitors using energy minimization calculations.

## Conclusions

A theoretical 3D model of 5-LOX was elaborated by homology with soybean LOXs based on consensus alignment of the sequences. The 5-LOX active site was characterized from a structural point of view and used to study the docking of selected inhibitors. This shed new light on the binding features of the enzyme. The active site pocket in the protein model constructed is conserved among all the LOXs. The residue Asn720 forms the fifth coordination with iron, hence is very important residue. The accuracy of the protein model is reflected in docking and minimization studies with benzyl propargyl ether inhibitors. The minimization results correlated well with the activity measured for all the inhibitors which further validates the homology model. Finally, hydrogen bond analysis identified the important hydrogen bonds between enzyme and inhibitors. Fundamental understanding of the molecular details of inhibitors/5-LOX interactions remains very rudimentary, in contrast with the extensive studies carried out on the localization and activation of the enzyme. The present study is a step towards the characterization of 5-LOX and its interaction with ligands. This model can be considered as a working tool for generating hypotheses and designing further experimental studies and more precise predictions of function and binding affinities of inhibitors. The studies presented here provide a pathway to design novel anti-asthma/ anti-cancer compounds.

## **Chapter -II**

**Development of 5-LOX inhibitors : Structure  
based lead optimization**

## 2.1. Introduction

### 2.1.1. Introduction to *de novo* design

The *de novo* design of protein ligands has recently gained increased attention [Miranker *et al.*, 1991; Ji *et al.*, 2003; Nugiel *et al.*, 2010; Tondi *et al.*, 2005]. Most effort so far has focused on the calculation of favorable binding sites and on the docking of given ligands into the binding pocket of a protein [Dessalew *et al.*, 2007]. Structure-based drug design (Fig. 28) encompasses both lead generation (through virtual screening, including molecular docking) and lead optimization/*de novo* design. While structure-based virtual screening is emerging as an increasingly powerful tool for lead discovery, structure based lead optimization has played a crucial role in drug discovery over the last 10 years. Given a high-resolution X-ray structure of a protein-ligand complex, computational methods are used to design potentially improved compounds that are predicted to make better or similar interactions with the target structure [Bohm, 1992; Bellows *et al.*, 2009]. A high-quality NMR structure or homology model may also be used. For use of a homology model, a high-resolution structure of a closely related protein may be required. Additional biological data (competition assay data, NMR binding data, etc.) to help confirm the binding mode in the actual target would also be desirable. With that level of structural information, an iterative process of designing, synthesizing and experimentally testing new compounds can develop.

Interactions between a protein and its ligand are usually formed through favorable non-bonded contacts such as hydrogen bonds or hydrophobic interactions. These contacts may be divided into individual interactions between

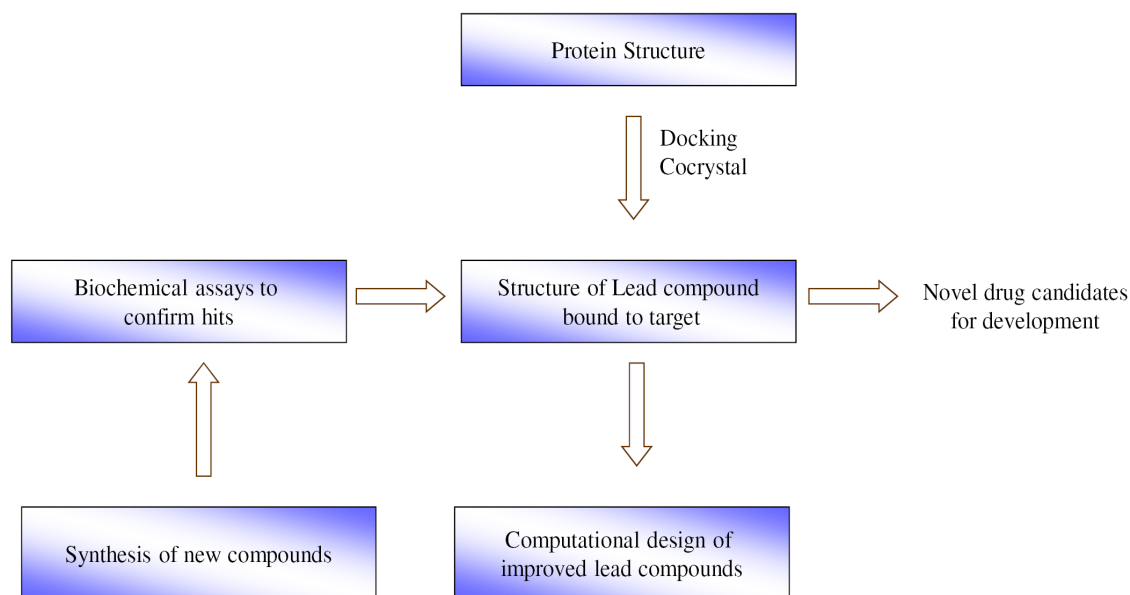


**Fig. 28:** *Structure-based lead generation and optimization*

single atoms or functional groups of the protein and the ligand. Thus, for every atom or functional group of the protein that is involved in binding with the ligand, there exists a counterpart on the ligand. This counterpart is again an atom or a functional group. For example, the counterpart for a carbonyl group C=O of the protein may be an amino group N-H of the ligand. A suitable position for such a functional group or atom of the ligand is referred to as its 'interaction

site'. A statistical analysis of hydrogen-bond geometries in crystal packings of small molecules [Bohm, 1992] reveals that there is a rather broad distribution of hydrogen-bond patterns. Therefore, for every functional group of the protein there exists not only a single position but also a region in space suitable for favorable interactions with the protein. This space can be used to optimize existing lead.

Even though there is fully automated *de novo* design software, it remains a crucial human task to pick the most promising candidates. In this study, we have used active site analysis method to identify various important amino acids in the active site and site point connection method for lead optimization.

*"It is essential that we learn to accept that de novo design will rarely yield novel lead structures with nanomolar activity in the first instance. Rather, the designed structures will probably represent examples of a prospective new lead series with micromolar activities that require further optimization"* [Schneider *et al.*, 2005, Nature Reviews, Drug Discovery].



## 2.2. Methodology

### 2.2.1. Site Point Connection method

Site-point connection method is one of the most widely used Ligand design method. A site point can be defined as a space in the active site at which a suitable ligand atom can make favorable interactions with one or more enzyme atoms. Site points with appropriate ligand atoms nearby are said to be satisfied. Site-point connection methods attempt to place small fragments in the active site so that one or more site points are satisfied and fragments are thereby placed in favorable regions [Biocampus 2003].

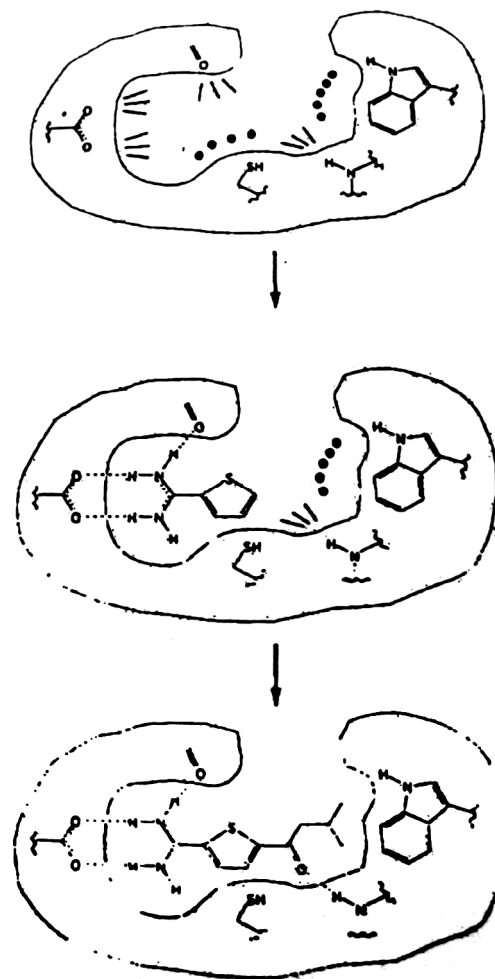


**Fig. 29:** Scheme of site-point methods  
(Source: Biocampus manual, 2003)

Fig. 29 shows the principle of site-point connection method. First, the site points for an active site are generated. Hydrogen bond acceptor and donor sites are marked with lines and hydrophobic sites are marked with dots. Then a small prototype molecule (here, 2-amidinothiophene) is positioned in the active site so

that it overlaps with several of the site points. Finally, additional building blocks are attached to the amidinothiophene to make contact with additional site points.

### 2.2.2. Binding site analysis

The 3D molecular model of 5-LOX was constructed in the previous studies. The molecular modeling was achieved with commercially available InsightII and Discover Studio software packages. All of the computational work was performed on Silicon Graphics workstations. The size and spatial orientation of the active site were identified by the grid analysis implemented in the Binding Site Analysis module within InsightII. The grid size for searching the proteins was set to 1 Å X 1 Å X 1 Å. All of the solvent accessible surfaces in the proteins were filled with grid points and only those having at least 125 grid points were accepted as possible ligand binding sites.

The *de novo* design program LUDI [LUDI user guide, Accelrys] was employed to further explore the important regions in the active site for ligand binding. The grid points produced by the InsightII/Binding Site Analysis module were divided into four subsites. The residues inside a 6 Å radius sphere, which centered on the centroid of each subsite, were used to generate the

interaction site. Three different types of interaction sites were defined in the program: lipophilic, hydrogen bond donor, and hydrogen bond acceptor. The standard default parameter and a fragment library supplied with the program were used during the LUDI search.

### 2.2.3. Lead Optimization

The 5-LOX-benzyl propargyl ether complex discussed earlier was taken. With the knowledge of interaction sites in the 5-LOX obtained from active site analysis method, the site points that were in the vicinity of the docked inhibitor and were unoccupied by any of the ligand atoms were closely visualized. In this study, only the site points corresponding to hydrogen bond donors and acceptors were considered. Four site points with potential of forming hydrogen bond interactions were identified. They were corresponding to Ser567, Gln521, His525 and Asp720 as shown in the Fig. 30.

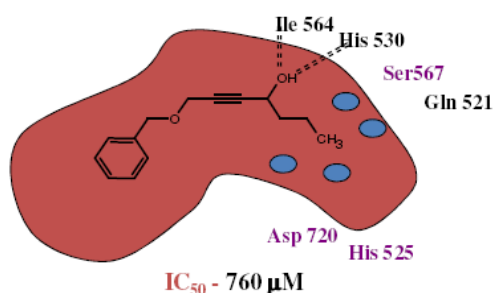


**Fig. 30:** The potential hydrogen bond interaction sites identified in the vicinity of the docked ligand. Interactions sites corresponding to Ser567, Gln521, His525 and Asp720 were targeted.

The lead molecules were constructed by manually linking new functional groups to the existing ligand. The new bond was constructed so that there was no introduction of significant internal strain in the candidate ligand. The synthetic accessibility of the generated structures was taken into account during the site point connection step. The newly formed ligand molecules were subsequently energy-minimized in the rigid protein to regularize the internal coordinates using the CVFF force field in the Discover 95.0 program within InsightII. The flexible ligand docking procedure in the Affinity module within InsightII was then used to define the lowest energy position for the generated molecules by using a Monte Carlo docking protocol. All of the atoms within a defined radius (6 Å) of the lead molecules were allowed to move. The solvation grid supplied with the Affinity program was used. If the resulting ligand/receptor system was within a predefined energy tolerance of the previous structure, the system was subjected to minimization. The resulting structure was accepted on the basis of an energy check, which used the Metropolis criterion and also a check of the RMSD of the new structure versus the structure found so far. The final conformations were obtained by following four stage protocol for energy minimization. Relative binding energies were calculated as described in Chapter-I. The interaction energies were calculated for each molecule. Each energy-minimized final docking position of the lead

molecules was evaluated using the interaction score function in the LUDI module.

The *Ludi* scoring method of interactions between a protein and its ligand was used to quantify the binding characteristics of the compounds to 5-LOX. In general a higher Ludi score represents a higher affinity and stronger binding of a ligand to the receptor.

*Ludi* can also score protein ligand interactions by statistically evaluating the fit of all potential ligands determined by the *Docking* module.

*Ludi* Score = -73.33 mol/kcal  $\Delta G$ , where:

$$\Delta G = \Delta G_o + \Delta G_{hb}f(\Delta R)f(\Delta a) + \Delta G_{ion}f(\Delta R)f(\Delta a) + \Delta G_{lipo}A_{lipo} + \Delta G_{rot}NR \Delta G;$$

$\Delta G_o$  represents the contribution to the binding energy that does not directly depend on any specific interactions with the receptor,  $\Delta G_{hb}$  and  $\Delta G_{ion}$  represent the contribution from an ideal hydrogen bond and unperturbed ionic interactions respectively,  $\Delta G_{lipo}$  represents the contribution from lipophilic interactions which is proportional to the lipophilic surface  $A_{lipo}$ ,  $\Delta G_{rot}NR$  represents the contribution due to freezing of internal degrees of freedom in the fragment, NR is the number of acyclic bonds,  $\Delta R$  is the deviation of the hydrogen bond length from the ideal value of 1.9 Å and  $\Delta a$  is the deviation of the hydrogen bond angle from the ideal value of 180 °.

In general, a higher *Ludi* score (0-1100 in range) represents higher affinity and stronger binding of a ligand to the receptor.

#### 2.2.4. *In vitro* 5-LOX inhibitory assay

5-LOX was purified and assayed as per the method described by Reddanna *et al.*, (1990). Enzyme activity was measured using polarographic method with a Clark's oxygen electrode on Strathkelvin Instruments, model 782, RC-300. Typical reaction mixture contained 50–100  $\mu\text{l}$  of enzyme and 10  $\mu\text{l}$  of substrate (133  $\mu\text{M}$  of arachidonic acid) in a final volume of 3 ml with 100 mM phosphate buffer pH 6.3. Rate of decrease in oxygen concentration was taken as a measure of enzyme activity. Stock solutions of test compounds, prepared immediately before use, were dissolved in DMSO. Various concentrations of test drug solutions were added and the LOX reaction was initiated by the addition of substrate. The reaction was allowed to proceed at 25  $^{\circ}\text{C}$  and the maximum slope generated was taken for calculating activity. Percent inhibition was

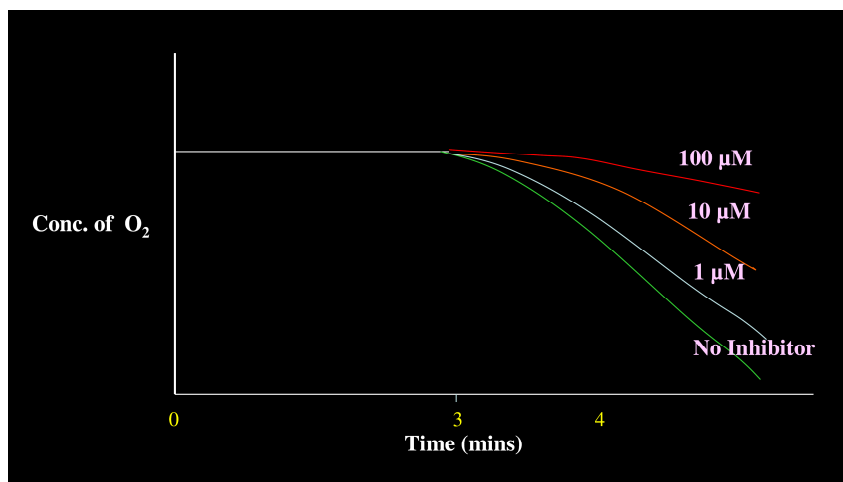


**Fig. 31:** O<sub>2</sub> conc. vs Time graph for various conc. of inhibitor

calculated by comparison of LOX activity in the presence and absence of inhibitor (Fig. 31). The concentration of the test compound causing 50% inhibition ( $IC_{50}$ ,  $\mu M$ ) was calculated from the concentration-inhibition response curve. Each assay was repeated thrice.

## 2.3. Results and discussion

### 2.3.1. Design of molecules

Prior to the design of a 5-LOX inhibitor, the active site of 5-LOX was investigated. Because the three-dimensional molecular model of 5-LOX from potato was a theoretical structure constructed from the crystallographic coordinates of Soybean LOX-3 [Jankun *et al.*, 2004], the active site of the crystal structure of the 1NO3 was also investigated for insights. We hoped that this crystal structure can afford some other useful information for inhibitor design. All of the possible ligand binding cavities on the 5-LOX were searched by the Binding Site Analysis program in InsightII. The largest cavity of 5-LOX obtained in Binding Site Analysis correlated with the inhibitor/substrate binding cavity of LOX-3 [Jankun *et al.*, 2004]. The other cavities were located far away from the active site. The shape and orientation of the active site of 5-LOX was similar to the shape and orientation of that of Soybean LOX-3. The key regions in the

active site that were essential for inhibitor binding were explored. 5-LOX-benzyl propargyl ether complex described in previous chapter was used. The interaction sites that were in the vicinity of the inhibitor and unoccupied were identified. New leads were designed so that hydrogen bond acceptor and donor sites in the vicinity are exploited as shown in Fig. 32. The propargyl group in Comp-1 was replaced with Benzyl group in S1. Methoxy group was added at 3', 4' and 5' position on the benzene ring.

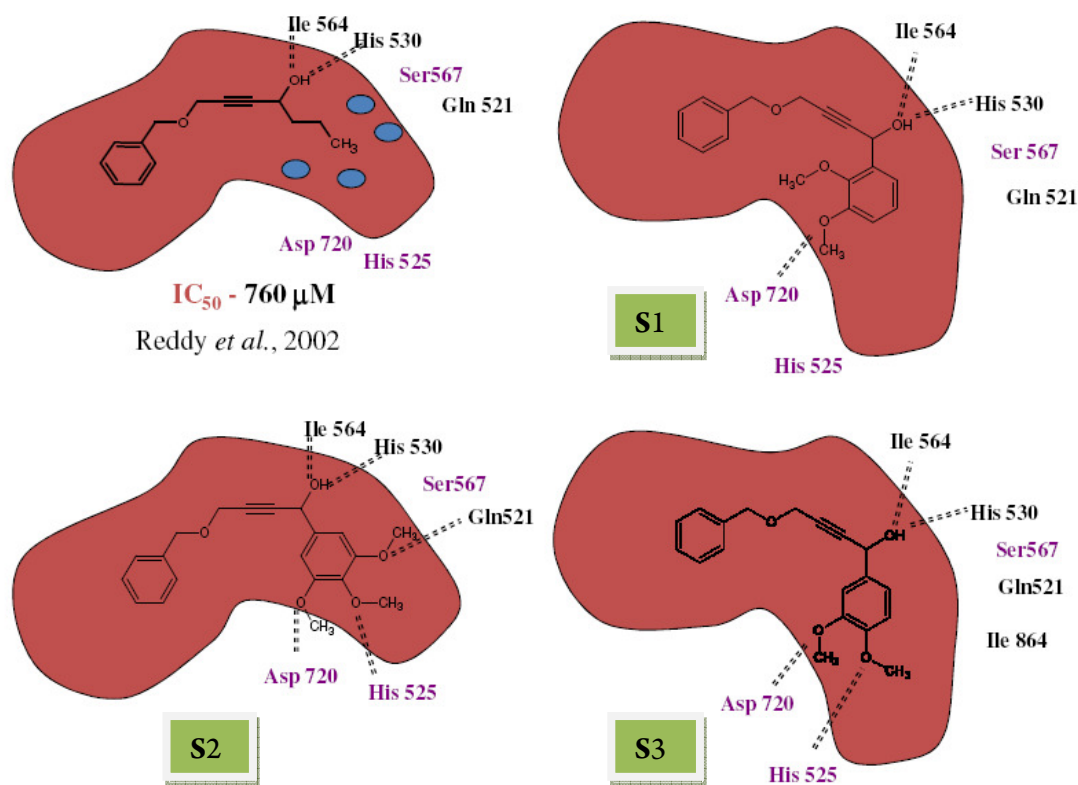


**Fig. 32:** Various molecules (S1-3) designed using site points



This was to make sure that the site points corresponding to the surrounding amino acids were satisfied. The designed molecules are shown in Fig. 33.

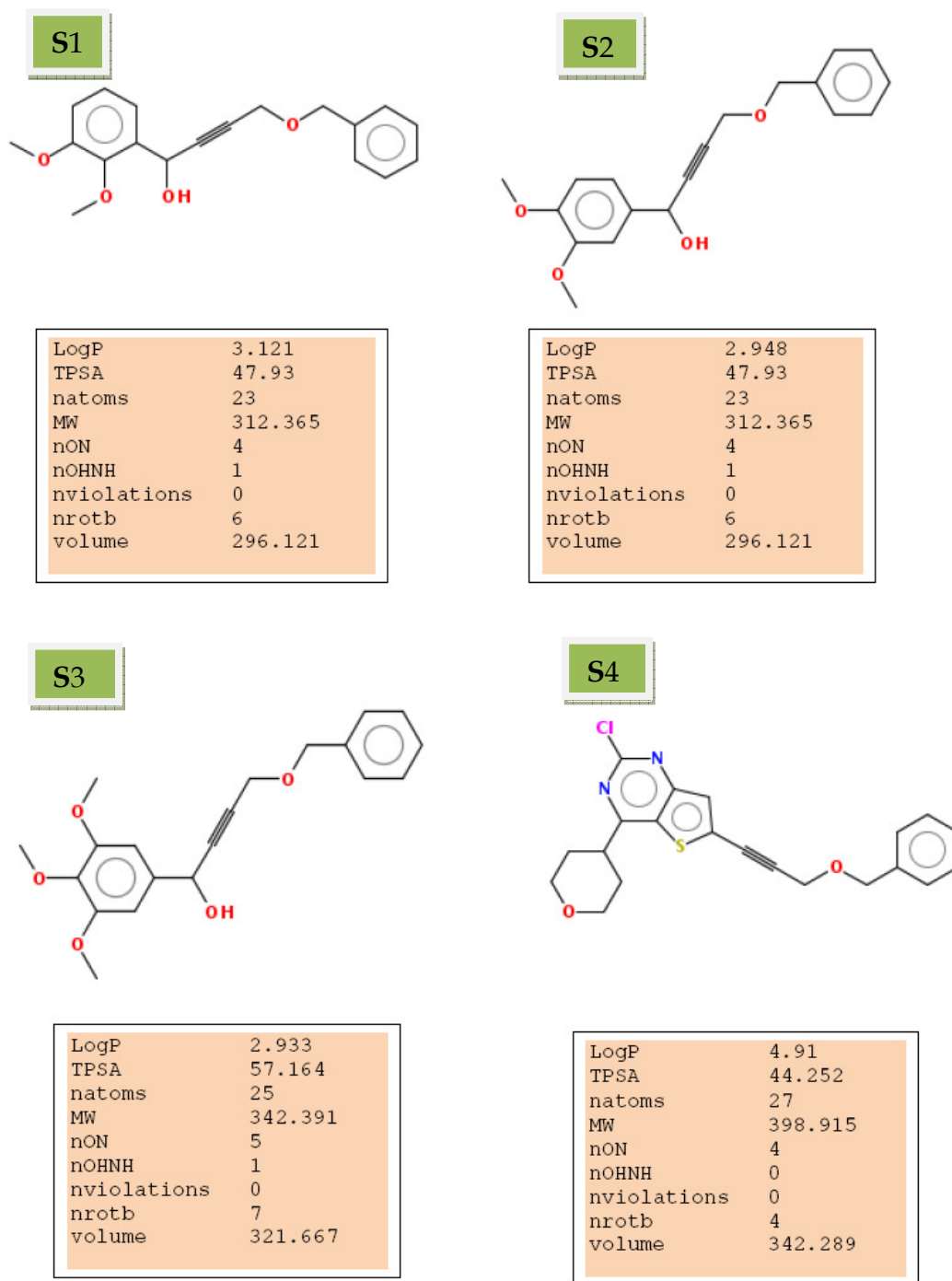


**Fig. 33:** The molecules designed and their molecular properties (S1-4). All the molecules follow Lipinski's rule of 5

### 4.3.2. Docking and scoring

The ligands were built using the Cerius2 program. The structures of the ligands were energy minimized to a RMSD of 0.001kcal/mol using MMFF94X forcefield. Docking of the inhibitors into 5-LOX was carried out using GOLD [Jones *et al.*, 1997]. The parameters used for GA were population size (100), selection pressure (1.1), number of operations (100,000), number of islands (5) and niche size (2). Operator parameters for crossover, mutation and migration were set to 95, 95 and 10 respectively. To quantitate the interactions in the protein-ligand complexes, the scoring function GOLD score was employed. Default cutoff values of 2.5 Å ( $d_{H-X}$ ) for hydrogen bonds and 4.0 Å for Vander Waals were employed. Based on the superimposition of the template, Soybean LOX-3 with 5-LOX 3D structure, active site was defined as a sphere of 10Å centered on the inhibitor in the template. During docking, the default algorithm was selected. Input parameters of the GOLD were set to allow octahedral coordination geometry to iron. The number of poses for each inhibitor was set to 100 and early termination was allowed if the top three bound conformations of a ligand were within 1.5 Å RMSD. After docking, the individual binding poses of each ligand were observed and their interactions with the protein were studied. The best and most energetically favorable conformation of each ligand was selected. The inhibitor-5-LOX complexes were formed and optimized by energy

minimization using four stage protocol mentioned earlier. After energy minimization, the lowest energy position in the active site for the generated lead molecule was determined by the flexible ligand docking procedure in the Affinity module of the InsightII program and the ligand was scored by LUDI. The LUDI score and interaction energies show that the molecules designed were more potential than the initial molecule i.e. comp 1 (Table-4).

**Table-4:** Calculated interaction energies (kcal/mol) for the designed compounds

Compound	$E_{vdw}$	$E_{elec}$	$E_{total}$ (kcal/mol)	LUDI score	$E_{bind}$ (kcal/mol)
1	-22.451	-6.153	-28.604	382	-11.6
S1	-34.823	-9.248	-44.071	526	-19.5
S2	-34.487	-16.401	-50.888	551	-20.1
S3	-39.214	-19.348	-58.562	622	-26.1
S4	-36.412	-17.612	-54.025	628	-25.5

Interaction study has shown the increased no. of hydrogen bonds from S1 to S4, thereby the LUDI score as well as the total interaction energies also increased. Hence, by using lead optimization studies more potent molecules were designed.

### 4.3.3. Biological evaluation

#### 4.3.3.1. *In vitro* LOX assay:

All the compounds were tested for their effect on 5-LOX inhibition and were assayed as per Reddanna *et al.* (1990). S1-S4 were the designed molecules while comp 1 is the already reported molecule. The % activity/inhibition *vs* molar concentration graphs of the compounds, their IC<sub>50</sub> values and hydrogen bond interactions are as shown in Fig. 34-37.

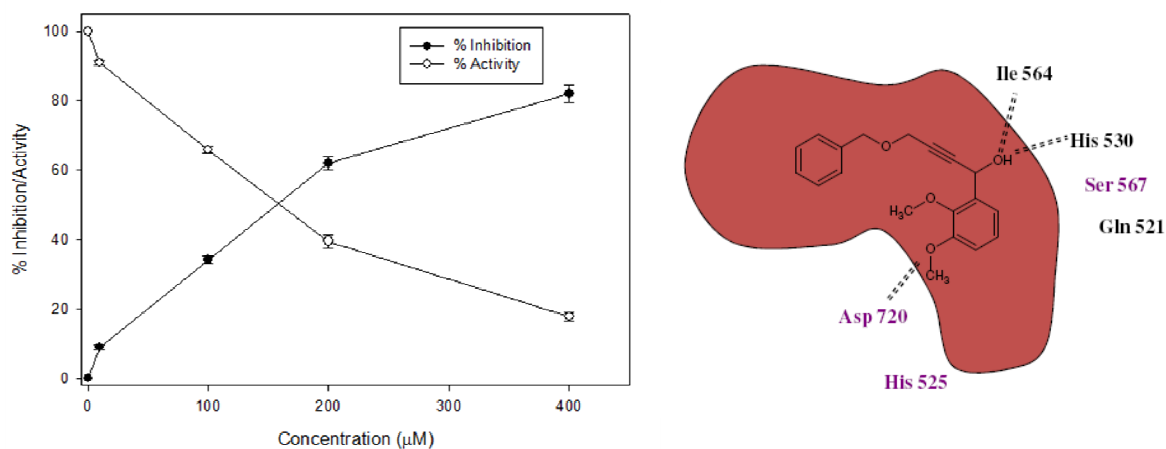


**Fig. 34:** Inhibition concentration curve of S1 (IC<sub>50</sub> -157 μM). Hydrogen bonds are denoted by dotted lines. Hydrogen bond analysis shows the utilization of site point corresponding to Asp720

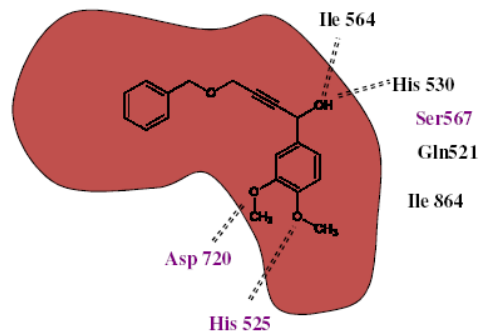
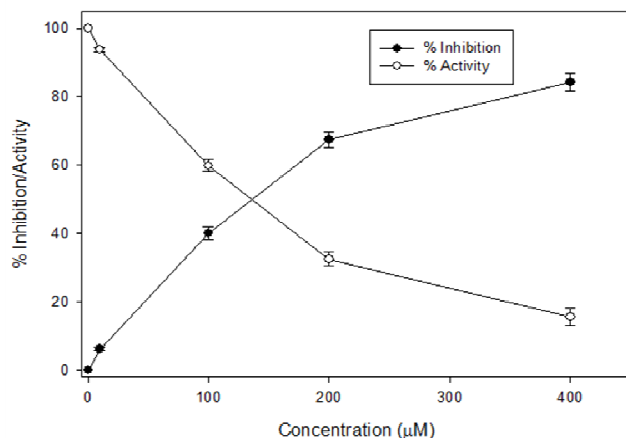


**Fig. 35:** Inhibition concentration curve of S2 (IC<sub>50</sub> -137 μM). Hydrogen bonds are denoted by dotted lines. Hydrogen bond analysis shows the utilization of site points corresponding to Asp720 and His525

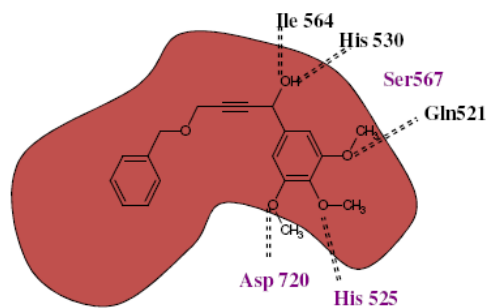
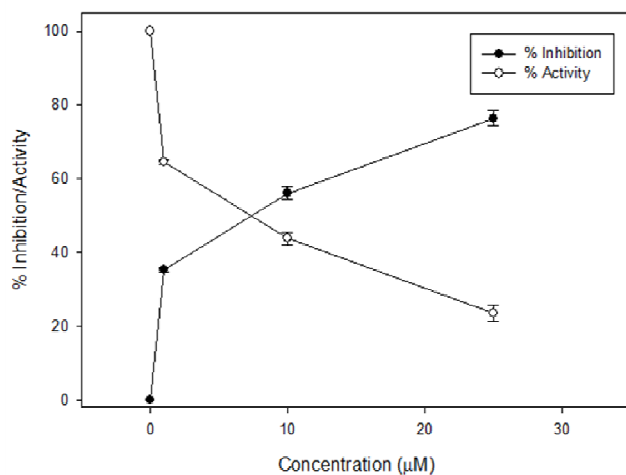


**Fig. 36:** Inhibition concentration curve of S3 (IC<sub>50</sub> -8 μM). Hydrogen bonds are denoted by dotted lines. Hydrogen bond analysis shows the utilization of site points corresponding to Asp720, His525 and Gln521

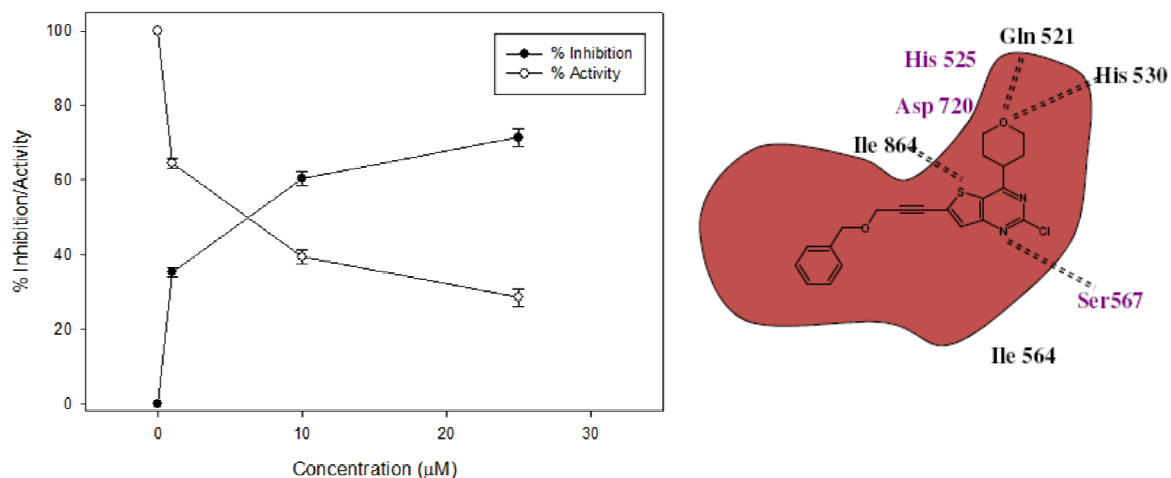


**Fig. 37:** Inhibition concentration curve of S4 ( $IC_{50}$  -6.4  $\mu$ M). Hydrogen bonds are denoted by dotted lines. Hydrogen bond analysis shows the utilization of site points corresponding to Gln521, His530, Gln521 and Ile864.

As shown in the Fig. 34-37, there is an inverse correlation between the number of hydrogen bonds and the  $IC_{50}$  values obtained. While S1 had only two groups (-OH, and -OCH<sub>3</sub>) in hydrogen bonding, S2 had three groups (-OH, -OCH<sub>3</sub>, and -OCH<sub>3</sub>) and S3 had four groups (-OH, -OH, -OCH<sub>3</sub> and -OH). S4 which showed the lowest  $IC_{50}$  value (6.4  $\mu$ M) had unique groups (-N=, -S- and -O-) in hydrogen bond interactions. Also, the overall trend for the interaction energy and LUDI scores were in good qualitative agreement with the experimental data. S3 and S4 which were scored higher and predicted to be the most active by LUDI score were the most potent. *In vitro* studies clearly validate the *in silico* prediction on the potency of designed molecules in the inhibition of

5-LOX. The foregoing studies clearly demonstrate the usefulness of the 5-LOX model built in designing the potent inhibitory molecules.

Homology models of lipoxygenase enzymes have been used in several previous studies for purposes other than inhibitor discovery. Specifically, these studies have used homology models, sometimes in combination with docking methods, to propose models for substrate binding and specificity in various LOXs. There have been very few reports on Structure based lead optimization/structure based *de novo* design of LOX inhibitors, mainly due to the lack of crystal structure for many of the human LOXs.

In a recent study, small molecule inhibitors of human platelet-type 12- and reticulocyte 15-LOX-1 (12-hLOX and 15-hLOX) were designed using structure-based methods. Homology models of 12-hLOX and 15-hLOX were developed, based on the structure of rabbit 15-LOX and virtual screening was performed. Of only 20 molecules tested for *In vitro* activity against 12- and 15-human LOX, three molecules showed inhibition of IC<sub>50</sub> less than 100  $\mu$ M affinity [Kenyon et al., 2006].

This study on Structure based lead optimization of 5-LOX inhibitors suggest that the homology models are capable of identifying low-micromolar

inhibitors at a rate that, in all likelihood, greatly exceeds random compound selection. The models of these protein–inhibitor complexes suggest strategies for future development of selective lipoxygenase inhibitors.

#### 4.4. Conclusions

Prior to this work, structure-based methods have not played a major role in the discovery of 5-LOX inhibitors, because experimental structures of 5-LOX do not exist. This study is a successful example reported for the inhibitor design of 5-LOX using the *de novo* design strategy. The studies presented here provide a pathway to design novel anti-asthma/anti-cancer compounds. A molecule of  $IC_{50}$  of 760  $\mu M$  was optimized to a more potential molecule with  $IC_{50}$  of 6.4  $\mu M$ . Site-point connection method showed good promise and it can be further used in developing a very potential 5-LOX inhibitor.

The overall trend for the interaction energy and LUDI scores are in good qualitative agreement with the experimental data. In addition, it should be pointed out that all of the lead molecules were designed on the basis of a homology derived molecular model of 5-LOX.



The new low-micromolar inhibitors appear to be suitable as leads for further inhibitor development efforts against 5-LOX based on the fact their size and chemical properties are appropriate to classify them as drug-like compounds. The lead optimization approach based on a homology model established in this study should have general implications for designing novel inhibitors of various LOXs. The methodology can be further used by exploiting various other site points to yield novel lead structures with higher activity against 5-LOX enzyme.

# Chapter -III

**Pharmacophore modeling of 5-LOX inhibitors:  
A ligand based drug design approach**

## 3.1. Introduction

### 3.1.1. Definition of pharmacophore

The essential functionalities of a molecule necessary for its pharmacological activity are called pharmacophores. Although the idea of pharmacophores existed for a long time, Ehrlich first introduced this terminology following the term chromophore which was used to describe the groups responsible for the color of a compound [Ehrlich, 1909]. The interest in the idea of pharmacophores has grown tremendously in the last few decades due to the availability of computer graphics [Marshall *et al.*, 1990], a number of computational methods to determine the pharmacophoric geometry [Kelebe, 1993] and various softwares for 3D database mining using the concept of a pharmacophore pattern match [Clark *et al.*, 1991]. However, the validity of a pharmacophore hypothesis came more from direct medicinal chemistry structure–activity relationships (SAR) studies rather than from any theoretical calculations. Such calculations may be possible in the near future with the availability of an ever increasing number of ligand–protein complex structures, better molecular mechanics force fields and better understanding of solvation factors. In such an approach, we have to show that the pharmacophoric groups provide the major contribution in binding affinity to the protein compared to the rest of the molecule.

In modern computational chemistry, pharmacophores are used to define the essential features of one or more molecules with the same biological activity. A database of diverse chemical compounds can then be searched for more molecules which share the same features located a similar distance apart from each other. Typical pharmacophore features represent the important functional groups i.e. hydrophobic, aromatic, a hydrogen bond acceptor, a hydrogen bond donor, a cation, or an anion. The features need to match different chemical groups with similar properties, in order to identify novel ligands. Ligands receptor interactions are typically “polar positive”, “polar negative” or “hydrophobic”. A well-defined pharmacophore model includes both hydrophobic volumes and hydrogen bond vectors.

### 3.1.2. Pharmacophore Modeling

The technique of developing a pharmacophore is based on first deriving preferred conformations *via* a conformational searching scheme, then defining common groups in terms of specific atom types. The molecules are then aligned and superimposed at the specific points in a defined way. The pharmacophore is then derived by joining the sites in common and calculating distances by averaging sites of superposition in a least squares fit calculation. A pharmacophore needs at least three points of connection but it can be more.

The complete pharmacophore can be represented geometrically as a triangle if three points are used or some other geometric figure if more points are available and describes the properties of the vertices as to the type of interaction with the receptor.

A wide range of experimental and theoretical data is routinely used to develop pharmacophoric patterns. This process is generally referred to as pharmacophore mapping and involves three main aspects: finding the features required for a particular biological activity; determining the molecular conformation required (i.e. the bioactive conformation); and developing a superposition or alignment rule for the series of compounds. The primary information used in pharmacophore mapping is derived naturally from the compounds synthesized and their measured biological activity. From this, structure activity relationships emerge and rudimentary pharmacophore hypothesis can be formulated. If the structure of the macromolecular target is known, either as determined experimentally or as computationally modeled, this information is obviously very useful to the pharmacophore mapping process. A variety of molecular modeling and computational chemistry techniques can then be applied, in conjunction with the experimental data, to develop pharmacophore models.

Automatic generation of pharmacophoric patterns is the goal of several modeling packages. This is a difficult procedure, however, because many bioactive molecules are flexible and their minimum energy conformations need not correspond to the receptor bound conformation. Automated pharmacophore mapping is now available in programs from Biocad, Biosym, Chemical Design Ltd., Tripos and Catalyst.

### 3.1.3. Catalyst

Catalyst (available from Accelrys Inc.) is one of the leading software products for pharmacophore modeling and 3D database searching. In this study, Catalyst was used for pharmacophore modeling of 5-LOX. HypoGen module in Catalyst was used in the study.

#### 3.1.3.1. HypoGen Theory

HypoGen attempts to derive SAR models from a set of molecules for which activity values ( $IC_{50}$ ) on a given biological target are available. It optimizes hypotheses that are present in the highly active compounds in the training set, but missing in the least active (or inactive) ones. It attempts to construct the simplest hypotheses that best correlate the activities (estimated

vs. measured). As displayed in Fig. 38. the predictive models are created in three steps in a HypoGen run: constructive, subtractive and optimization.

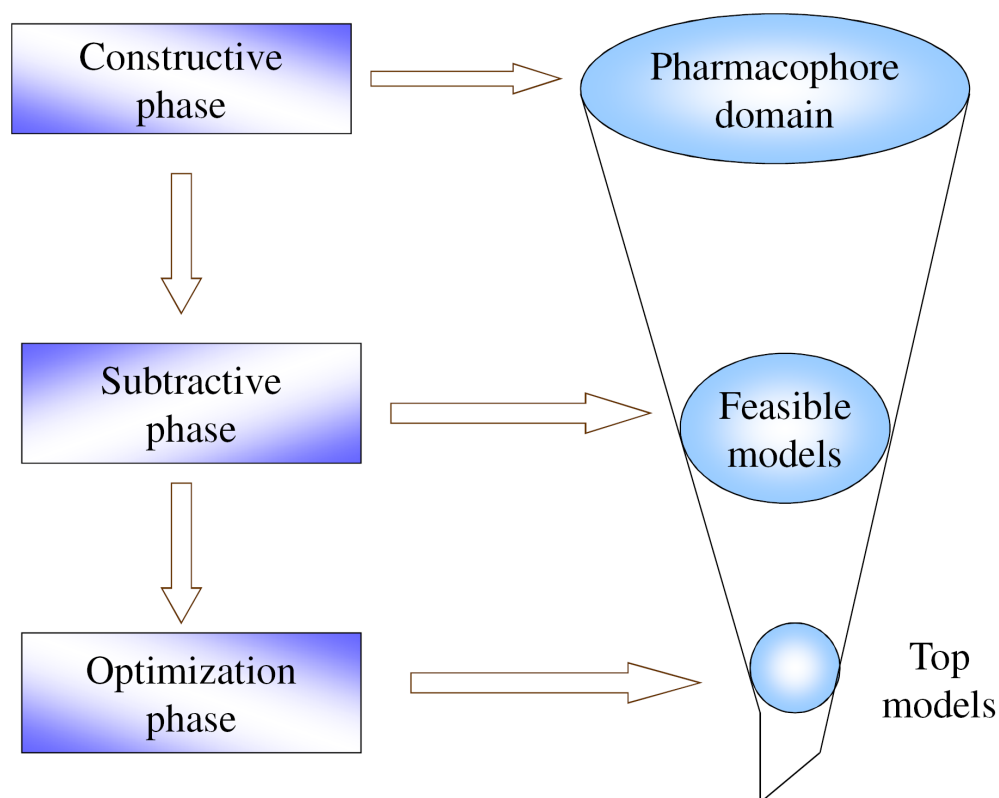


**Fig. 38:** *HypoGen theory* [Biocampus manual, 2003].

*Constructive phase:*

The constructive phase identifies hypotheses that are common to the most active set of compounds. The most active set is determined by the following equation:

$$MA * Unc_{MA} - (A/Unc_A) > 0$$

where MA is the activity of the most active compound, Unc is the uncertainty in the measured activity and A is the activity of the compound. The most active set of compounds is limited to a maximum of 8. Once the set is determined, HypoGen enumerates all possible pharmacophore configurations using all combinations of pharmacophore features for each of the conformations of the two most active compounds.

*Subtractive phase:*

The subtractive phase identifies pharmacophore confirmations developed in the constructive phase that are also present in the least active set of molecules and remove them. The first step is the identification of the least active compounds. This is accomplished by the use of equation:

$$\log(A) - \log(MA) > 3.5$$

where A is the activity of the current compound and MA is the activity of the most active compound. In simple terms, all compounds whose activity is 3.5 orders of magnitude less than that of the most active compounds are considered to be in the set of least active molecules. The value 3.5 is a user adjustable parameter, if needed.

The important guidelines in the selection of training set are:

- i. Have at least two diverse compounds in the most active set (to maximize the number of enumerated pharmacophore configurations)



- ii. The compounds in the training set should cover a wide range of activities of at least four orders of magnitude (in order to have an effective subtractive)

*Optimization phase:*

The optimization phase involves improvement of the hypothesis score. Small perturbations are applied to those pharmacophore configurations that survived the subtractive phase and are scored based on errors in activity estimates from regression and complexity of the hypothesis. The total cost of each pharmacophore is computed by the sum of three costs: weight, error and configuration. While the weight component increases with the deviation of the feature weight from the ideal value of 2.0, the error component increases with the RMSD between the measured and estimated activities. The configuration cost is fixed and depends on the complexity of the pharmacophore and is generated in this phase. Upon completion of this phase, HypoGen reports top scoring 10 unique pharmacophores.

### **3.1.3.2. HipHop Theory**

HipHop is very similar to constructive phase of HypoGen. The objective is to identify and enumerate all possible pharmacophore configurations that are common to the training set. The implementation of this objective within

HipHop is, however, very different from that of HypoGen. HipHop performs an exhaustive search starting with the simplest pharmacophore configurations i.e. all possible combinations of two-feature pharmacophore. Once all the two-feature are exhausted, it moves to the three-feature combinations. The process continues until HipHop can no longer generate common pharmacophore combinations. The process is schematically shown in Fig. 39.

The user specifies how many molecules must map completely or partially to the pharmacophore. Hence, broader and more diverse pharmacophore can be built in this manner. The resultant pharmacophore models are scored. The final output of a HipHop run is an user determined number of unique pharmacophore sorted from the highest scoring to the lowest [Biocampus manual, 2003].

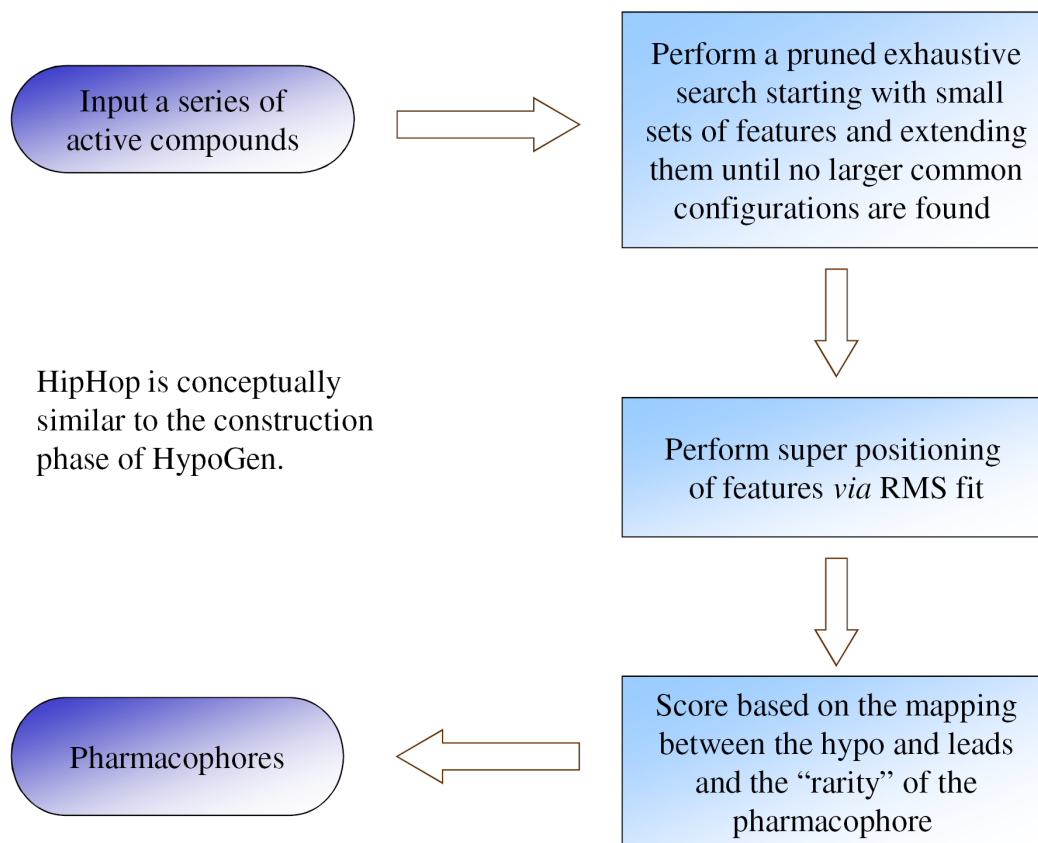


**Fig. 39:** *HipHop theory* [Biocampus manual, 2003].

#### 3.1.4. Pharmacophore Model of 5-LOX

A good pharmacophore model could be used as query for searching small molecule databases in order to discover novel chemical entities. A reliable pharmacophore model can be built using HypoGen (a part of the Catalyst suite of software), provided, we have experimental affinities of protein-ligand interactions. The ligands should have a variety of scaffolds and

the range of affinity should vary at least a thousand fold. The pharmacophore model generated can be used to search small molecule databases in order to identify molecules that represent similar shape and chemical features from a given database.

Due to the therapeutic potential of inhibitors of 5-LOX, many pharmaceutical companies and academic research groups have been involved in the development of effective 5-LOX inhibitors. This has resulted in the identification of many novel inhibitors. These provide a good basis for elucidating the structure-activity relationship of these inhibitors, which will aid in identification of more inhibitors. Lack of crystal structure information of 5-LOX has been an obstacle for application of the structure based drug design strategies in practice. As an alternative, homology modeling was used in generation of 3-D models of various LOXs which were inturn used in various drug design strategies [Aparoy *et al.*, 2008; Du *et al.*, 2006; Charlier *et al.*, 2006; Hammarberg *et al.*, 2000; Bindu *et al.*, 2004; Hemak *et al.*, 2002; Werz *et al.*, 2005]. Ligand based drug design is an alternative in such cases. In a ligand-based design, identification of a pharmacophore is one of the most important steps.

Pharmacophore model is a widely used approach to quantitatively explore common chemical characteristics among a considerable number of

structures with great diversity and qualified pharmacophore model could also be used as a query for searching chemical databases to find new chemical entities [Xie *et al.*, 2009; Taha *et al.*, 2008; Wang *et al.*, 2008; Lu *et al.*, 2007]. Recent advances in virtual screening approach for inhibitor identification are summarized in Table-5.

**Table-5:** Summary of successful application of pharmacophore based virtual screening.  
CHK1: checkpoint kinase-1; HIV: Human Immuno deficiency virus; HCV: hepatitis C virus; SARS-CoV: Severe acute respiratory syndrome corona virus; PPAR: Peroxisome Proliferator Activated Receptor

Disease	Target	Method	Activity ( $\mu\text{M}$ )	Ref
Cancer	Microtubule	Catalyst	0.187	Liou <i>et al.</i> , 2006
		PharmoMap <sup>TM</sup> , PharmoScan <sup>TM</sup>	15.7	Kim <i>et al.</i> , 2006
	Aurora A kinase	Catalyst	3.8	Deng <i>et al.</i> , 2008
	CHK1	Plurality	0.45	Lyne <i>et al.</i> , 2004
Virus infection	HIV protease	Catalyst	1.9	Pandit <i>et al.</i> , 2006
		Ligandscout	35	Steindl <i>et al.</i> , 2007
	HCV Polymerase	PharmoMap <sup>TM</sup> , PharmoScan <sup>TM</sup>	20	Ryu <i>et al.</i> , 2009
	SARS-CoV protease	Catalyst, Dock4.0.2, Dock5.0, CoMFA, CoMSIA	3	Tsai <i>et al.</i> , 2006
Alzheimer	tau	Catalyst	12	Larbig G <i>et al.</i> , 2007
Diabetes	PPARs	Catalyst	1.5, 44	Markt P <i>et al.</i> , 2008

In our studies, we identified pharmacophore model of the 5-LOX inhibitors. Then the best quantitative pharmacophore model generated was used as a 3D query to screen several commercial databases comprising of compounds which follow Lipinski's rule of five [Lipinski, 2000] and docking study [Wang *et al.*, 2008]. Finally, the identified potential lead compounds were evaluated biologically for their inhibitory activities, as well as further structural modification studies.

## 3.2. Materials and methods

### 3.2.1. General methodology

All the pharmacophore modeling calculations were carried out by using the Catalyst 4.11 software package on SGI workstation [CATALYST 4.11; Accelrys: San Diego, CA, 2005]. The HipHop and HypoGen modules within Catalyst were used for the construction of qualitative and quantitative models, respectively. Chemical feature based pharmacophore hypotheses can be generated automatically using the HypoGen algorithm within Catalyst, provided that structure activity relationship data of a well balanced set of compounds are available.

### 3.2.2. Training set selection and generation:

For the pharmacophore modeling study compounds from the literature with a range of 5-LOX inhibitory activities, spanning at least four orders of magnitude were collected. 24 molecules with IC<sub>50</sub> values ranging from 0.003 μM to 41 μM for 5-LOX were selected and included in the training set (Fig. 40). All structures in the training set were built in 2D/3D Visualizer within Catalyst and minimized to the closest local minimum based on a modified CHARMM force field within the confirm module [Brooks *et al.*, 1983]. Catalyst generated a representative family of conformational models for each compound using a Monte-Carlo-like algorithm together with Poling [Smellie *et al.*, 1995]. Diverse conformational models for each compound were generated using an energy range of 15 kcal/mol of the calculated potential energy minimum. Maximum number of conformers was specified to 250 for each molecule to ensure maximum exploration of the conformational space.

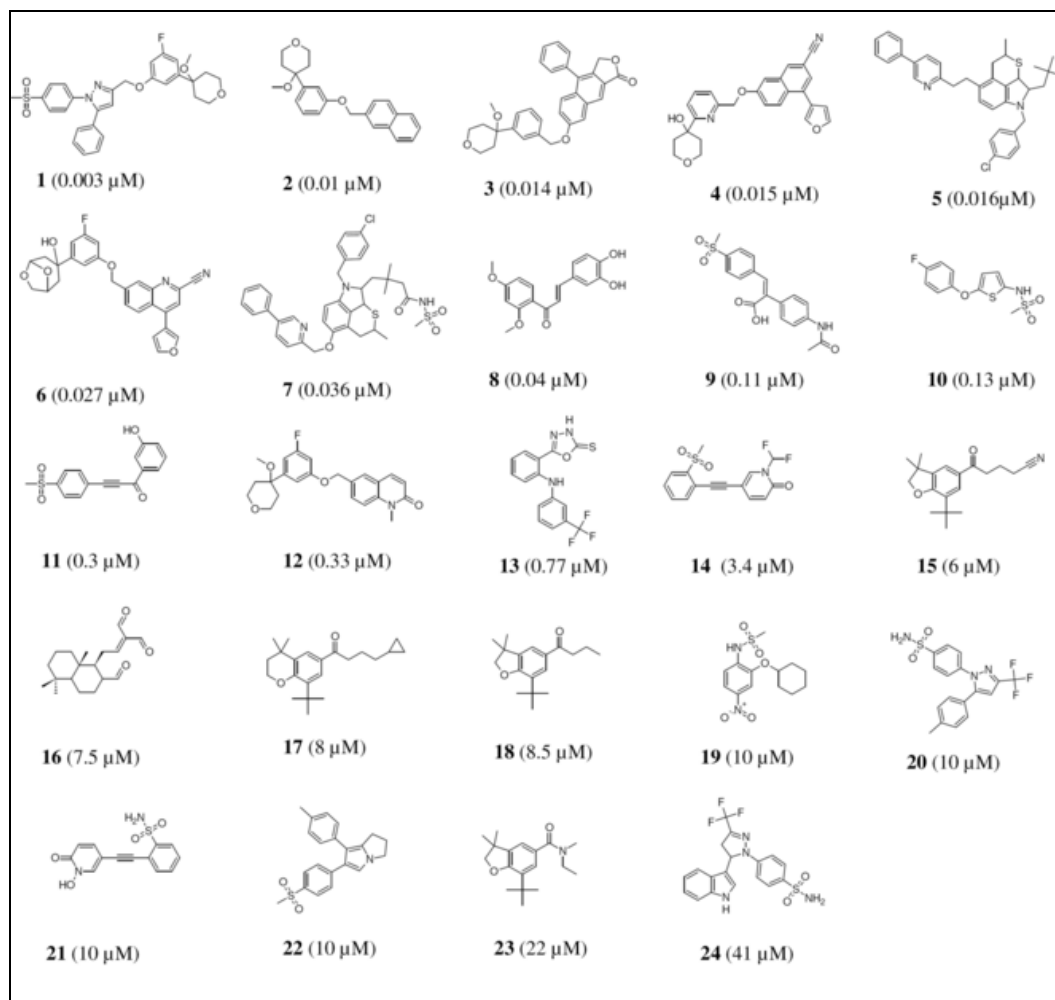


**Fig. 40:** Chemical structures of 5-LOX inhibitors in training set (compounds 1–24) together with their biological activity data ( $IC_{50}$  values, in parentheses).

### 3.2.3. Generation of Hypotheses

Catalyst generates hypotheses consisting of features. These features are displayed as round mesh balls, which represent an area in space relative to the



other features where a characteristic of a molecule should be to induce the desired activity (location constraints).

Catalyst generates hypotheses with a heavy emphasis on a group of molecules which are the most active of the training set with activities falling into a certain activity range. The upper limit of this activity range is defined by Catalyst to be the product of the uncertainty value multiplied by the activity of the most active compounds in the training set. The lower limit of this activity range is defined by Catalyst to be the division of the uncertainty value with the activity of the most inactive compounds in the training set. It is very important that the hypotheses generated are not biased by any one chemical structure type, so it is necessary to ensure that compounds of more than one structural type are included in the most active group in the training set.

In this study, the qualitative HipHop model was generated based on the five most active compounds (1-5) in training set before performing the quantitative pharmacophore modeling, the purpose of which is to identify pharmacophore features necessary for potent 5-LOX inhibitors. In the HipHop run, the most active compound 1 was considered as 'reference compound' specifying a 'principal' value of 2 and a 'MaxOmitFeat' value of 0. The 'principal' and 'MaxOmit-Feat' values were set to 1 for the remaining four

compounds. HipHop parameters were kept at their default values. The HipHop pharmacophore hypothesis clearly indicated the importance of hydrogen-bond acceptor, hydrogen-bond acceptor lipid, hydrogen-bond donor, hydrophobic moiety, hydrophobic aliphatic moiety, hydrophobic aromatic moiety and ring aromatic feature.

Further, hypotheses were generated using HypoGen with default parameters including a minimum no. of features of 3. The allowed set of features was hydrogen-bond acceptor, hydrogen-bond acceptor lipid, hydrogen-bond donor, hydrophobic and ring aromatic features. A ring aromatic feature is defined as a feature which maps 5- or 6- numbered aromatic rings (which may be next to a charge). Hydrogen bond donor (HBD) groups were used, although Catalyst never included any HBD feature in the generated pharmacophore. The removal of HBD feature caused a difference in Total Cost and Correlation values and therefore it was used in the HypoGen run even though it was not included in the final pharmacophore model developed.

### 3.2.4. Pharmacophore evaluation

The generated HypoGen models were evaluated according to Debnath in terms of cost functions and statistical parameters, which were calculated by HypoGen module during hypothesis generation. A pharmacophore model should have a high correlation coefficient, lowest total cost and RMSD values. The total cost should be close to the fixed cost and away from the null cost. The difference between the cost of the generated hypothesis and the cost of the null hypothesis signifies the reliability of a pharmacophore model. A value of 40–60 bits between them for a pharmacophore hypothesis may indicate that it has 75–90 % probability of correlating the data.

For the qualitative pharmacophore model of 5-LOX inhibitors, test set method was used for validation. The test set used here contains a total of 65 inhibitors as shown in Fig. 41. Further the validation of quantitative pharmacophore model was done by cross validation method. The cross validation was performed by using CatScramble program within Catalyst. The CatScramble strategy tries to scramble the experimental activities in the training set randomly and the resulting training sets were used for HypoRefine run. The confidence level was set to 95%, thereby CatScramble program

generated 19 random spreadsheets to construct hypotheses using exactly the same conditions as used in generating the original pharmacophore hypotheses.

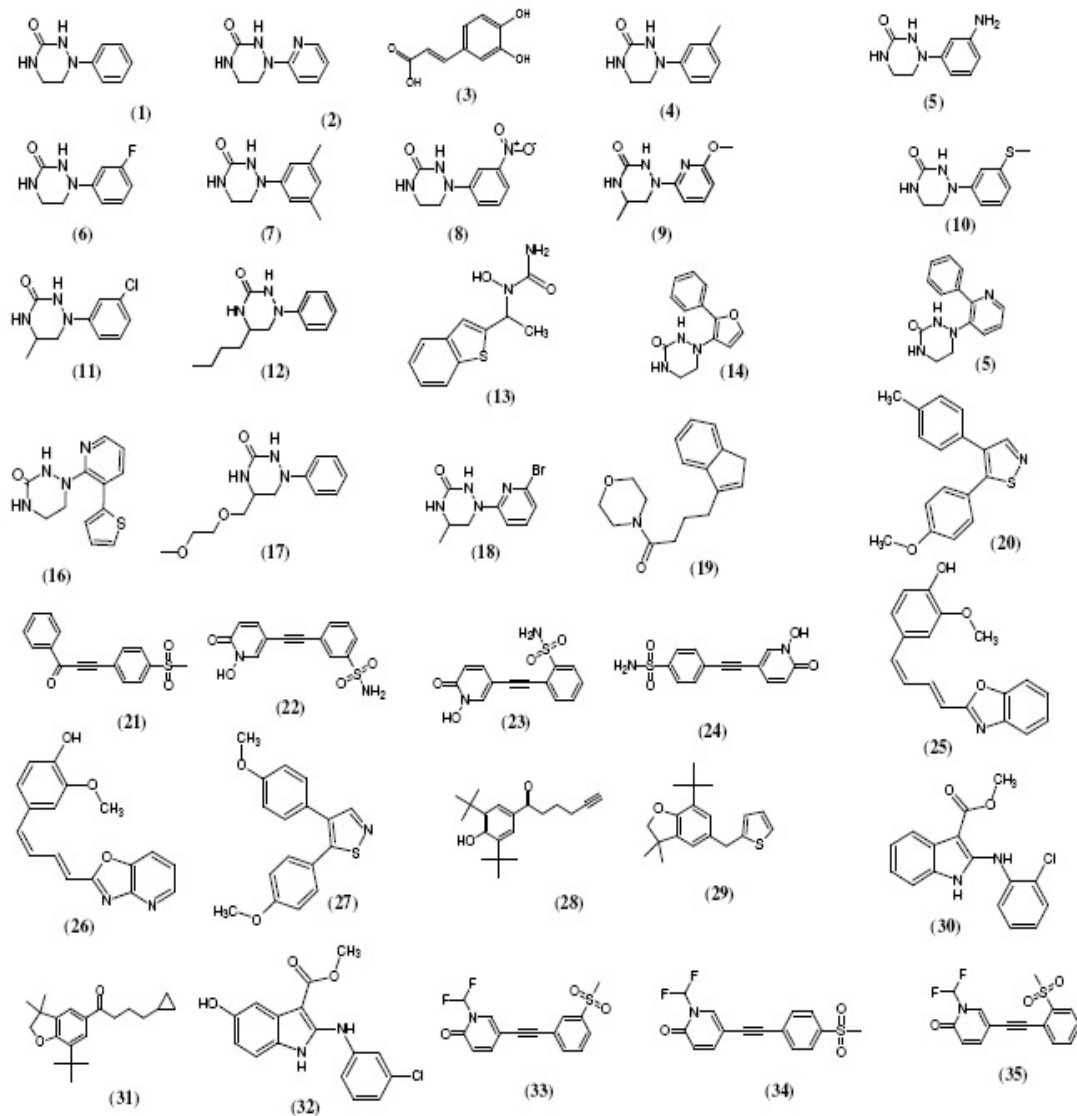


Fig. 41: Chemical structures of 5-LOX inhibitors in test set (compounds 1-65)

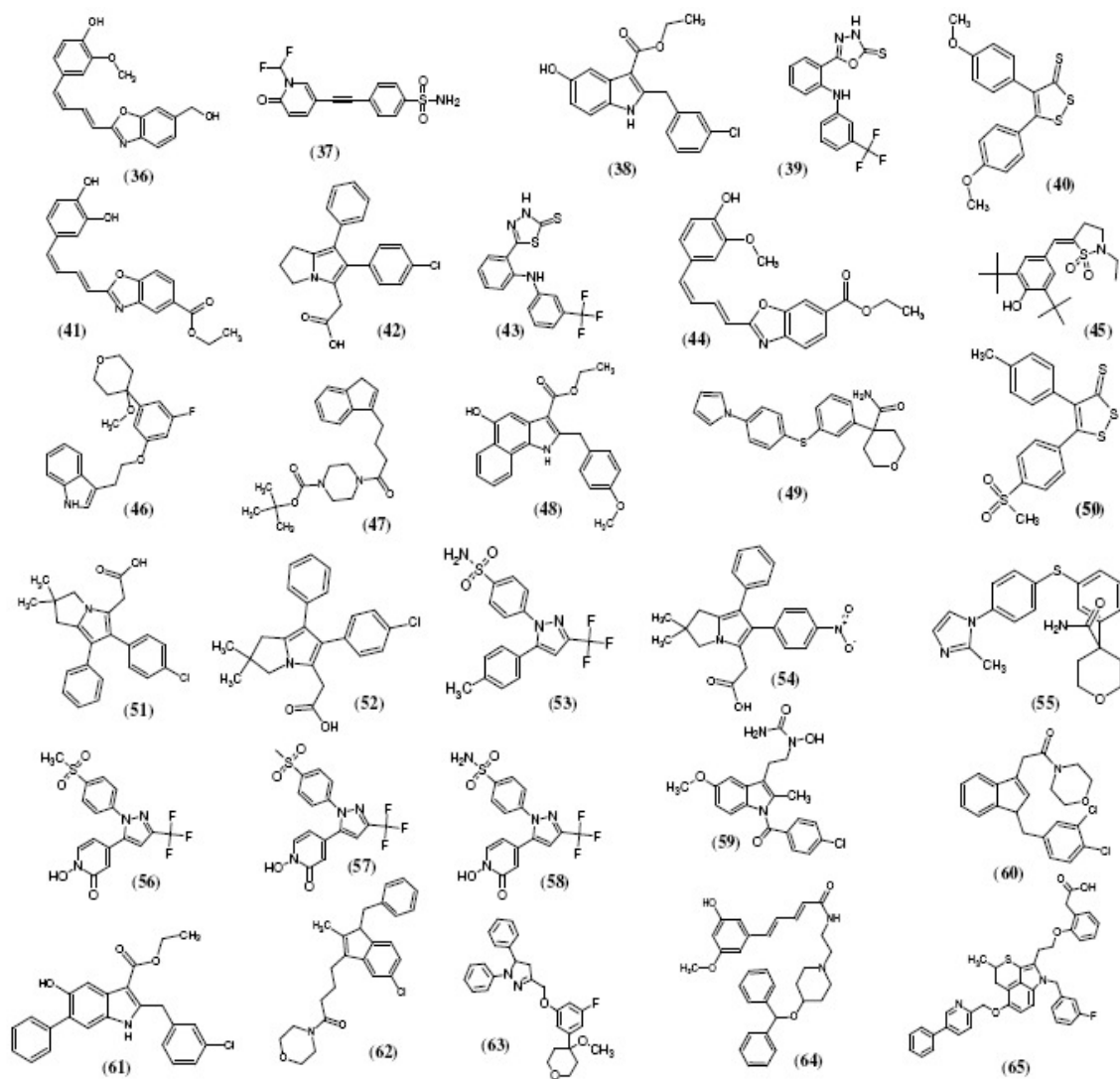


Fig. 41: Chemical structures of 5-LOX inhibitors in test set (compounds 1-65)

### 3.3. Results and Discussion

#### 3.3.1 Generation of the model

Catalyst generates hypotheses by assigning chemical features to the training set molecules, then arranging the features so that the molecules map with a ranking which correlates with their activity. The hypothesis generation places a greater importance on the molecules contained in the most active group of the training set.

Catalyst produces 10 hypotheses (sometimes 9) which are arranged in a hierarchical manner according to the Catalyst cost analysis, which takes into account many factors including the size of the training set. The most influential parameter contributing to this cost analysis is the correlation between the hypothesis estimated activity values and the real activity values. The correlation value can lie between 0 and 1, with 1 being a perfect correlation. Catalyst cost analysis also takes into account a configurational parameter which describes the complexity of the problem (this parameter should be under 18). Catalyst cost analysis also employs the principle of Occam's razor whereby a hypothesis should be as simple as possible. This cost analysis allows one to assess the validity of the produced hypotheses. This involves the use of three cost parameters as discussed earlier:

- i. The null cost parameter assumes that all training set molecules have the same activity, so that there is no statistically significant structure in the training set. This cost parameter has the highest numerical value of all the cost parameters.
- ii. The fixed cost parameter assumes all training set molecules fit the simplest possible hypothesis perfectly. This cost parameter has the smallest numerical value of all the hypotheses cost parameters.
- iii. The total cost parameter results in a ranking of generated hypothesis. This parameter takes into account the correlation of the training set molecules, tested activities with the activity estimated by the hypothesis.

The difference between the total cost and the null hypothesis cost gives rise to the resultant cost, which determines the statistical significance of the pharmacophore model generated.

In this study, the approach we used is to develop a pharmacophore model using the HypoGen module in Catalyst which can be used to correlate the observed biological activities for a series of compounds with their chemical structures. In our trials, we found that taking hydrogen-bond acceptor,

hydrogen-bond acceptor lipid, hydrogen-bond donor, hydrophobic moiety and ring aromatic feature generated a good quality pharmacophore model.

The top 10 ranked hypotheses as well as their statistical parameters are presented in Table-6. The best pharmacophore model (Hypo1), which was characterized by the lowest total cost value (108.338) and the highest cost difference (58.281), contains four features, namely, two hydrogen bond acceptors, one hydrophobic and one ring aromatic feature. A 'measured' versus 'estimated' activity for the training set exhibited a correlation coefficient ( $r$ ) =0.974978 with root-mean-square deviation (RMSD) =0.6025. The good score value indicated a reliable ability to predict activities within the training set. The config costs of the runs were high and exceeded the maximum limit of 18. This may be because of the training set compounds, which seem to increase the entropy of the hypothesis. The reasonable cost difference of the hypothesis and high correlation obtained and further evaluation of the resulting model with Fischer Randomization test and with test set compounds should surpass any drawbacks related to the less than optimal config cost.



**Table-6:** Statistical parameters of the top 10 hypotheses of 5-LOX inhibitors generated by HypoGen program

Hypo No.	Total Cost <sup>a</sup>	Cost Diff. <sup>b</sup>	RMSD	Correlation (r)	Features
1	108.338	58.281	0.602576	0.974978	AAZR
2	109.789	56.830	0.68082	0.967973	ALZR
3	110.088	56.531	0.755627	0.959451	AZRR
4	110.388	56.231	0.721508	0.963781	ALZR
5	110.805	55.814	0.740654	0.961824	ALZR
6	111.068	55.551	0.769418	0.958449	ALZR
7	111.770	54.849	0.854401	0.947673	ALRR
8	111.882	54.737	0.825159	0.951754	LLZR
9	112.050	54.569	0.711489	0.96675	ALZR
10	112.257	54.362	0.814461	0.953537	AAZR

<sup>a</sup> The total cost value of a hypothesis is calculated by summing three cost factors, a weight cost (data not shown), an error cost (data not shown) and a configuration cost (a constant among all the hypotheses).

<sup>b</sup> The difference between the total cost of a hypothesis and that of the null hypothesis, roughly correlates with significance. The larger the difference, the greater is the significance of the hypothesis. A true correlation in the data will very likely be estimated by models that exhibit a cost difference (Null cost - Total cost) (fixed cost = 102.934, configuration cost = 21.0826 and null cost = 166.619). All cost values are in bits.

<sup>c</sup> A, hydrogen bond acceptor; L, hydrogen bond acceptor lipid; Z, hydrophobic feature; and R, ring aromatic moiety.

The 3D space and distance constraints of these pharmacophore features were shown in Fig. 42A and 42B. Fig. 42C and 42D present the Hypo1 aligned with the most active compound 1 (IC<sub>50</sub>: 0.003  $\mu$ M) and the least active compound 24 (IC<sub>50</sub>: 41  $\mu$ M) in the training set, respectively. All features of Hypo1 model were nicely mapped with the corresponding chemical functional groups on compound 1. By contrast, the compound 24 just mapped three

features while the other feature of Hydrogen Bond Acceptor was not mapped. Table-7 shows the experimental and estimated inhibitory activities of the 24 training set compounds. All highly active compounds were predicted correctly. In comparison to other compounds, compound 2 has shown high error value of +6.2. The error costs of all the other compounds in test set are below 3, indicating the hypothesis developed is effective.

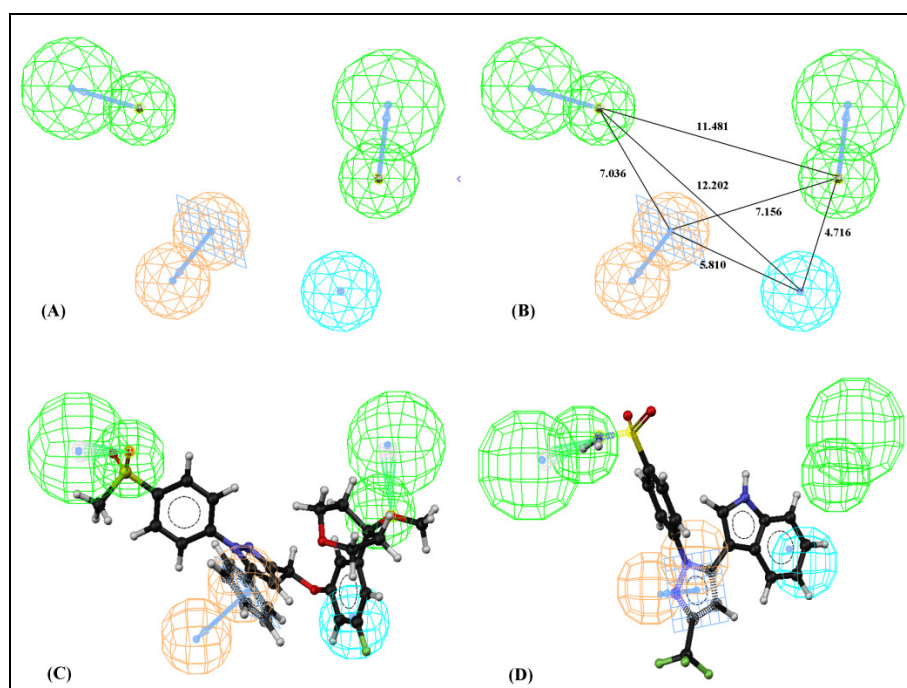


**Fig 42:** Pharmacophore model of 5-LOX inhibitors generated by HypoGen. (A) The best HYPOGEN model Hypo1. (B) 3D spatial relationship and geometric parameters of Hypo1. (C) Hypo1 mapping with the most active compound 1 (IC<sub>50</sub>: 0.005 μM) (D) Hypo1 mapping with the least active compound 24 (IC<sub>50</sub>: 41 μM). Pharmacophore features are color-coded with light-blue for hydrophobic feature, orange for ring aromatic feature and green for hydrogen-bond acceptor.

**Table-7:** Experimental and estimated (by Hypo1) IC<sub>50</sub> values (μM) together with the error values (defined as the ratio between experimental activity and estimated activity) of the training set compounds 1-24.

Molecule	<sup>a</sup> Exptl. IC <sub>50</sub> (μM)	<sup>b</sup> Estimated IC <sub>50</sub> (μM)	<sup>c</sup> Error	Fit Value	Reference
1	0.003	0.0019	-1.6	8.62	Barbey, <i>et al.</i> , 2002
2	0.01	0.062	+6.2	7.1	Ducharme <i>et al.</i> , 1994
3	0.014	0.018	+1.3	7.63	Ducharme <i>et al.</i> , 1994
4	0.015	0.005	-2.6	8.13	Hamel <i>et al.</i> , 1997
5	0.016	0.034	+2.1	7.36	Hutchinson <i>et al.</i> , 1993
6	0.027	0.028	+1	7.44	Dube <i>et al.</i> , 1998
7	0.036	0.062	+1.7	7.10	Hutchinson <i>et al.</i> , 1993
8	0.04	0.076	+1.9	7.01	Nakamura <i>et al.</i> , 2002
9	0.11	0.12	+1.1	6.81	Moreau <i>et al.</i> , 2006
10	0.13	0.13	-1	6.78	Kirchner <i>et al.</i> , 1997
11	0.3	0.57	+1.9	6.13	Rao <i>et al.</i> , 2005
12	0.33	0.24	-1.4	6.51	Ducharme <i>et al.</i> , 1994
13	0.77	0.46	-1.7	6.23	Charlier <i>et al.</i> , 2003
14	3.4	1.4	-2.5	5.75	Chawdhury <i>et al.</i> , 2009
15	6	10	+1.7	4.87	Janusz <i>et al.</i> , 1998
16	7.5	6.4	-1.2	5.08	Abe <i>et al.</i> , 2006
17	8	11	+1.4	4.83	Chawdhury <i>et al.</i> , 2008
18	8.5	10	+1.2	4.87	Janusz <i>et al.</i> , 1998
19	10	10	+1	4.87	Barbey, <i>et al.</i> , 2002
20	10	5.8	-1.7	5.12	Chawdhury <i>et al.</i> , 2008
21	10	11	+1.1	4.86	Chawdhury <i>et al.</i> , 2008
22	10	11	+1.1	4.85	Ulbrich <i>et al.</i> , 2002
23	22	10	-2.1	4.87	Janusz <i>et al.</i> , 1998
24	41	11	-3.8	4.85	Reddy <i>et al.</i> , 2008

<sup>a</sup> Exptl. = experimental activity (IC<sub>50</sub> values, μM).

<sup>b</sup> Estimated activity (IC<sub>50</sub> values, μM). <sup>c</sup> The negative value indicates that the experimental IC<sub>50</sub> is higher than the predicted IC<sub>50</sub>.

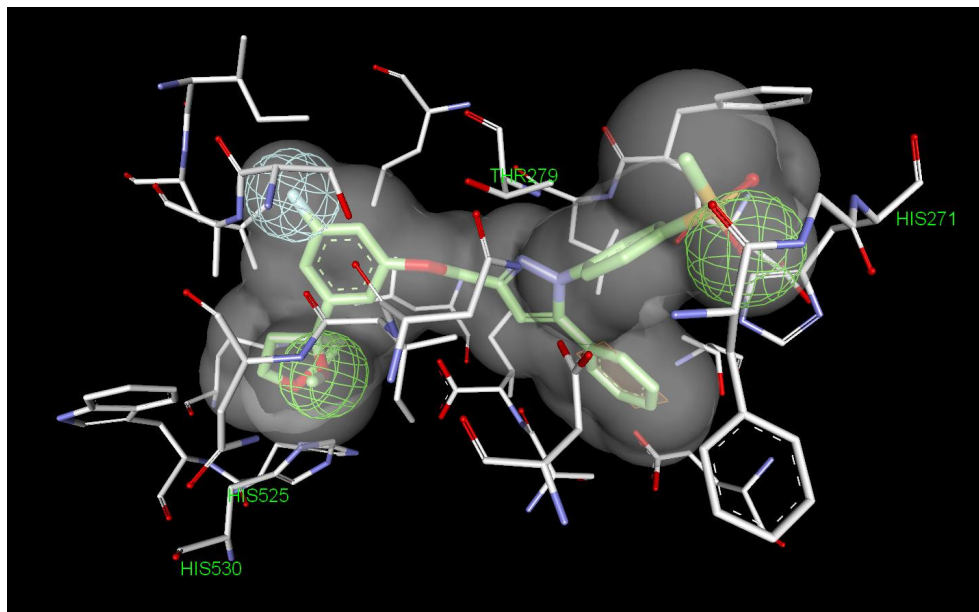


**Fig. 43:** Interactions of most active molecule (compound 1,  $IC_{50}$ :  $0.003\mu M$ ) in training set. Hydrogen Acceptors are shown in green, hydrophobic in blue and ring aromatic in brown

Interactions of the most active compound with the homology model of 5-LOX discussed earlier were studied. The interactions are in good agreement with the pharmacophore model of 5-LOX developed. Strong hydrogen bond interactions were formed with His271, His525 and His530 as shown in Fig. 43.

### 3.3.1 Validation of the model

Fischer randomization test method [Fischer, 1966] was used to evaluate the statistical relevance of Hypo1 by using the CatScramble program

implemented in Catalyst. The confidence level was set to 95%. Thereby CatScramble program generated 19 random spreadsheets to construct hypotheses using exactly the same conditions as used in generating the original pharmacophore hypothesis. The total costs of pharmacophore models obtained in the 19 HypoGen runs as well as the original HypoGen run are presented in Fig. 44. From Fig. 44, one can see that the original hypothesis is better than those of the 19 random hypotheses generated.

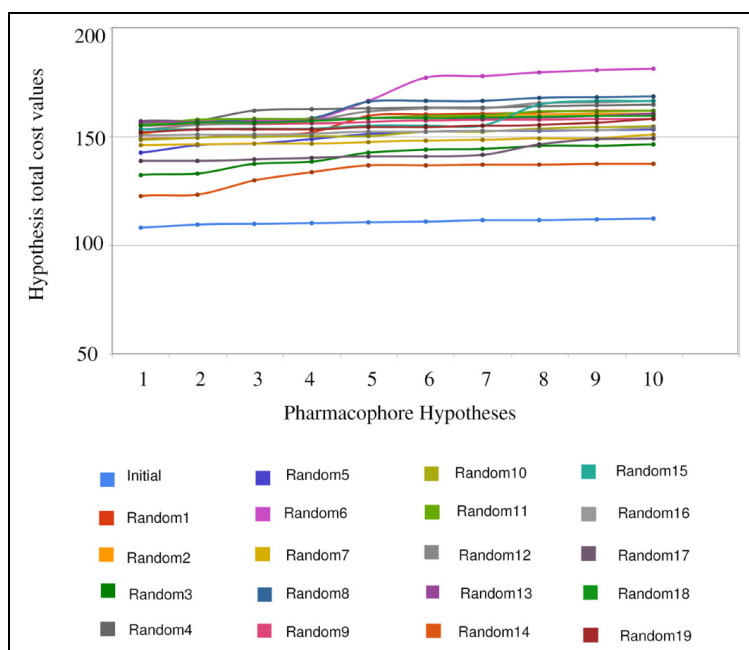


**Fig. 44:** The difference in total cost of hypotheses between the initial spreadsheet and 19 random spreadsheets after CatScramble run.

These results provide confidence on our pharmacophore model. An independent test set which contains 65 external compounds was used to validate the established model (Hypo1). The experimental and predicted

activities of the test set compounds are shown in Table-8. Further, a fairly good correlation coefficient of 0.75 was observed for regression analysis of the experimental and predicted inhibitory activity values for the test set compounds (Fig. 45). The high correlation coefficient value denotes the predictive capability of the model.

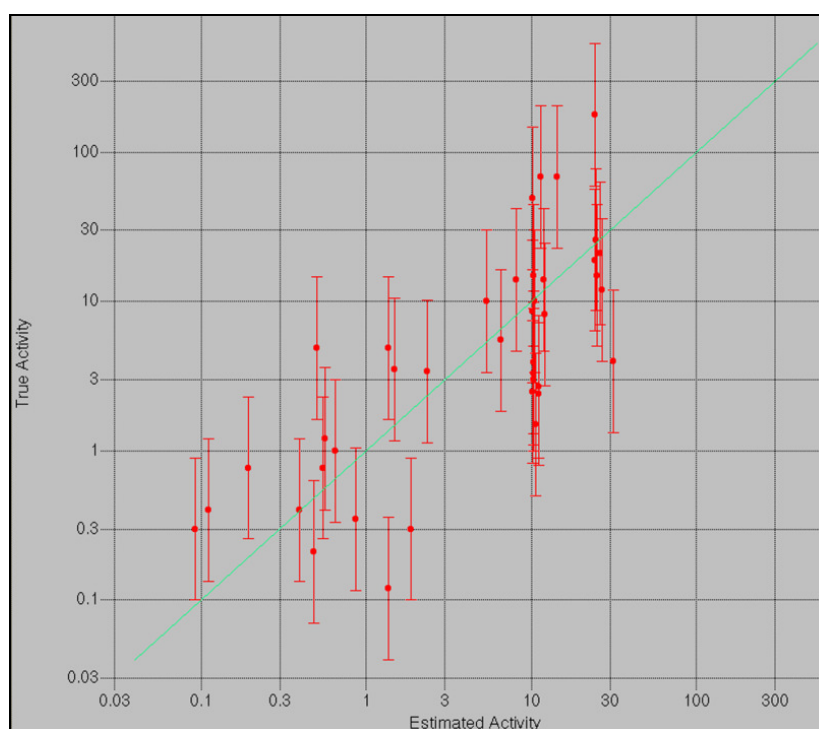


**Fig. 45:** Correlation plot(r) between the experimental activity and the predicted activity by Hypo1 for test set molecules (in red).

**Table-8:** Experimental and estimated (by Hypo1) IC<sub>50</sub> values (μM) together with the error values (defined as the ratio between experimental activity and estimated activity) of the test set compounds 01-65.

Compound	Experimental Activity (μM)	Estimated Activity (μM)	Error
1	21	26	1.2
2	26	25	-1
3	4	31	7.8
4	15	25	1.7
5	178	24	-7.3
6	19	24	1.3
7	12	27	2.2
8	49	10	-4.8
9	5.5	6.5	1.2
10	14	12	-1.2
11	2.7	11	4.1
12	1.5	11	7.1
13	2.9	0.31	-9.3
14	4.9	1.4	-3.6
15	30	5	-6
16	8.2	12	1.5
17	14	8.2	-1.7
18	2.4	11	4.6
19	2.06	1.5	-1.4
20	8	16	2

21	1	0.65	-1.5
22	15	10	-1.4
23	10	5.4	-1.9
24	68	12	-5.9
25	0.33	0.33	-1
26	0.37	0.35	-1.1
27	20	10	-1.9
28	3	10	3.4
29	68	14	-4.7
30	10.2	6.1	-1.7
31	68	11	-6
32	0.3	1.8	5.9
33	3.2	0.5	-6.4
34	3.3	10	3.1
35	3.4	2.3	-1.5
36	0.3	0.096	-3.1
37	3.5	1.5	-2.4
38	2	4	2
39	0.77	0.55	-1.4
40	10	11	1.1
41	0.02	0.015	-1.3
42	1.6	1	-1.6
43	0.77	0.19	-4
44	0.13	0.032	-4
45	2.5	10	4.1



46	0.85	0.21	-4
47	0.74	2.2	2.9
48	0.15	0.063	-2.4
49	0.27	0.074	-3.6
50	9	10	1.2
51	0.21	0.48	2.3
52	0.18	0.9	5
53	10	10	1
54	1.5	0.87	-1.7
55	0.14	0.047	-3
56	0.35	0.86	2.5
57	0.35	0.99	2.8
58	4.9	0.5	-9.7
59	0.4	0.11	-3.6
60	0.87	0.31	-2.8
61	1.2	0.57	-2.1
62	0.95	0.12	-7.8
63	0.57	0.065	-8.7
64	0.15	0.09	-1.7
65	0.023	0.017	-1.4

Results obtained by using the test set method show a fairly good correlation between the experimental and predicted  $IC_{50}$  values, indicating a good predictive ability. The validation results show the reliability of the model. Charlier *et al.*, (2006) have reported a pharmacophore model generated for 16 non redox 5-LOX inhibitors with Catalyst (HipHop module). It includes two hydrophobic groups, an aromatic ring, and two hydrogen bond acceptors. In their study they have only used HipHop module taking a narrow range of active compounds. In comparison, in this study, we have taken a diverse set of compounds, diverse in structure as well as activity and run the quantitative HypoGen. We have found out that two hydrogen bond acceptors, one ring aromatic and one hydrophobic feature are most important in the activity of 5-LOX inhibitors. In both the studies, hydrogen bond donor feature has been shown not to play a role for activity against 5-LOX.

In conclusion, the chemical features that a molecule should possess in order to be a 5-LOX enzyme inhibitor are all represented in our pharmacophore, although it has been generated using a ligand based approach and without considering structural information of the target.

### 3.4. Conclusion

In conclusion, in this study, chemical feature based pharmacophore modeling of inhibitors of 5-LOX has been carried out by using HypoGen module within Catalyst program package. The best HypoGen model, which was characterized by the lowest total cost (108.338), the lowest RMSD (0.602576) and the best correlation coefficient (0.974978), consists of two hydrogen bond acceptors, one hydrophobic and one ring aromatic feature. Both test set and cross validation methods have been used to validate the pharmacophore model, Hypo1. Results obtained by using the test set method show a fairly good correlation between the experimental and predicted IC<sub>50</sub> values, indicating a good predictive ability. The statistical confidence of Hypo1 has also been confirmed by using CatScramble program within Catalyst. Thus, the pharmacophore model that we developed should be helpful in identifying novel lead compounds with improved inhibitory activity through 3D database searches and useful in designing novel 5-LOX inhibitors.

# **Chapter-IV**

## **Identification of 5-LOX inhibitors: Pharmacophore based approach**

## 4.1. Introduction

Virtual screening is a strategy for bringing a more focused approach to HTS by using computational analysis to select a subset of compounds considered to be appropriate for a given receptor. Clearly, this strategy implies that some information is available regarding either the nature of the receptor binding site or the type of ligand that is expected to bind productively, or both [McInnes *et al.*, 2007; Villoutreix *et al.*, 2009]. It should be stressed that virtual screening encompasses a variety of computational screens, from the simplistic to the sophisticated and hence can usefully exploit different types of information describing the receptor [Klebe, 2006]. Likewise it can be used to produce either a much focused subset of compounds (for example, if only close structural analogs of a lead compound are of interest) or a very open ended subset (for example, a restriction on size, as described by molecular weight, may be the only constraint applied). Such issues relate to the objectives of a particular research project. For example, an HTS program may be already up and running, and the problem to be addressed is which set of 1,00,000 compounds from a database of one million should be assayed first. At the other end of the scale, a newly discovered receptor may have a low-throughput binding assay, and a far more focused set of compounds needs to be selected [Waszkowycz *et al.*, 2001]. In theory, the applicability of virtual screening is limited only by what properties of a compound can be calculated

computationally and the perceived relevance of those properties to the problem in hand.

On a practical level, further considerations include:

1. The timescale for calculation of the properties, which may be considerable for a database of, say, one million compounds
2. The accuracy or meaningfulness of the properties, particularly so when computationally cheap methods are applied
3. Methods for analysis of the data—not a trivial problem, since high-throughput modeling, as with HTS, generates very large volumes of data
4. The software and hardware required to yield a timely answer

The main computational filters that are available to virtual screening (in terms of increasing sophistication and computational cost) can be summarized as:

1. Selection on the basis of two-dimensional (2D) property profiles
2. Selection by means of a target-specific pharmacophore
3. Selection on the basis of more detailed three-dimensional (3D) modeling: e.g., receptor–ligand docking

These methods are described below.

#### 4.1.1. Selection on the basis of 2D property profiles.

Regardless of whether any useful information is available to describe the receptor or known ligands, it is often preferable to limit HTS to “drug-like” compounds. “Drug likeness” is used to indicate a broad range of properties or structural features that are generally important in various stages of drug optimization, such as stability, solubility, and lipophilicity, which can all influence drug absorption and excretion. Selection of drug-like compounds is particularly important when compounds are sourced from suppliers’ catalogs (where many compounds are more reagent-like than drug-like) or from a combinatorial library. The current trend in the pharmaceutical industry is for pharmacokinetic profiles and toxicological profiles to be evaluated at earlier stages in the drug discovery process. Therefore, it is useful to bring some of these concepts into the virtual screening stage, while accepting that the calculable properties currently available are at best only vague indicators of metabolic fate or toxicity [Waszkowycz *et al.*, 2001].

Lipinski’s “rule-of-five” is a well-known rule-of thumb that encodes a simple profile for orally bioavailable compounds, basing the classification on a limit on molecular weight, lipophilicity (in terms of the partition coefficient,  $\log P$ ), and hydrophilicity (in terms of counts of hydrogen bond donors and

acceptors) [Lipinski *et al.*, 2000]. These properties can be calculated quickly and can be easily applied to filtering a large database. Likewise, filters can be applied on specific chemical substructures, e.g., those associated with problems in chemical stability or toxicity. This approach is useful if the limitations are borne in mind and is particularly appropriate for dividing and prioritizing a very large database into subsets that fulfill different design criteria.

#### **4.1.2. Selection by means of a target-specific pharmacophore.**

A pharmacophore is a simplified 3D description of the key structural features of a set of known ligands or of the target receptor. The structural features are usually described in terms of discrete hydrogen bond donors or acceptors, lipophilic centers, ring centroids and so on, separated in terms of distances (more usually, distance ranges). Usually a small number of such sites are defined, e.g. two to five. Typically these sites are derived from a set of ligands and hence represent those features common to the ligands that are deemed to be relevant to activity [Marshall *et al.*, 1990].

A pharmacophore is readily used to search a database of chemical structures. These structures need to contain 3-D models, and preferably a conformationally flexible search is necessary so that compounds are not



rejected on the trivial basis that an inappropriate conformer is stored in the database. The value of the pharmacophore search is that a reasonably focused query on 3-D structural grounds can be applied relatively quickly to a large database (Fig. 46). The limitations are that the query may rapidly become over-defined. It is often the case that a typical three or four-point pharmacophore will be too restrictive and yield few interesting hits, whereas a slightly more open-ended query may yield too many hits.

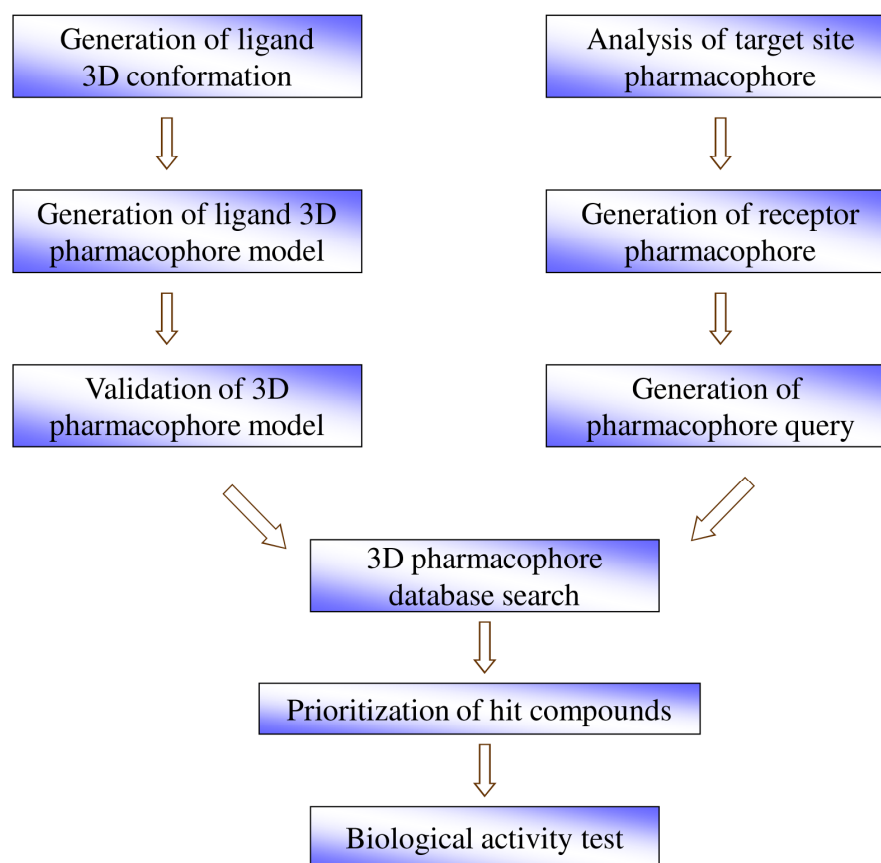


**Fig. 46:** Process for the ligand and receptor pharmacophore based virtual screening. A typical process consists of the preparation of pharmacophore model, three-dimensional database screening and selection of hit compounds. (Modified from Kim *et al.*, 2010)

Either way, the problem with managing the hit list is that there is usually no effective way of ranking or scoring the hits, other than methods based on evaluation of similarity to the initial ligands. Therefore, there is a tendency for pharmacophore searches to yield solutions similar to those already known, rather than a well-focused set of novel solutions.

#### **4.1.3. Selection by means of receptor–ligand docking**

The next stage up from a pharmacophore search in terms of computational expense is explicit docking of the compound database to the biological target of interest (Fig. 47). This stage involves objective docking of each compound (either as a rigid or conformationally flexible model) into a model of the receptor that is treated either as rigid or with limited side-chain flexibility. Generally the extent of the expected binding site is defined to limit the search. This virtual screening strategy requires a 3D database of ligands, a 3-D structure of the target receptor (either derived experimentally or from a model built by homology to related protein structures) and a docking software comprising an efficient searching algorithm and an accurate scoring function.

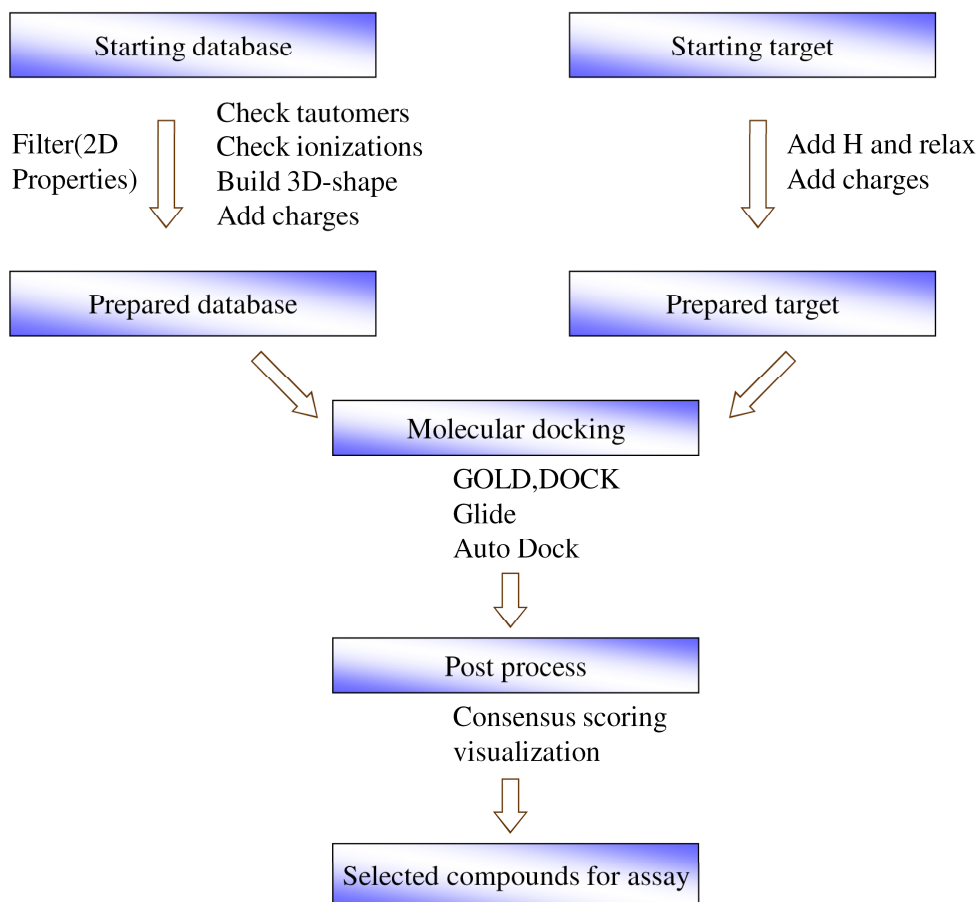


**Fig. 47:** *Process for the structure based virtual screening.* A pictorial description of the workflow of a structure based virtual screen run. The typical workflow consists of a preparation phase for the database and the target, followed by a molecular docking phase and concludes with the post-processing and compound selection phases (Modified from Lyne, 2002).

The attraction of explicit receptor–ligand docking is that it represents the most detailed and relevant computational model for identifying a receptor-focused subset. In addition, it is also one of the least biased approaches. Application of pharmacophore queries or focused 2D property profiles may significantly inhibit the diversity of the compound subset because they are biased by the

properties of known ligands. In contrast, the molecular docking program can process an entire chemical database with minimal prefiltering (e.g., to eliminate unstable or toxic moieties) so that the final selection is based on the quality of the docked models rather than a subjective opinion of what properties are expected in a ligand. This route is a very promising one in finding structurally novel ligands, which may make receptor interactions similar to known ligands or may achieve different interactions within other binding sites. Some of the published virtual screening studies are summarized in Fig. 48.

Target	Software Package	Ligand Data Set
Thymidylate synthase	DOCK	153 000 ACD compounds
FK506-binding protein	SANDOCK	ACD and Cambridge Crystallographic Database
Retinoic acid receptor	ICM	153 000 ACD compounds
HIV-1 RNA transactivation response element	ICM	153 000 ACD compounds
Farnesyl transferase	EUDOC	67 928 ACD compounds
DNA gyrase	LUDI, CATALYST	350 000 ACD + in-house compounds
Kinesin	DOCK	110 000 ACD compounds
Hypoxanthine-guanine-xanthine phosphoribosyl transferase	DOCK	599 compound virtual library
Thrombin; factor Xa; estrogen receptor	PRO_LEADS	10 000 ChemBridge compounds
Estrogen receptor (agonist and antagonist forms)	PRO_LEADS	1.1 million ACD-SC compounds

**Fig. 48:** Summary of recently published virtual screening studies based on receptor–ligand docking (taken from Waszkowycz *et al.*, 2001)

The output of a docking-based screen is a set of 3D models of the predicted binding mode of each compound against the receptor, together with a ranking that is a measure of the quality of fit, if not a prediction of the binding affinity itself. The 3D models represent the most detailed basis available for determining which molecules are capable of fitting within the very strict structural constraints of the receptor binding site. For a particular receptor, ligand binding modes may be further classified with respect to the specific receptor contacts that are achieved. Thus, the 3D models represent a very valuable source of data for understanding the nature of ligand binding in a given receptor and, hence, as a source of inspiration for the design of analogs or indeed novel ligands.

#### **4.1.4. Recent applications of pharmacophore based virtual screening**

In recent years, the number of studies on pharmacophore based virtual screening for various disease targets has dramatically increased. Advances in the screening tools that rely on chemical feature-based pharmacophore models have significantly influenced the rational design of new molecular entities. Catalyst, leading software for chemical feature based pharmacophore modeling, is arguably the most widely used program. A number of previous studies focused on the validation of pharmacophore-based virtual screening –

by evaluating pharmacophore models, by pharmacophore identification and by the associated methodologies for screening – with respect to the reproduction of the binding affinity or enrichment of hit lists from a database of decoys.

As the 3D structure of 5-LOX was computationally derived (Chapter-I), to decrease the changes of biased output in virtual screening, in this study, pharmacophore based virtual screening was employed for the screening of commercial databases. Structure based virtual screening was only used as a later stage approach to rank the hits, so that false hits can be eradicated. After virtual screening, five of the potential molecules identified were procured and were validated for 5-LOX inhibition in 5-LOX enzyme. Later, the molecules showing 5-LOX inhibition were tested for their anti-proliferative effects in COLO cell line. 5-LOX over expression has been reported in colon polyps and colon cancer cell lines and 5-LOX inhibitors were shown to be anti-proliferative in colon cancer cell lines [Melstrom *et al.*, 2008], hence the 5-LOX inhibitors identified were checked for their anti-proliferative effects in COLO cell line.

## 4.2. Methodology

### 4.2.1. Virtual screening

In this work, we performed ligand- based virtual screening of a large database of lead-like commercially available compounds to identify novel 5-LOX inhibitors. In second stage the top ranked hits from pharmacophore based screening were docked and scored so as to remove any false hits. The virtual screening workflow is depicted in Fig. 49.

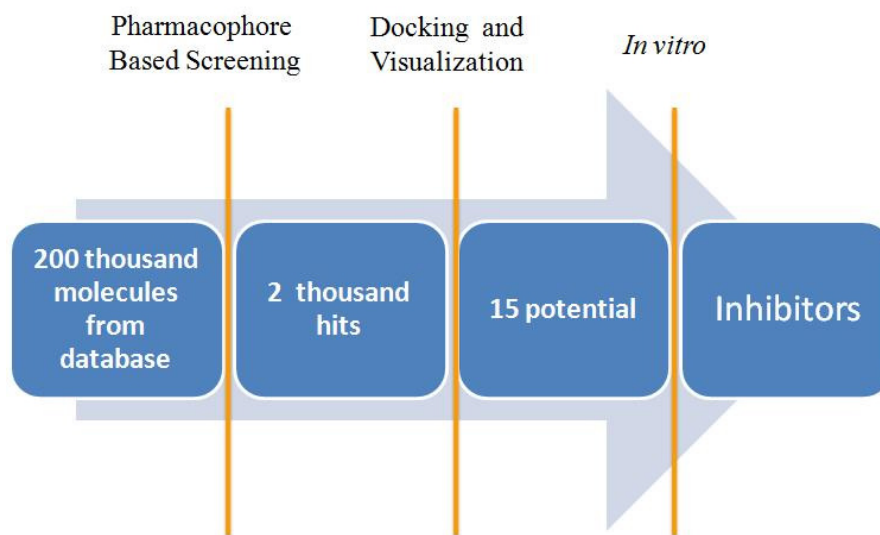


**Fig. 49** : The virtual screening work flow. First, the pharmacophore filter is used. The false positives are removed by the second filter, docking and visualization.

#### Methodologies employed

- (a) on the basis of 2D property profiles : Lipinski rule of five
- (b) means of a target-specific pharmacophore
- (c) means of receptor–ligand docking

The Pharmacophore query was used as a 3-D structural query in the screening of NCI, Maybridge and Enamine databases. NCI and Maybridge databases comprise 2,38,819 and 59,652 molecules respectively. The chemical function based pharmacophore model was used for database searching by the best flexible search method in Catalyst. Drug like small molecule databases comprising molecules which follow Lipinski's rule of 5 were obtained from Enamine Ltd., Ukraine. These databases contain molecules which follow Lipinski's rule of 5.

The top 5,000 molecules with molecular weight with in 250 to 600 were taken. In the second step, we conducted structure-based virtual screening by docking the top molecules with the above described homology model of 5-LOX. Docking of the molecules into 5-LOX was carried out using GOLD version 3.1 (Cambridge Crystallographic Data Center, Cambridge, United Kingdom) [Jones *et al.*, 1997]. GOLD is based on the genetic algorithm. It performs docking of flexible ligands into proteins with partial flexibility in the



neighborhood of the active site. The parameters used for GA were population size (100), selection pressure (1.1), number of operations (100,000), number of islands (5) and niche size (2). Operator parameters for crossover, mutation and migration were set to 95, 95 and 10 respectively. To quantitate the interactions in the protein-ligand complexes, the scoring function GOLD score was employed. Default cutoff values of 2.5 Å ( $d_{H-X}$ ) for hydrogen bonds and 4.0 Å for Vander Waals were employed. During docking, the default algorithm speed was selected and the ligand binding site in the 5-LOX was defined as discussed in docking studies section of Chapter I. The number of poses for each inhibitor was set to 100, and early termination was allowed if the top three bound conformations of a ligand were within 1.5 Å RMSD. After docking, the individual binding poses of each ligand were observed and their interactions with the protein were studied. The best and most energetically favorable conformation of each ligand was selected. Top 1000 molecules were taken and were complexed with 5-LOX.

In the third step, the complexes were taken and scored using Ludi and Ligandfit in Accelrys Discover Studio. Since there is no generally applicable scoring function so far, the compounds which were commonly scored top by various applications were ranked higher. After screening the protein-ligand interactions were visualized and potential compounds were identified.

Among the potential compounds identified only few compounds were readily available with the vendors. 5 compounds were selected (L11-L15) and purchased from Enamine Ltd., Ukraine to further test their efficacy with 5-LOX and thus to validate the pharmacophore model developed.

#### 4.2.2. Biological evaluation

##### 4.2.2.1. *In vitro* 5-LOX inhibitory assay

5-LOX was purified and assayed as per the method described by Reddanna *et al.*, (1990). Enzyme activity was measured using polarographic method with a Clark's oxygen electrode on Strathkelvin Instruments, model 782, RC-300. Typical reaction mixture contained 50–100  $\mu$ l of enzyme and 10  $\mu$ l of substrate (133  $\mu$ M of arachidonic acid) in a final volume of 3 ml with 100 mM phosphate buffer pH 6.3. Rate of decrease in oxygen concentration was taken as a measure of enzyme activity. Stock solutions of test compounds L11-L15 were prepared immediately before use, were dissolved in DMSO. Various concentrations of test drug solutions were added and the LOX reaction was initiated by the addition of substrate. The reaction was allowed to proceed at 25 °C and the maximum slope generated was taken for calculating activity. Percent inhibition was calculated by comparison of LOX activity in the

presence and absence of inhibitor. The concentration of the test compound causing 50% inhibition ( $IC_{50}$ ,  $\mu M$ ) was calculated from the concentration-inhibition response curve. Each assay was repeated thrice.

#### 4.2.2.2. In vitro anti-proliferative effects on COLO cell line

COLO-205 cell line used in this study was maintained in monolayer in tissue culture Petri dishes. Medium for the cell line was RPMI-1640 supplemented with 10% heat inactivated fetal bovine serum (FBS) 100 IU/ml penicillin, 100  $\mu g/ml$  streptomycin and 2 mM L-glutamine. The cell line was maintained in a humidified atmosphere with 5%  $CO_2$  at 37 °C. The cultured cells were passaged twice a week, seeding at a density of  $5 \times 10^3$  cells per well in 96 well plate before the day of experiment. Before the treatment with test compound cells were washed with PBS and fresh medium was added.

Cell proliferation was assessed using the 3-(4,5-dimethylthiazol-2-yl)-2,5- diphenyl tetrazolium bromide (MTT) staining as described by Mosmann *et al.* (1983). The MTT assay is based on the reduction of the tetrazolium salt, MTT, by viable cells. The NADH or NADPH generated in the living cells, convert the yellow form of the MTT salt to insoluble, purple formazan crystals. The absorbance of the formazan solution can be measured

spectrophotometrically after dissolving the crystals in an organic solvent (DMSO). Cells ( $5 \times 10^3$  cells per well) were incubated in 96-well plates in the presence or absence of the test compounds (0.1-100  $\mu\text{M}$ ) for 24 h in a final volume of 100  $\mu\text{l}$ . At the end of the treatment, 20  $\mu\text{l}$  of MTT (5 mg/ml in PBS) was added to each well and incubated for an additional 4 h at 37 °C. The purple-blue MTT formazan precipitate was dissolved in 100  $\mu\text{l}$  of DMSO. The activity of the mitochondria, reflecting cellular growth and viability, was evaluated by measuring the optical density at 570 nm on Quant Bio-tek Instruments, Inc. micro titer plate reader. Each concentration was tested in three different experiments run in three replicates.

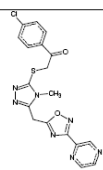
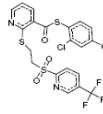
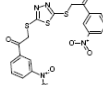
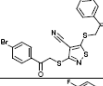
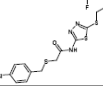
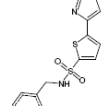
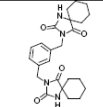
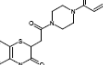
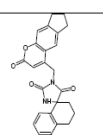
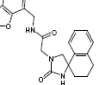
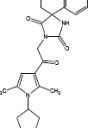
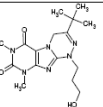
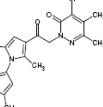
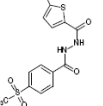
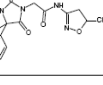
## 4.3. Results and discussion

### 4.3.1. Screening and identification of potential 5-LOX inhibitors

Three chemical databases (Maybridge, NCI, Enamine) containing 2 million compounds in total were screened utilizing the 5-LOX pharmacophore model developed as a query and 15,162 unique structures (8% of all virtually screened compounds) were able to match the pharmacophore model. The top 5000 molecules were further docked into 5-LOX active site using GOLD software. Most of the molecules showed positive Gold Score and were ranked

using GoldScore function. The top 1000 molecules were complexed with 5-LOX and the protein-ligand interactions were scored using LUDI of Accelrys Discover Studio. The molecules which were commonly scored higher by all the programs were identified and were ranked as potential. As the molecules from the drug like databases of Enamine Ltd., Ukraine were readily available and followed Lipinski's rule of 5, potential molecules from that database were given preference in the study.

**Table-9:** Some of the potential hits (L1 to L15) identified

Compounds	Structure	GOLD score	LUDI score
L1		76	821
L2		77	906
L3		90	832
L4		84	842
L5		78	827
L6		81	682
L7		72	702
L8		72	723
L9		75	743
L10		70	950
L11		79	807
L12		71	712
L13		74	747
L14		64	628
L15		68	717

Some of the potential molecules (L1-L15) are listed in Table- 9. Of the potential molecules identified, 5 compounds (L11-L15) that were available readily and structurally diverse were procured. In order to know whether any biological activity of the molecules was previously reported these compounds were used as queries for a SciFinder database search. None of the selected molecules could be retrieved in the search. The selected molecules and their properties like LogP, Mol Wt., number of hydrogen bond acceptors, hydrogen bond donors, no. of rotatable bonds and number of violations of Lipinski's rule are summarized in Fig. 51.

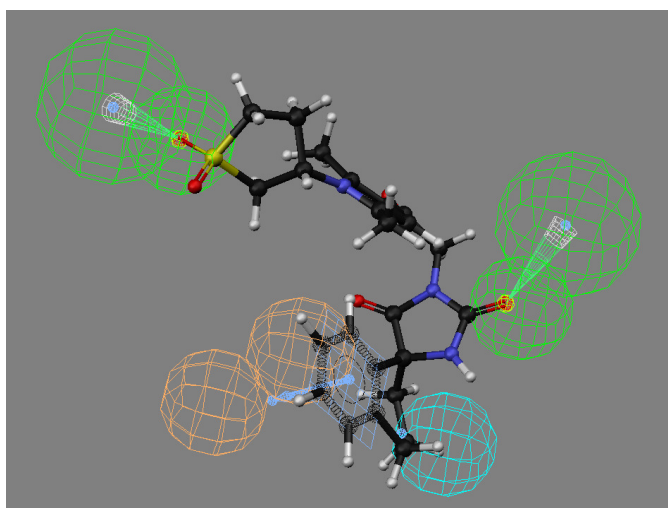


**Fig. 50:** One of the potential molecules identified, L11 mapped on to the pharmacophore model. Pharmacophore features are color-coded with light-blue for hydrophobic feature, orange for ring aromatic feature and green for hydrogen-bond acceptor.

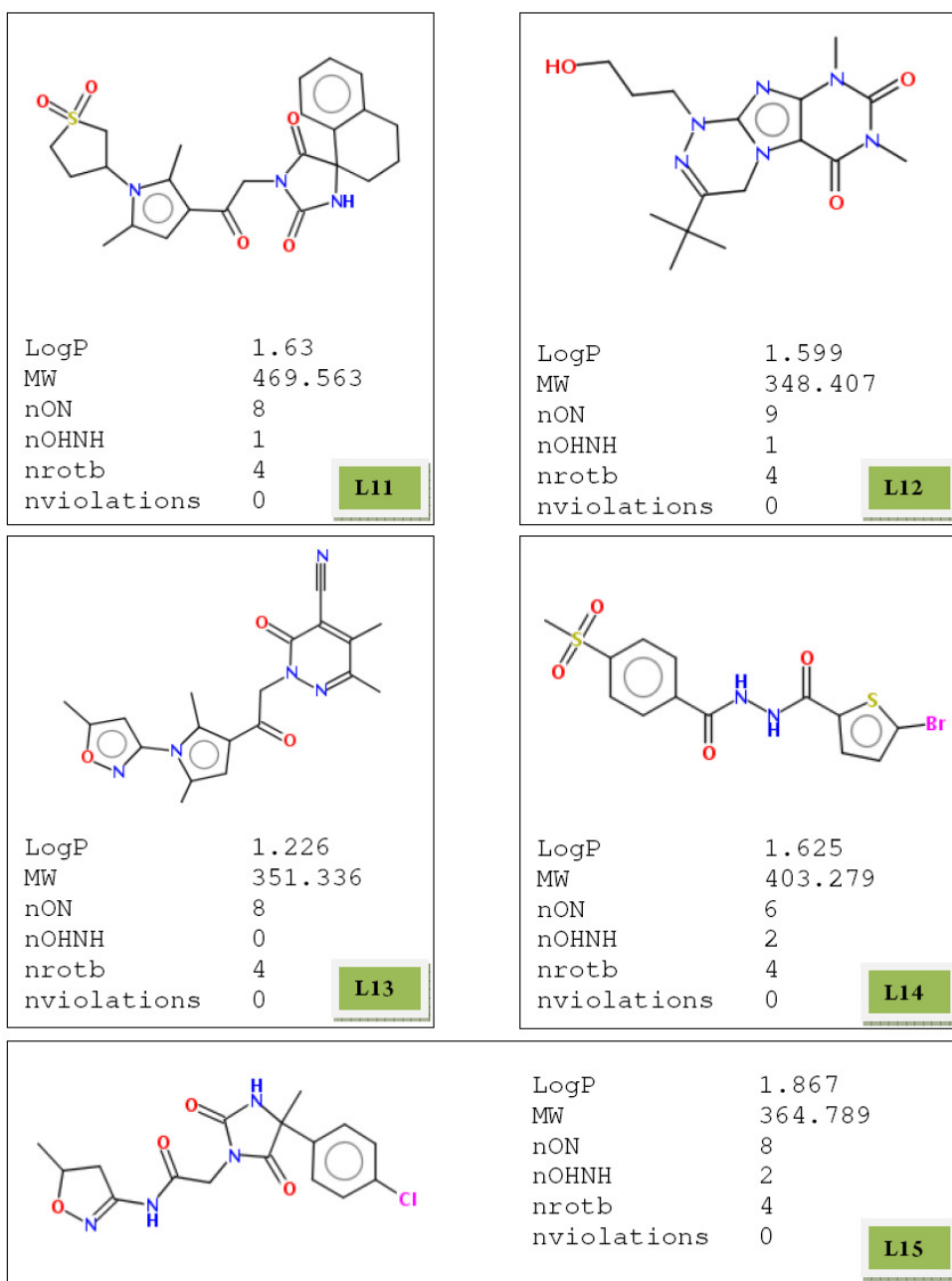


**Fig. 51:** Selected molecules (hits) and their molecular properties. All the properties lie within Lipinski's rule of 5 range with no violations

### 4.3.2. Biological evaluation of the hits

#### 4.3.2.1. *In vitro* assay

The potential 5-LOX inhibitory molecules, selected basing on *in silico* pharmacophore screening, were tested *in vitro* for their inhibitory properties against 5-LOX enzyme using the assay described by Reddanna *et al.*, (1990). Out of the five molecules tested only L11 and L13 showed inhibition at a concentration of 100  $\mu$ M. The other three compounds (L12, L14 and L15) showed no inhibition up to 100  $\mu$ M concentration. The most active molecule of the two, L11 showed potent inhibition of 5-LOX (Fig. 52) with an  $IC_{50}$  value of 14  $\mu$ M.

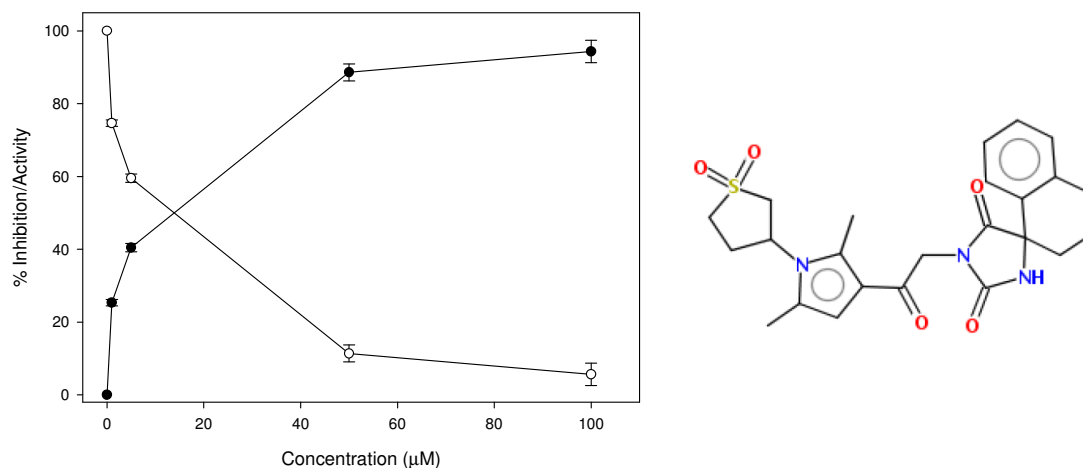


**Fig. 52:** Effect of L11 on 5-LOX activities. Data are the mean of three independent assays.



L13 showed inhibition activity towards 5-LOX with an  $IC_{50}$  of 35  $\mu M$  (Fig. 53).

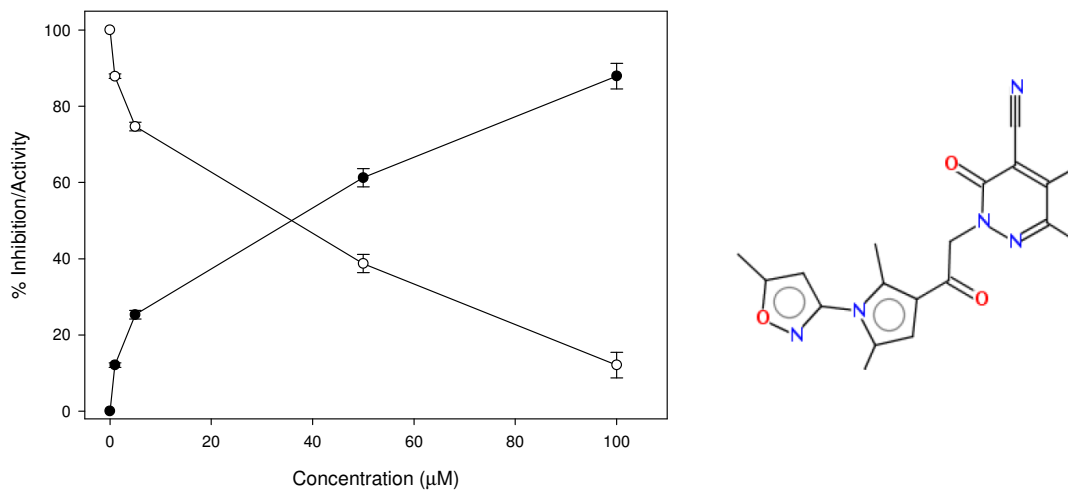


**Fig. 53:** Effect of L13 on 5-LOX activities. Data are the mean of three independent assays

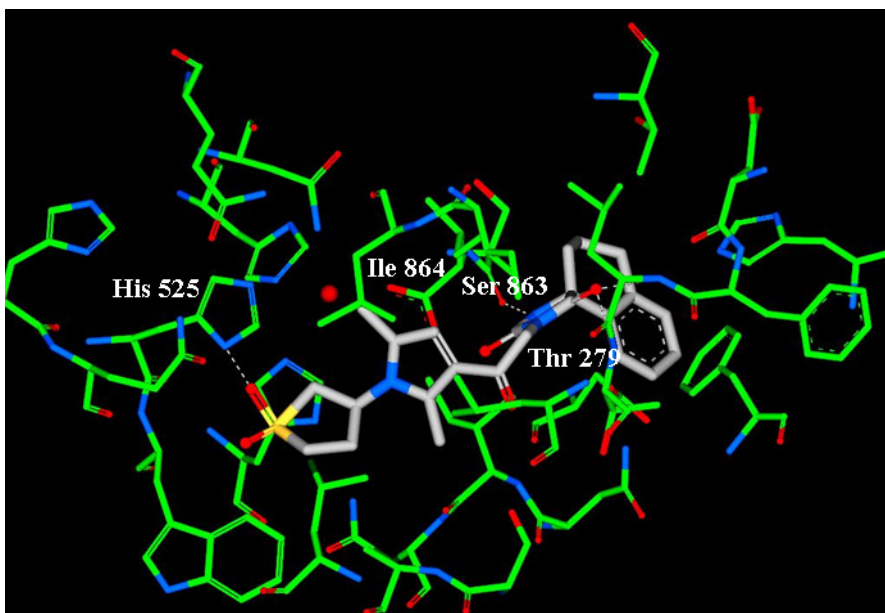


**Fig. 54:** Interactions of L11 with 5-LOX. The labeled amino acids Thr279, His525, Ser863 and Ile864 form hydrogen bond interactions within 5-LOX active site

#### 4.3.2.2. *In vitro* anti-proliferative effects

To test the anti-cancer/ anti-proliferative effects of the 5-LOX inhibitors, cancer cell line- COLO-205 (colon cancer) was used. The cells were incubated with different concentrations of compounds for 24 h and the cell viability was measured by MTT assay. The  $GI_{50}$  values for different compounds obtained were shown in Fig. 55. As can be seen in the figure L11 and L13 showed anti-proliferative effects in a dose dependent manner, with  $GI_{50}$  of 46.5  $\mu$ M and 67.0  $\mu$ M respectively.

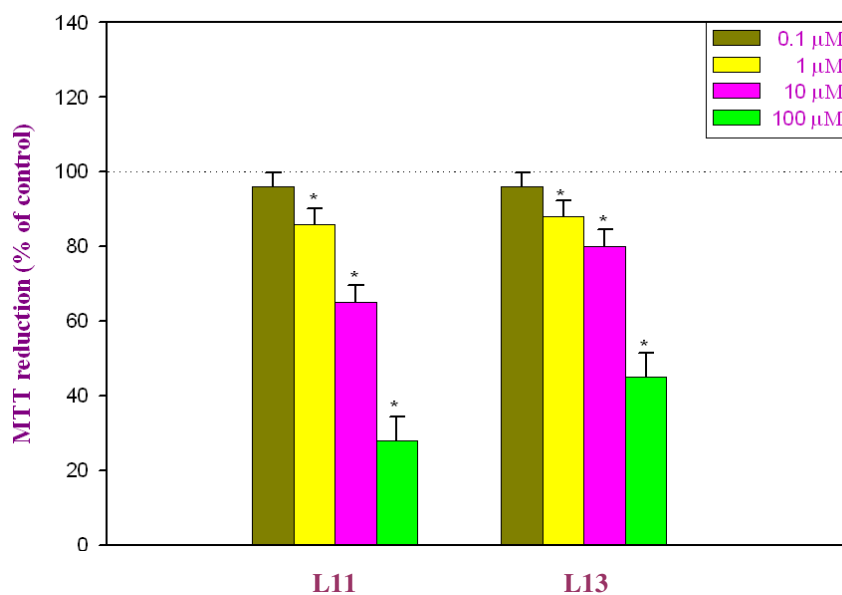


**Fig. 55:** Effect of the two molecules on the proliferation of COLO-205 cell line. The cells were incubated with different concentrations of compounds for 24 h and the cell viability was measured by MTT assay. Dose dependent growth inhibition was observed in the tested cell line. The number of cells in the control was taken as 100%. The values represent the mean  $\pm$  S.E.M from three independent experiments.

\*Indicates statistical significance with  $P < 0.05$ .

5-LOX association with asthma, GERD and various other inflammatory disorders is well known. Recently, several studies have shown that eicosanoids produced by 5-LOX play important roles in the development of cancer [Goosens *et al.*, 2007]. Earlier reports suggest that 5-LOX is up-regulated in colorectal cancer and that inhibition of its expression might be valuable in the prevention and treatment of colorectal cancer [Soumaoro *et al.*, 2006]. Two studies have shown a relationship between 5-LOX over expression in colon cancer and poor prognosis. Hence the 5-LOX inhibitors identified by pharmacophore based virtual screening have been screened for their anti-proliferative properties. These studies showed a dose dependent inhibition in the growth of COLO-205 cell line by both L11 and L13 and showed GI<sub>50</sub> of 46.5  $\mu$ M and 67  $\mu$ M respectively. Further studies however are needed to understand the mechanism(s) involved in the growth inhibition of COLO-205 cells by the 5-LOX inhibitors identified in this study.

#### 4.4. Conclusion

In the present study, 5-LOX inhibitors were successfully identified by employing pharmacophore based virtual screening which validates the pharmacophore model generated and explains its usefulness in predicting activities of large datasets of molecules. In Summary, by using pharmacophore based virtual screening and docking, two compounds L11 and L13 were

identified as 5-LOX inhibitors with  $IC_{50}$  of 14  $\mu$ M and 35  $\mu$ M respectively. The molecules also showed anti proliferative effects on COLO-205 cell line. These studies thus validate the pharmacophore model generated and suggest the usefulness of the model in screening of various small molecule libraries.

A decorative graphic in the top-left corner of the page. It consists of two solid red squares of equal size, positioned side-by-side. A thin, dark vertical line extends downwards from the bottom edge of the left square, continuing past the 'Overall Conclusions' header.

## Overall Conclusions

5-Lipoxygenase (5-LOX) is the key enzyme involved in the biosynthesis of leukotrienes, the mediators of allergy, asthma, GERD, Crohn's disease and other inflammatory disorders. Recent studies have shown its role in cancer stem cells in CML. 5-LOX is also shown associated with various cancers. As 5-LOX is implicated in many inflammatory disorders, there is growing emphasis by many pharmaceutical companies and academic research groups on the development of effective 5-LOX inhibitors. Lack of crystal structure information of 5-LOX, however, has been an obstacle for the application of structure based drug design strategies. Homology models of lipoxygenase enzymes have been used in several previous studies for purposes other than inhibitor discovery. Specifically, homology models were sometimes used in combination with docking methods, to propose models for substrate binding in various LOXs.

In the present study, homology modeling strategy was employed to generate 3D model of 5-LOX, which was further used in various lead optimization studies. An inactive molecule with  $IC_{50}$  of 760  $\mu$ M was modified into active molecule of  $IC_{50}$  of 6.4  $\mu$ M using site point connection methods. Even though the studies did not yield novel lead structures with nano molar activity, the designed structures will probably represent examples of a prospective lead series with micro molar activities that require further

optimization. The model can be considered as a working tool for generating hypotheses and designing further experimental studies and more precise predictions of function and binding affinities of inhibitors. The structure based lead optimization studies presented provides a pathway to design novel anti-asthma/ anti-cancer compounds.

Based on the fact the chemical properties of the designed molecules are appropriate, it is reasonable to classify them as drug-like compounds. Our work will hopefully find application in the platform construction for structure-based 5-LOX inhibitor discovery.

Pharmacophore model is widely employed to quantitatively explore common chemical characteristics among a considerable number of structures with great diversity. Such a model could also be used as a query for searching chemical databases and find new chemical entities. In our study, 5-LOX pharmacophore model was developed using HypoGen module in Catalyst. Then the best quantitative pharmacophore model generated was used as a 3D query to screen several commercial databases.

Our ligand based virtual screening studies resulted in the identification of two 5-LOX inhibitors with an  $IC_{50}$  of 14  $\mu$ M and 35  $\mu$ M respectively. Of only

5 molecules tested for *in vitro* activity against 5-LOX, two molecules showed inhibition of IC<sub>50</sub> less than 100  $\mu$ M. The 5-LOX inhibitors also showed anti-proliferative effects on COLO-205 cell line, a colon cancer line in which 5-LOX is known to be over expressed with a GI<sub>50</sub> of 46.5  $\mu$ M and 67  $\mu$ M respectively. Our results suggest that virtual screening against the pharmacophore models is capable of identifying potential inhibitors at a rate higher than in random compound selection. The pharmacophore model can be helpful in identifying novel 5-LOX inhibitors through 3D database searches and useful in designing more potential molecules.

These studies thus provide a homology model and pharmacophore model, which will be helpful in designing novel 5-LOX inhibitors. This study assumes importance in the light of key role played by 5-LOX in various pathological manifestations and lack of crystal structure for use in molecular modeling and design studies.



## 6. References

- ✚ Abe, M., Ozawa, Y., Uda, Y., Morimitsu, Y., Nakamura, Y., and Osawa, T. 2006. A novel labdane-type trialdehyde from myoga (*Zingiber mioga* Roscoe) that potently inhibits human platelet aggregation and human 5-lipoxygenase. *Biosci Biotechnol Biochem* 70, 2494-2500.
- ✚ Accelrys Inc. InsightII; version 2000ed.: San Diego, CA.
- ✚ Anderson, K.M., Seed, T., Vos, M., Mulshine, J., Meng, J., Alrefai, W., Ou, D., and Harris, J.E. 1998. 5-Lipoxygenase inhibitors reduce PC-3 cell proliferation and initiate nonnecrotic cell death. *Prostate* 37, 161-173.
- ✚ Aparoy, P., Reddy, R.N., Guruprasad, L., Reddy, M.R., and Reddanna, P. 2008. Homology modeling of 5-lipoxygenase and hints for better inhibitor design. *J Comput Aided Mol Des* 22, 611-619.
- ✚ Avis, I.M., Jett, M., Boyle, T., Vos, M.D., Moody, T., Treston, A.M., Martinez, A., and Mulshine, J.L. 1996. Growth control of lung cancer by interruption of 5-lipoxygenase-mediated growth factor signaling. *J Clin Invest* 97, 806-813.
- ✚ Barbey, S., Goossens, L., Taverne, T., Cornet, J., Choesmel, V., Rouaud, C., Gimeno, G., Yannic-Arnoult, S., Michaux, C., Charlier, C., Houssin, R., and Henichart, J.P. 2002. Synthesis and activity of a new methoxytetrahydropyran derivative as dual cyclooxygenase-2/5-lipoxygenase inhibitor. *Bioorg Med Chem Lett* 12, 779-782.
- ✚ Barhate, N. B., Madhava Reddy, C., Srinivasa Reddy, P., Wakharkar, R. D. and Reddanna, P. 2002. Synthesis and biochemical evaluation of benzyl propargyl ethers as inhibitors of 5-lipoxygenase. *Indian J Biochem Biophys* 39, 264-273.
- ✚ Bellows, M.L., and Floudas, C.A. 2009. Computational Methods for De Novo Protein Design and its Applications to the Human Immunodeficiency Virus 1, Purine Nucleoside Phosphorylase, Ubiquitin Specific Protease 7, and Histone Demethylases. *Curr Drug Targets*.
- ✚ Berman, H.M., Westbrook, J., Feng, Z., Gilliland, G., Bhat, T.N., Weissig, H., Shindyalov, I.N., and Bourne, P.E. 2000. The Protein Data Bank. *Nucleic Acids Res* 28, 235-242.

- ✚ Bindu, P.H., Sastry, G.M., and Sastry, G.N. 2004. Characterization of calcium and magnesium binding domains of human 5-lipoxygenase. *Biochem Biophys Res Commun* 320, 461-467.
- ✚ Biocampus Manual, Protein Modelling and Rational Drug Design, Volume II, 2003.
- ✚ Blundell, T.L., Sibanda, B.L., Sternberg, M.J., and Thornton, J.M. 1987. Knowledge-based prediction of protein structures and the design of novel molecules. *Nature* 326, 347-352.
- ✚ Boeglin, W.E., Kim, R.B., and Brash, A.R. 1998. A 12R-lipoxygenase in human skin: mechanistic evidence, molecular cloning, and expression. *Proc Natl Acad Sci U S A* 95, 6744-6749.
- ✚ Bohm, H.J. 1992. LUDI: rule-based automatic design of new substituents for enzyme inhibitor leads. *J Comput Aided Mol Des* 6, 593-606.
- ✚ Brash, A.R. 1999. Lipoxygenases: occurrence, functions, catalysis, and acquisition of substrate. *J Biol Chem* 274, 23679-23682.
- ✚ Brooks, B. R., Bruccoleri, R. E., Olafson, B. D., States, D. J., Swaminathan, S., Karplus, M. 1983. CHARMM: A program for macromolecular energy, minimization, and dynamics calculations. *J Comput. Chem* 4; 187-217.
- ✚ CATALYST 4.11; Accelrys: San Diego, CA, 2005, <http://www.accelrys.com>.
- ✚ Cavasotto, C.N., and Phatak, S.S. 2009. Homology modeling in drug discovery: current trends and applications. *Drug Discov Today* 14, 676-683.
- ✚ Chen, X., Reddanna, P., Reddy, G.R., Kidd, R., Hildenbrandt, G., and Reddy, C.C. 1998. Expression, purification, and characterization of a recombinant 5-lipoxygenase from potato tuber. *Biochem Biophys Res Commun* 243, 438-443.
- ✚ Charlier, C., and Michaux, C. 2003. Dual inhibition of cyclooxygenase-2 (COX-2) and 5-lipoxygenase (5-LOX) as a new strategy to provide safer non-steroidal anti-inflammatory drugs. *Eur J Med Chem* 38, 645-659.

- ✚ Charlier, C., Henichart, J.P., Durant, F., and Wouters, J. 2006. Structural insights into human 5-lipoxygenase inhibition: combined ligand-based and target-based approach. *J Med Chem* 49, 186-195.
- ✚ CHARMM user guide, Accelrys, Inc., San Diego, USA; 1999
- ✚ Chang, M., Rao, M.K., Reddanna, P., Li, C.H., Tu, C.P., Corey, E.J., and Reddy, C.C. 1987. Specificity of the glutathione S-transferases in the conversion of leukotriene A4 to leukotriene C4. *Arch Biochem Biophys* 259, 536-547.
- ✚ Chen, Y., Hu, Y., Zhang, H., Peng, C., and Li, S. 2009. Loss of the Alox5 gene impairs leukemia stem cells and prevents chronic myeloid leukemia. *Nat Genet* 41, 783-792.
- ✚ Chowdhury, M.A., Abdellatif, K.R., Dong, Y., Das, D., Suresh, M.R., and Knaus, E.E. 2008. Synthesis of celecoxib analogs that possess a N-hydroxypyrid-2(1H)one 5-lipoxygenase pharmacophore: biological evaluation as dual inhibitors of cyclooxygenases and 5-lipoxygenase with anti-inflammatory activity. *Bioorg Med Chem Lett* 18, 6138-6141.
- ✚ Chowdhury, M.A., Abdellatif, K.R., Dong, Y., Rahman, M., Das, D., Suresh, M.R., and Knaus, E.E. 2009. Synthesis of 1-(methanesulfonyl- and aminosulfonylphenyl)acetylenes that possess a 2-(N-difluoromethyl-1,2-dihydropyridin-2-one) pharmacophore: evaluation as dual inhibitors of cyclooxygenases and 5-lipoxygenase with anti-inflammatory activity. *Bioorg Med Chem Lett* 19, 584-588.
- ✚ Chowdhury, M.A., Abdellatif, K.R., Dong, Y., Das, D., Yu, G., Velazquez, C.A., Suresh, M.R., and Knaus, E.E. 2009. Synthesis and biological evaluation of salicylic acid and N-acetyl-2-carboxybenzenesulfonamide regioisomers possessing a N-difluoromethyl-1,2-dihydropyrid-2-one pharmacophore: dual inhibitors of cyclooxygenases and 5-lipoxygenase with anti-inflammatory activity. *Bioorg Med Chem Lett* 19, 6855-6861.
- ✚ Clark, D.E., Willett, P., and Kenny, P.W. 1991. Pharmacophoric pattern matching in files of three-dimensional chemical structures: use of smoothed bounded distances for incompletely specified query patterns. *J Mol Graph* 9, 157-160.

- ✚ Colovos, C., and Yeates, T.O. 1993. Verification of protein structures: patterns of nonbonded atomic interactions. *Protein Sci* 2, 1511-1519.
- ✚ Davidson, E.M., Rae, S.A., and Smith, M.J. 1983. Leukotriene B<sub>4</sub>, a mediator of inflammation present in synovial fluid in rheumatoid arthritis. *Ann Rheum Dis* 42, 677-679.
- ✚ Deng, X.Q., Wang, H.Y., Zhao, Y.L., Xiang, M.L., Jiang, P.D., Cao, Z.X., Zheng, Y.Z., Luo, S.D., Yu, L.T., Wei, Y.Q., and Yang, S.Y. 2008. Pharmacophore modelling and virtual screening for identification of new Aurora-A kinase inhibitors. *Chem Biol Drug Des* 71, 533-539.
- ✚ Dessalew, N., and Bharatam, P.V. 2007. Structure based de novo design of novel glycogen synthase kinase 3 inhibitors. *Bioorg Med Chem* 15, 3728-3736.
- ✚ Dixon, R.A., Diehl, R.E., Opas, E., Rands, E., Vickers, P.J., Evans, J.F., Gillard, J.W., and Miller, D.K. 1990. Requirement of a 5-lipoxygenase-activating protein for leukotriene synthesis. *Nature* 343, 282-284.
- ✚ Du, L., Zhang, Z., Luo, X., Chen, K., Shen, X., and Jiang, H. 2006. Binding investigation of human 5-lipoxygenase with its inhibitors by SPR technology correlating with molecular docking simulation. *J Biochem* 139, 715-723.
- ✚ Dube, D., Blouin, M., Brideau, C., Chan, C.C., Desmarais, S., Ethier, D., Falgoutret, J.P., Friesen, R.W., Girard, M., Girard, Y., Guay, J., Riendeau, D., Tagari, P., and Young, R.N. 1998. Quinolines as potent 5-lipoxygenase inhibitors: synthesis and biological profile of L-746,530. *Bioorg Med Chem Lett* 8, 1255-1260.
- ✚ Ducharme, Y., Brideau, C., Dube, D., Chan, C.C., Falgoutret, J.P., Gillard, J.W., Guay, J., Hutchinson, J.H., McFarlane, C.S., Riendeau, D., and et al. 1994. Naphthalenic lignan lactones as selective, nonredox 5-lipoxygenase inhibitors. Synthesis and biological activity of (methoxyalkyl)thiazole and methoxytetrahydropyran hybrids. *J Med Chem* 37, 512-518.

- ✚ Ehrlich, P. 1909. *Über den jetzigen Stand der Chemotherapie*, Chem. Ber., 42, 17.
- ✚ Erion, M.D., Takabayashi, K., Smith, H.B., Kessi, J., Wagner, S., Honger, S., Shames, S.L., and Ealick, S.E. 1997. Purine nucleoside phosphorylase. 1. Structure-function studies. *Biochemistry* 36, 11725-11734.
- ✚ Fischer, R. The Design of Experiments; Hafner Publishing: New York, 1966. Chapter 2.
- ✚ Fiser, A., Do, R.K., and Sali, A. 2000. Modeling of loops in protein structures. *Protein Sci* 9, 1753-1773.
- ✚ Funk, C.D. 1996. The molecular biology of mammalian lipoxygenases and the quest for eicosanoid functions using lipoxygenase-deficient mice. *Biochim Biophys Acta* 1304, 65-84.
- ✚ Funk, C.D. 2001. Prostaglandins and leukotrienes: advances in eicosanoid biology. *Science* 294, 1871-1875.
- ✚ Gerwick, W.H. 1994. Structure and biosynthesis of marine algal oxylipins. *Biochim Biophys Acta* 1211, 243-255.
- ✚ Gorbitz, C.H., and Etter, M.C. 1992. Structure of L-phenylalanine L-phenylalaninium formate. *Acta Crystallogr C* 48 ( Pt 7), 1317-1320.
- ✚ Greer, J. 1990. Comparative modeling methods: application to the family of the mammalian serine proteases. *Proteins* 7, 317-334.
- ✚ Hamel, P., Riendeau, D., Brideau, C., Chan, C.C., Desmarais, S., Delorme, D., Dube, D., Ducharme, Y., Ethier, D., Grimm, E., Falgoutret, J.P., Guay, J., Jones, T.R., Kwong, E., McAuliffe, M., McFarlane, C.S., Piechuta, H., Roumi, M., Tagari, P., Young, R.N., and Girard, Y. 1997. Substituted (pyridylmethoxy)naphthalenes as potent and orally active 5-lipoxygenase inhibitors; synthesis, biological profile, and pharmacokinetics of L-739,010. *J Med Chem* 40, 2866-2875.
- ✚ Hammarberg, T., Provost, P., Persson, B., and Radmark, O. 2000. The N-terminal domain of 5-lipoxygenase binds calcium and mediates calcium stimulation of enzyme activity. *J Biol Chem* 275, 38787-38793.

- ✚ Hemak, J., Gale, D., and Brock, T.G. 2002. Structural characterization of the catalytic domain of the human 5-lipoxygenase enzyme. *J Mol Model* 8, 102-112.
- ✚ Krieger, E., Nabuurs, S.B., Vriend, G. 2003. Homology modeling. *Methods Biochem Anal* 44, 509-523.
- ✚ Homology user guide, Accelrys, Inc., San Diego, USA; 1999.
- ✚ Hutchinson, J.H., Riendeau, D., Brideau, C., Chan, C., Delorme, D., Denis, D., Falgoutret, J.P., Fortin, R., Guay, J., Hamel, P. 1993. Substituted thiopyrano[2,3,4-c,d]indoles as potent, selective, and orally active inhibitors of 5-lipoxygenase. Synthesis and biological evaluation of L-691,816. *J Med Chem* 36, 2771-2787.
- ✚ Janusz, J.M., Young, P.A., Scherz, M.W., Enzweiler, K., Wu, L.I., Gan, L., Pikul, S., McDow-Dunham, K.L., Johnson, C.R., Senanayake, C.B., Kellstein, D.E., Green, S.A., Tulich, J.L., Rosario-Jansen, T., Magrisso, I.J., Wehmeyer, K.R., Kuhlenbeck, D.L., Eichhold, T.H., and Dobson, R.L. 1998. New cyclooxygenase-2/5-lipoxygenase inhibitors. 2. 7-tert-butyl-2,3-dihydro-3,3-dimethylbenzofuran derivatives as gastrointestinal safe antiinflammatory and analgesic agents: variations of the dihydrobenzofuran ring. *J Med Chem* 41, 1124-1137.
- ✚ Janusz, J.M., Young, P.A., Ridgeway, J.M., Scherz, M.W., Enzweiler, K., Wu, L.I., Gan, L., Chen, J., Kellstein, D.E., Green, S.A., Tulich, J.L., Rosario-Jansen, T., Magrisso, I.J., Wehmeyer, K.R., Kuhlenbeck, D.L., Eichhold, T.H., and Dobson, R.L. 1998. New cyclooxygenase-2/5-lipoxygenase inhibitors. 3. 7-tert-butyl-2, 3-dihydro-3,3-dimethylbenzofuran derivatives as gastrointestinal safe antiinflammatory and analgesic agents: variations at the 5 position. *J Med Chem* 41, 3515-3529.
- ✚ Ji, H., Zhang, W., Zhang, M., Kudo, M., Aoyama, Y., Yoshida, Y., Sheng, C., Song, Y., Yang, S., Zhou, Y., Lu, J., and Zhu, J. 2003. Structure-based de novo design, synthesis, and biological evaluation of non-azole inhibitors specific for lanosterol 14 $\alpha$ -demethylase of fungi. *J Med Chem* 46, 474-485.

- ✚ Jones, G., Willett, P., Glen, R.C., Leach, A.R., and Taylor, R. 1997. Development and validation of a genetic algorithm for flexible docking. *J Mol Biol* 267, 727-748.
- ✚ Kelebe, G. 1993. Structural alignment of molecules, In Kubinyi, H. (Ed.) 3D QSAR in drug design: theory, methods and applications, ESCOM, Leiden, pp. 173-199.
- ✚ Kim do, Y., Kim, K.H., Kim, N.D., Lee, K.Y., Han, C.K., Yoon, J.H., Moon, S.K., Lee, S.S., and Seong, B.L. 2006. Design and biological evaluation of novel tubulin inhibitors as antimitotic agents using a pharmacophore binding model with tubulin. *J Med Chem* 49, 5664-5670.
- ✚ Kirchner, T., Argentieri, D.C., Barbone, A.G., Singer, M., Steber, M., Ansell, J., Beers, S.A., Wachter, M.P., Wu, W., Malloy, E., Stewart, A., and Ritchie, D.M. 1997. Evaluation of the antiinflammatory activity of a dual cyclooxygenase-2 selective/5-lipoxygenase inhibitor, RWJ 63556, in a canine model of inflammation. *J Pharmacol Exp Ther* 282, 1094-1101.
- ✚ Klebe, G. 2006. Virtual ligand screening: strategies, perspectives and limitations. *Drug Discov Today* 11, 580-594.
- ✚ Kyte, J., and Doolittle, R.F. 1982. A simple method for displaying the hydropathic character of a protein. *J Mol Biol* 157, 105-132.
- ✚ Kyun-Hwan Kim, Nam Doo Kim & Baik-Lin Seong. 2010 Pharmacophore-based virtual screening: a review of recent applications *Expert Opin Drug Discov*
- ✚ Larbig, G., Pickhardt, M., Lloyd, D.G., Schmidt, B., and Mandelkow, E. 2007. Screening for inhibitors of tau protein aggregation into Alzheimer paired helical filaments: a ligand based approach results in successful scaffold hopping. *Curr Alzheimer Res* 4, 315-323.
- ✚ Laskowski, R.A., Moss, D.S., and Thornton, J.M. 1993. Main-chain bond lengths and bond angles in protein structures. *J Mol Biol* 231, 1049-1067.
- ✚ Liou, J.P., Mahindroo, N., Chang, C.W., Guo, F.M., Lee, S.W., Tan, U.K., Yeh, T.K., Kuo, C.C., Chang, Y.W., Lu, P.H., Tung, Y.S., Lin, K.T., Chang, J.Y., and Hsieh, H.P. 2006. Structure-activity relationship studies



- of 3-aroylindoles as potent antimitotic agents. *ChemMedChem* 1, 1106-1118.
- # Lipinski, C.A. 2000. Drug-like properties and the causes of poor solubility and poor permeability. *J Pharmacol Toxicol Methods* 44, 235-249.
  - # Lu, A., Zhang, J., Yin, X., Luo, X., and Jiang, H. 2007. Farnesyltransferase pharmacophore model derived from diverse classes of inhibitors. *Bioorg Med Chem Lett* 17, 243-249.
  - # LUDI user guide, Accelrys, Inc., San Diego, USA; 1999
  - # Lyne, P. D. Structure-based virtual screening: an overview. *Drug Discov Today* 2002, 7, 1047-55.
  - # Lyne, P.D., Kenny, P.W., Cosgrove, D.A., Deng, C., Zabudoff, S., Wendoloski, J.J., and Ashwell, S. 2004. Identification of compounds with nanomolar binding affinity for checkpoint kinase-1 using knowledge-based virtual screening. *J Med Chem* 47, 1962-1968.
  - # Markt, P., Petersen, R.K., Flindt, E.N., Kristiansen, K., Kirchmair, J., Spitzer, G., Distinto, S., Schuster, D., Wolber, G., Laggner, C., and Langer, T. 2008. Discovery of novel PPAR ligands by a virtual screening approach based on pharmacophore modeling, 3D shape, and electrostatic similarity screening. *J Med Chem* 51, 6303-6317.
  - # Marshall, G.R. and Naylor, C.B., *Use of molecular graphics for structural analysis of small molecules*, In Hansch, C., Sammes, P.G., Taylor, J.B. and Ramsden, C.A. (Eds.) *Comprehensive medicinal chemistry: Vol. 4*, Pergamon Press, Oxford, 1990, pp. 431-458.
  - # Marshall, G.R., Barry, C.D., Bosshard, H.E., Dammkoehler, R.A. and Dunn, D.A., *The conformational parameter in drug design*, Computer Assisted Drug Design, ACS Symp. Ser. 112, 1979, pp. 205-226.
  - # McInnes, C. 2007. Virtual screening strategies in drug discovery. *Curr Opin Chem Biol* 11, 494-502.
  - # Melstrom, L.G., Bentrem, D.J., Salabat, M.R., Kennedy, T.J., Ding, X.Z., Strouch, M., Rao, S.M., Witt, R.C., Ternent, C.A., Talamonti, M.S., Bell, R.H., and Adrian, T.A. 2008. Overexpression of 5-lipoxygenase in colon



- polyps and cancer and the effect of 5-LOX inhibitors in vitro and in a murine model. *Clin Cancer Res* 14, 6525-6530.
- ✚ Meruvu, S., Walther, M., Ivanov, I., Hammarstrom, S., Furstenberger, G., Krieg, P., Reddanna, P., and Kuhn, H. 2005. Sequence determinants for the reaction specificity of murine (12R)-lipoxygenase: targeted substrate modification and site-directed mutagenesis. *J Biol Chem* 280, 36633-36641.
  - ✚ Minor, W., Steczko, J., Stec, B., Otwinowski, Z., Bolin, J.T., Walter, R., and Axelrod, B. 1996. Crystal structure of soybean lipoxygenase L-1 at 1.4 Å resolution. *Biochemistry* 35, 10687-10701.
  - ✚ Miranker, A., and Karplus, M. 1991. Functionality maps of binding sites: a multiple copy simultaneous search method. *Proteins* 11, 29-34.
  - ✚ MOE Program, Chemical Computing Group Inc., Montréal, Québec, Canada, 2003.
  - ✚ Montgomery, J.A., Niwas, S., Rose, J.D., Secrist, J.A., 3rd, Babu, Y.S., Bugg, C.E., Erion, M.D., Guida, W.C., and Ealick, S.E. 1993. Structure-based design of inhibitors of purine nucleoside phosphorylase. 1. 9-(arylmethyl) derivatives of 9-deazaguanine. *J Med Chem* 36, 55-69.
  - ✚ Moreau, A., Rao, P.N., and Knaus, E.E. 2006. Synthesis and biological evaluation of acyclic triaryl (Z)-olefins possessing a 3,5-di-tert-butyl-4-hydroxyphenyl pharmacophore: dual inhibitors of cyclooxygenases and lipoxygenases. *Bioorg Med Chem* 14, 5340-5350.
  - ✚ Nakamura, C., Kawasaki, N., Miyataka, H., Jayachandran, E., Kim, I.H., Kirk, K.L., Taguchi, T., Takeuchi, Y., Hori, H., and Satoh, T. 2002. Synthesis and biological activities of fluorinated chalcone derivatives. *Bioorg Med Chem* 10, 699-706.
  - ✚ Needleman, S.B., and Wunsch, C.D. 1970. A general method applicable to the search for similarities in the amino acid sequence of two proteins. *J Mol Biol* 48, 443-453.
  - ✚ Nie, D., Che, M., Grignon, D., Tang, K., and Honn, K.V. 2001. Role of eicosanoids in prostate cancer progression. *Cancer Metastasis Rev* 20, 195-206.

- ✚ Nikolaev, V., Reddanna, P., Whelan, J., Hildenbrandt, G., and Reddy, C.C. 1990. Stereochemical nature of the products of linoleic acid oxidation catalyzed by lipoxygenases from potato and soybean. *Biochem Biophys Res Commun* 170, 491-496.
- ✚ Nugiel, D.A., Krumrine, J.R., Hill, D.C., Damewood, J.R., Bernstein, P.R., Sobotka-Briner, C.D., Liu, J., Zacco, A., and Pierson, M.E. De Novo Design of a Picomolar Nonbasic 5-HT(1B) Receptor Antagonist. *J Med Chem* 53, 1876-1880.
- ✚ Pandit, D., So, S.S., and Sun, H. 2006. Enhancing specificity and sensitivity of pharmacophore-based virtual screening by incorporating chemical and shape features--a case study of HIV protease inhibitors. *J Chem Inf Model* 46, 1236-1244.
- ✚ Peitsch, M.C., Schwede, T., and Guex, N. 2000. Automated protein modelling--the proteome in 3D. *Pharmacogenomics* 1, 257-266.
- ✚ Prigge, S.T., Boyington, J.C., Faig, M., Doctor, K.S., Gaffney, B.J., and Amzel, L.M. 1997. Structure and mechanism of lipoxygenases. *Biochimie* 79, 629-636.
- ✚ Profile-3D user guide, Accelrys, Inc., San Diego, USA; 1999.
- ✚ QUANTA, Accelrys Inc., San Diego, CA, USA.
- ✚ Rao, P.N., Chen, Q.H., and Knaus, E.E. 2005. Synthesis and biological evaluation of 1,3-diphenylprop-2-yn-1-ones as dual inhibitors of cyclooxygenases and lipoxygenases. *Bioorg Med Chem Lett* 15, 4842-4845.
- ✚ Rapoport, S.M., Schewe, T., Wiesner, R., Halangk, W., Ludwig, P., Janicke-Hohne, M., Tannert, C., Hiebsch, C., and Klatt, D. 1979. The lipoxygenase of reticulocytes. Purification, characterization and biological dynamics of the lipoxygenase; its identity with the respiratory inhibitors of the reticulocyte. *Eur J Biochem* 96, 545-561.
- ✚ Reddanna, P., Rao, M.K., and Reddy, C.C. 1985. Inhibition of 5-lipoxygenase by vitamin E. *FEBS Lett* 193, 39-43.

- ✚ Reddanna, P., Whelan, J., Reddy, P.S., and Reddy, C.C. 1988. Isolation and characterization of 5-lipoxygenase from tulip bulbs. *Biochem Biophys Res Commun* 157, 1348-1351.
- ✚ Reddanna, P., Whelan, J., Maddipati, K.R., and Reddy, C.C. 1990. Purification of arachidonate 5-lipoxygenase from potato tubers. *Methods Enzymol* 187, 268-277.
- ✚ Reddanna, P., Prabhu, K.S., Whelan, J., and Reddy, C.C. 2003. Carboxypeptidase A-catalyzed direct conversion of leukotriene C4 to leukotriene F4. *Arch Biochem Biophys* 413, 158-163.
- ✚ Reddy, M.R., and Erion, M.D. 1998. Structure-based drug design approaches for predicting binding affinities of HIV1 protease inhibitors. *J Enzyme Inhib* 14, 1-14.
- ✚ Reddy, M.R., and Erion, M.D. 2005. Computer-aided drug design strategies used in the discovery of fructose 1, 6-bisphosphatase inhibitors. *Curr Pharm Des* 11, 283-294.
- ✚ Reddy, M.V., Mallireddigari, M.R., Cosenza, S.C., Pallela, V.R., Iqbal, N.M., Robell, K.A., Kang, A.D., and Reddy, E.P. 2008. Design, synthesis, and biological evaluation of (E)-styrylbenzylsulfones as novel anticancer agents. *J Med Chem* 51, 86-100.
- ✚ Reddy, R.N., Mutyala, R., Aparoy, P., Reddanna, P., and Reddy, M.R. 2007. Computer aided drug design approaches to develop cyclooxygenase based novel anti-inflammatory and anti-cancer drugs. *Curr Pharm Des* 13, 3505-3517.
- ✚ Ryu, K., Kim, N.D., Choi, S.I., Han, C.K., Yoon, J.H., No, K.T., Kim, K.H., and Seong, B.L. 2009. Identification of novel inhibitors of HCV RNA-dependent RNA polymerase by pharmacophore-based virtual screening and in vitro evaluation. *Bioorg Med Chem* 17, 2975-2982.
- ✚ Sali, A., and Blundell, T.L. 1993. Comparative protein modelling by satisfaction of spatial restraints. *J Mol Biol* 234, 779-815.
- ✚ Sanchez, R., and Sali, A. 1997. Advances in comparative protein-structure modelling. *Curr Opin Struct Biol* 7, 206-214.

- ✚ Sansom, C.E., Wu, J., and Weber, I.T. 1992. Molecular mechanics analysis of inhibitor binding to HIV-1 protease. *Protein Eng* 5, 659-667.
- ✚ Schneider, G., and Fechner, U. 2005. Computer-based de novo design of drug-like molecules. *Nat Rev Drug Discov* 4, 649-663.
- ✚ Shibata, D., and Axelrod, B. 1995. Plant lipoxygenases. *J Lipid Mediat Cell Signal* 12, 213-228.
- ✚ Singh, U.C., Weiner, P.K., Caldwell, J.K. and Kollman P.A. AMBER version 3.0, University of California, San Francisco, CA,1986.
- ✚ Skrzypczak-Jankun, E., Borbulevych, O.Y., and Jankun, J. 2004. Soybean lipoxygenase-3 in complex with 4-nitrocatechol. *Acta Crystallogr D Biol Crystallogr* 60, 613-615.
- ✚ Smellie, A., Teig, S.L., Towbin, P. 1995. Polling: promoting conformational variation. *J Comput Chem* 16, 171-187
- ✚ Soumaoro, L.T., Iida, S., Uetake, H., Ishiguro, M., Takagi, Y., Higuchi, T., Yasuno, M., Enomoto, M., and Sugihara, K. 2006. Expression of 5-lipoxygenase in human colorectal cancer. *World J Gastroenterol* 12, 6355-6360.
- ✚ Steindl, T.M., Schuster, D., Laggner, C., Chuang, K., Hoffmann, R.D., and Langer, T. 2007. Parallel screening and activity profiling with HIV protease inhibitor pharmacophore models. *J Chem Inf Model* 47, 563-571.
- ✚ Sternberg, M.J., Bates, P.A., Kelley, L.A., and MacCallum, R.M. 1999. Progress in protein structure prediction: assessment of CASP3. *Curr Opin Struct Biol* 9, 368-373.
- ✚ Taha, M.O., Atallah, N., Al-Bakri, A.G., Paradis-Bleau, C., Zalloum, H., Younis, K.S., and Levesque, R.C. 2008. Discovery of new MurF inhibitors via pharmacophore modeling and QSAR analysis followed by in-silico screening. *Bioorg Med Chem* 16, 1218-1235.
- ✚ Thompson, J.D., Higgins, D.G., and Gibson, T.J. 1994. CLUSTAL W: improving the sensitivity of progressive multiple sequence alignment

through sequence weighting, position-specific gap penalties and weight matrix choice. *Nucleic Acids Res* 22, 4673-4680.

- ✚ Tondi, D., Morandi, F., Bonnet, R., Costi, M.P., and Shoichet, B.K. 2005. Structure-based optimization of a non-beta-lactam lead results in inhibitors that do not up-regulate beta-lactamase expression in cell culture. *J Am Chem Soc* 127, 4632-4639.
- ✚ Tsai, K.C., Chen, S.Y., Liang, P.H., Lu, I.L., Mahindroo, N., Hsieh, H.P., Chao, Y.S., Liu, L., Liu, D., Lien, W., Lin, T.H., and Wu, S.Y. 2006. Discovery of a novel family of SARS-CoV protease inhibitors by virtual screening and 3D-QSAR studies. *J Med Chem* 49, 3485-3495.
- ✚ Ulbrich, H., Fiebich, B., and Dannhardt, G. 2002. Cyclooxygenase-1/2 (COX-1/COX-2) and 5-lipoxygenase (5-LOX) inhibitors of the 6,7-diaryl-2,3-1H-dihydropyrrolizine type. *Eur J Med Chem* 37, 953-959.
- ✚ Villoutreix, B.O., Eudes, R., and Miteva, M.A. 2009. Structure-based virtual ligand screening: recent success stories. *Comb Chem High Throughput Screen* 12, 1000-1016.
- ✚ Vriend, G. 1990. WHAT IF: a molecular modeling and drug design program. *J Mol Graph* 8, 52-56, 29.
- ✚ Wang, D., and Dubois, R.N. 2010. Eicosanoids and cancer. *Nat Rev Cancer* 10, 181-193.
- ✚ Wang, H.Y., Cao, Z.X., Li, L.L., Jiang, P.D., Zhao, Y.L., Luo, S.D., Yang, L., Wei, Y.Q., and Yang, S.Y. 2008. Pharmacophore modeling and virtual screening for designing potential PLK1 inhibitors. *Bioorg Med Chem Lett* 18, 4972-4977.
- ✚ Waszkowycz, B., Perkins, T.D.J., Sykes, R.A., Li, J. 2001. Large-scale virtual screening for discovering leads in the postgenomic era, *IBM Syst J* 40, 360-376.
- ✚ Werz, O., Tretiakova, I., Michel, A., Ulke-Lemee, A., Hornig, M., Franke, L., Schneider, G., Samuelsson, B., Radmark, O., and Steinhilber, D. 2005. Caspase-mediated degradation of human 5-lipoxygenase in B lymphocytic cells. *Proc Natl Acad Sci U S A* 102, 13164-13169.

- ✚ Whelan, J., Reddanna, P., Nikolaev, V., Hildebrandt, G., Reddy, C.C. 1988. In: Reddy CC, Hamilton GA, Madyastha KM (eds) Biological oxidation systems, vol 2. Academic Press, San Diego, CA, p 765
- ✚ Xie, H.Z., Li, L.L., Ren, J.X., Zou, J., Yang, L., Wei, Y.Q., and Yang, S.Y. 2009. Pharmacophore modeling study based on known spleen tyrosine kinase inhibitors together with virtual screening for identifying novel inhibitors. *Bioorg Med Chem Lett* 19, 1944-1949.
- ✚ Zhang, Y.Y., Lind, B., Radmark, O., and Samuelsson, B. 1993. Iron content of human 5-lipoxygenase, effects of mutations regarding conserved histidine residues. *J Biol Chem* 268, 2535-2541.

## List of publications

### Published articles:

1. **Aparoy P**, Kumar Reddy K, Kalangi SK, Chandramohan Reddy T, Reddanna P. Pharmacophore modeling and virtual screening for designing potential 5-Lipoxygenase inhibitors. *Bioorg Med Chem Lett*. 2010 Feb 1;20(3):1013-8. Epub 2009 Dec 21. PubMed PMID: 20045317.
2. Reddy RN, Mutyala RR, **Aparoy P**, Reddanna P, Reddy MR. An analysis of hydrophobic interactions of thymidylate synthase with methotrexate: free energy calculations involving mutant and native structures bound to methotrexate. *J Mol Model*. 2010 Feb;16(2):203-9. Epub 2009 Jun 28. PubMed PMID: 19562390.
3. **Aparoy P**, Chatterjee M, Guruprasad L, Reddanna P. Structure prediction of neuroendocrine convertase -2: a potential target in various cancers. *Protein Pept Lett*. 2009;16(4):383-91. PubMed PMID: 19356135.
4. **Aparoy P**, Leela T, Reddy RN, Reddanna P. Computational analysis of R and S isoforms of 12-lipoxygenases: homology modeling and docking studies. *J Mol Graph Model*. 2009 Feb;27(6):744-50. Epub 2008 Nov 27. PubMed PMID: 19147381.
5. **Aparoy P**, Reddy RN, Guruprasad L, Reddy MR, Reddanna P. Homology modeling of 5-lipoxygenase and hints for better inhibitor design. *J Comput Aided Mol Des*. 2008 Sep;22(9):611-9. Epub 2008 Jan 30. PubMed PMID: 18231862.
6. Reddy RN, Mutyala R, **Aparoy P**, Reddanna P, Reddy MR. Computer aided drug design approaches to develop cyclooxygenase based novel anti-inflammatory and anti-cancer drugs. *Curr Pharm Des*. 2007;13(34):3505-17. Review. PubMed PMID: 18220787.

### Articles Accepted/In press:

7. **Aparoy P**, Kuntal K Bhushan, Reddanna P. Development of tools and database for analysis of metal binding sites in protein. *Protein Pept Lett*. 2010.
8. **Aparoy P**, Reddy RN, Guruprasad L, Reddanna P. Computational Analysis of Interactions of Argadin with Chitotriosidase, Chitinase and Acidic

Mammalian Chitinase: Hints for Specific Inhibitor Design. Letters in Drug Designing and Discovery. 2010

9. Gullipalli D, Arif A, **Aparoy P**, Svenson GJ, Whiting MF, Reddanna P, Dutta-Gupta A. Identification of a developmentally and hormonally regulated Delta-Class glutathione S-transferase in rice moth *Corcyra cephalonica*. Comp Biochem Physiol B Biochem Mol Biol. 2010 Feb 4. [Epub ahead of print] PubMed PMID: 20138238.

#### Articles under review:

10. **Aparoy P**, Reddy MR, Reddanna P Relative Binding Free Energies of Fructose 1,6-Bisphosphatase inhibitors Calculated Using an Ab InitioQM/MM-Based Free Energy Perturbation Method: Dependence of Results on Simulation Length.
11. Reddy NP, **Aparoy P**, Reddy TC, Chandrani A, Reddanna P. Design, synthesis and biological evaluation of chalcone derivatives as 5-LOX inhibitors.
12. **Aparoy P**, Reddy KK, Priyankeswari K, Reddanna P. Identification of specific patterns in 5-, 12R- and 15-Lipoxygenases.
13. Reddy TC, **Aparoy P**, Kishore Babu N, Suresh Kumar K and Reddanna P. Kinetics and Docking studies of a COX-2 inhibitor isolated from *Terminalia bellerica* fruits.
14. Reddy TC, Bharat Reddy D, Aparna A, **Aparoy P**, Arunasree K, Lakshmi pathi V, Subramanyam A, Reddanna P. Gallic acid, a natural antioxidant isolated from *Terminalia bellerica* fruits, induces apoptosis in human chronic myeloid leukemia cell line-K562.